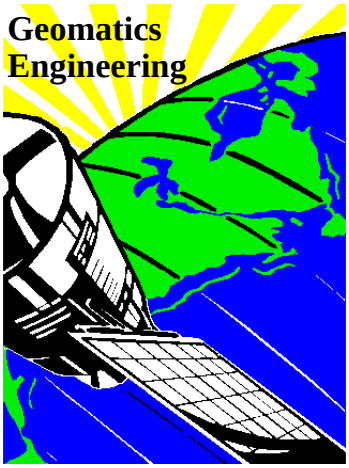

UCGE REPORTS
Number 20061

Department of Geomatics Engineering

High Accuracy Airborne Differential GPS Positioning Using a Multi-Receiver Configuration

by

Jing Shi

April 1994

(www.geomatics.ucalgary.ca/GradTheses.html)

THE UNIVERSITY OF CALGARY

HIGH ACCURACY AIRBORNE DIFFERENTIAL GPS POSITIONING USING A MULTI-RECEIVER CONFIGURATION

by

JING SHI

A THESIS

SUBMITTED TO THE FACULTY OF GRADUATE STUDIES

IN PARTIAL FULFILLMENT OF THE REQUIREMENTS FOR THE

DEGREE OF MASTER OF SCIENCE

DEPARTMENT OF GEOMATICS ENGINEERING

CALGARY, ALBERTA

APRIL, 1994

ABSTRACT

Precise airborne DGPS positioning using a multi-receiver configuration is investigated with the emphasis on the centimetre level accuracy over large operational areas. The critical errors from the atmosphere, orbit, Selective Availability and multipath are reviewed and analyzed. The effects of these errors on the positioning solutions are identified and assessed for monitor-remote separations ranging from 50 to 200 km. Theoretical analysis in two frequently used kinematic GPS algorithms is presented and methods for accuracy evaluation are studied. To demonstrate the achievable accuracy of airborne DGPS positioning over a large area, results from flight tests with a multi-receiver configuration are extensively investigated. Under the present satellite constellation, the accuracy of airborne DGPS positioning with monitor-remote separations of 50 - 200 km is at the level of 10 cm if high quality receivers are used and the effects due to all critical errors are taken into account.

ACKNOWLEDGMENTS

I wish to express my appreciation to my supervisor, Professor M. Elizabeth Cannon for her advice, support and encouragement throughout the course of my graduate studies.

Professor Cannon is also acknowledged for providing the SEMIKIN™ software. Thanks go to many students in our research group for beneficial discussions related to this thesis. Specifically, I would like to thank Mr. Gang Lu and Mr. Dingsheng Cheng for sharing their research experiences in GPS. Mr. Keith Van Dierendonck is thanked for his assistance in data collection as well as for providing field information on the flight test. Mr. Douglas Roberts is acknowledged for providing precise ephemeris data. Mr. Hazen Gehue, Mr. Roberts and Mr. Van Dierendonck are all gratefully acknowledged for proofreading the thesis manuscript.

Financial support for my graduate studies came from a Natural Science and Engineering Research Council Strategic Grant and The University of Calgary through a Graduate Research Assistantship. An NSERC/CRD grant with Canagrav Research provided funds for the acquisition of the test data. Their contributions are greatly acknowledged.

Finally, special thanks go to my wife, Xiaoping, for her support and understanding.

TABLE OF CONTENTS

Page

ABSTRACT iii

ACKNOWLEDGMENTS iv

TABLE OF CONTENTS v

LIST OF TABLES viii

LIST OF FIGURES x

NOTATION xiv

CHAPTER

1 INTRODUCTION 1

1.1 Background and Objectives 1

1.2 Thesis Outline 4

2 ERROR SOURCES AND CORRECTIONS 6

2.1 GPS Observables and Errors 6

2.2 Tropospheric Error and Correction 10

2.3 Ionospheric Error and Correction 12

2.4 Orbital Error and Precise Orbit 15

2.4.1 Broadcast Ephemeris Error and Selective Availability 16

2.4.2 Precise Ephemerides and Applications 19

2.5 Multipath 22
3 ALGORITHMS AND ANALYSIS 24
3.1 Kinematic GPS Algorithms 25
3.2 Analytical Estimation of Orbital Error Effect on Estimated Positions 31
3.3 Theoretical Analysis on Solutions From a Triple Receiver System 37
4 CONFIGURATIONS AND OPERATIONAL STRATEGIES 41
4.1 Error Budget and Limitations 42
4.2 Configuration of GPS Receivers 46
4.2.1 Configuration on the Ground 46
4.2.2 Configuration on the Aircraft 47
4.3 Operational Strategies 48
5 DATA PROCESSING STRATEGIES AND ACCURACY EVALUATION 51
5.1 Data Processing Strategies 51
5.2 Methods for Accuracy Checking and Analysis 53
6 TEST DESCRIPTION, RESULTS AND ANALYSIS 57
6.1 Test Description 57
6.2 Data Processing 62
6.3 Positioning Results 64
6.3.1 Results with P-code L1 and C/A-code L1 64

6.3.2 Results with P-code L2 71
6.3.3 Results with Cross Correlation L2 74
6.4 Critical Error Effects and Analysis 76
6.4.1 Tropospheric Effect 77
6.4.2 Ionospheric Effect 79
6.4.3 Orbital Error Effect 86
6.4.4 Multipath Effect 94
6.5 Comparison and Accuracy Evaluation 102
6.5.1 Comparison with Known Baseline on the Aircraft 102
6.5.2 Comparison Between Forward and Reverse Processing 108
6.5.3 Triangle Misclosure Test 110
6.5.4 Positioning Solution from Different Monitor Stations 113
7 SUMMARY, CONCLUSIONS, AND RECOMMENDATIONS 116
7.1 Summary of Research 116
7.2 Conclusions 117
7.3 Recommendations 121
REFERENCES 123

LIST OF TABLES

Table		Page
4.1	Residual GPS Errors for the Case of L1 Measurements with SA On	43
4.2	Residual GPS Errors for the Case of L1/L2 Measurments with SA On	44
4.3	Residual GPS Errors for the Case of L1 Measurements with Precise Ephemerides	45
6.2.1	Kinematic Data Processing Scenario	63
6.3.1	Flight Misclosures, P-code L1, April 27	66
6.3.2	Flight Misclosures, C/A-code L1, April 28	66
6.3.3	Contrast of DD Residuals Statistics Between the OSHA-AFT and and FORE-AFT Kinematic Runs	71
6.3.4	Flight Misclosures, P-code L2, April 27	72
6.3.5	Contrast Between P-code L1 and P-code L2 DD Residuals Statistics	73
6.3.6	Flight Misclosures, Cross-correlation L2, April 28	75
6.4.1	DD Resdiduals Statistics Comparison Between with and without Tropospheric Correction Solutions	79
6.4.2	Statistics of Residuals Using Ionospherically Corrected Measurement	80

6.4.3 Statistics of the Satellite Orbital Error in Position and Related Features..... 88
6.4.4 Comparison Between Statistics of Residuals Using Broadcast and Precise Orbits..... 93
6.5.1 Statistics of Difference Between Trajectories from Forward and Reverse Time Processing 110
6.5.2 Statistics of the Triangle Misclosure Formed by OSHA-FORE, OSHA-AFT and FORE-AFT Kinematic Vector 111

LIST OF FIGURES

Figure **Page**

2.4.1 Comparison Between Orbital Errors from Block I and Block II.....18

6.1.1 GPS Receiver Configurations on the Ground and on the Aircraft 59

6.1.2 Satellite Skyplot.....59

6.1.3 Flight Path on April 27, 1993.....61

6.1.4 Flight Path Changing in Latitude, Longitude and Height over GPS Time.....61

6.3.1 DD Residuals for PRNs 31-11 Using the OSHA-AFT Kinematic Run (P-code L1, April 27).....67

6.3.2 DD Residuals for PRNs 19-11 Using the OSHA-AFT Kinematic Run (P-code L1, April 27).....68

6.3.3 DD Residuals for PRNs 31-11 Using the OSHA-AFT Kinematic Run (C / A-code L1, April 28).....68

6.3.4 DD Residuals for PRNs 28-11 Using the OSHA-AFT Kinematic Run (C / A-code L1, April 28).....69

6.3.5 DD Residuals for PRNs 19-11 Using the FORE-AFT Kinematic Run (P-code L1, April 27).....70

6.3.6 DD Residuals for PRNs 19-11 Using the FORE-AFT Kinematic Run (C / A-code L1, April 28).....70

6.3.7 DD Residuals for PRNs 31-11 Using the OSHA-AFT Kinematic Run (P-code L2, April 27).....73

6.3.8 RMS of Flight Misclosures on April 27 and 28.....75
6.3.9 DD Residuals for PRNs 19-11 Using the FORE-AFT Kinematic Run (Cross-correlation L2, April 28).....76
6.4.1 Tropospheric Error Effect on the Position of the FORE Antenna Using the OSHA-FORE Kinematic Run.....78
6.4.2 Comparison of Residuals Using P-code L1, L2 and L1/L2 Measurements.....81
6.4.3 Comparison Between Residuals Using P-code L1 and L2 versus Monitor-Remote Separation.....83
6.4.4 Comparison Between Residuals Using C/A-code L1 and Cross-correlation L2 versus Monitor-Remote Separation.....83
6.4.5 Comparison Between Residuals Using P-code L1 on April 27 and C/A-code L1 on April 28 versus Monitor-Remote Separation.....84
6.4.6 Ratios of Residual RMS Using P-code L2 to P-code L1 and Using Cross-correlation L2 to C/A-code L1.....84
6.4.7 Difference Between Aircraft Trajectories Using P-code L1 and L1/L2 Measurements, April 27.....86
6.4.8 Differences Between Broadcast and Precise Orbits for All Satellites Used on April 27.....87
6.4.9 Difference Between Aircraft Trajectories Using Precise and Broadcast Orbits on April 27 (OSHA-AFT Kinematic Run with P-code L1).....90
6.4.10 Difference Between Aircraft Trajectories Using Precise and Broadcast Orbits on April 27 (OSHA-AFT Kinematic Run

with P-code L1 and No Broadcast Updating During Mission) 90
6.4.11 Difference Between Aircraft Trajectories Using Precise and Broadcast Orbits on April 28 (OSHA-FORE Kinematic Run with C / A-code L1) 92
6.4.12 Comparison Between Residuals Using Precise and Broadcast Orbit 92
6.4.13 Multipath Effect on Residuals in Static Mode after Landing 98
6.4.14 Multipath Effect on Residuals by Using Static Data in Kinematic Mode after Landing 99
6.4.15 Multipath Effect on Coordinates by Using Static Data in Kinematic Mode after Landing 100
6.4.16 Residuals Using the AFT-FORE Kinematic Run on the Flight Test Leg 2 101
6.5.1 Difference in Known and Estimated Aircraft Antenna Separation Using the OSHA-FORE and OSHA-AFT Kinematic Runs (P-code L1, April 27) 105
6.5.2 Difference in Known and Estimated Aircraft Antenna Separation Using the FORE-AFT Kinematic Run (P Code L1, April 27) 105
6.5.3 Difference in Known and Estimated Aircraft Antenna Separation Using the OSHA-FORE and OSHA-AFT Kinematic Runs (C / A-code L1 , April 28) 106
6.5.4 Difference in Known and Estimated Aircraft Antenna Separation Using the FORE-AFT Kinematic Run

(C / A-code L1, April 28) 106

6.5.5 Difference in Known and Estimated Aircraft Antenna Separation Using the AFT-FORE Kinematic Run on the Flight Test Leg 2 107

6.5.6 Trajectory Differences Between Forward and Reverse Time Processing Solutions (P-code L1, April 27) 109

6.5.7 Misclosure Formed by the OSHA-FORE, OSHA-AFT and FORE-AFT Kinematic Vectors (P-code L1, April 27) 112

6.5.8 Correlation Between Aircraft Differences Determined from Two Monitor Receiver and the Error Between Two Monitor Receivers When Processed in Kinematic Mode 115

6.5.9 Difference Between Measured and Estimated Baseline Using Independent Aircraft Trajectories (on the flight test leg 2) 115

NOTATION

i) **Symbol**

$\mathbf{A}$	design matrix
$\mathbf{a}$	coefficient vector
c	speed of light
$\mathbf{C}^x$	Kalman state vector covariance matrix
$\mathbf{C}^w$	Kalman system process noise covariance matrix
$\mathbf{C}_l$	measurement noise covariance
$\mathbf{C}^{\Delta x}$	increment vector covariance
d_{ion}	ionospheric delay
d_{trop}	tropospheric delay
$d_{ion}(t_i)$	absolute ionospheric correction to the L1 carrier phase at epoch t_i
d'_{ion}	relative ionospheric correction to the L1
$d\rho$	orbital error
$d\rho_n$	nominal orbital error
$d\rho_{SA}$	orbital error due to AS
dt	satellite clock error
dT	receiver clock error
$\delta\mathbf{x}_r$	position error vector of the remote caused by satellite orbital errors
δx_r, δy_r, δz_r	coordinate errors of the remote caused by satellite

	orbital errors
$\delta\mathbf{x}^i$	position error vector of the satellite, i
δx^i, δy^i, δz^i	coordinate errors of the satellite, i
ε	measurement noise vector
$\varepsilon(\Phi)$	carrier measurement noise
$\varepsilon(\Phi_{rx})$	receiver noise
$\varepsilon(\Phi_{mult})$	multipath error
f	carrier phase frequency
Φ	carrier phase observation or transition matrix
Φ_{L1}	L1 carrier phase measurement
Φ_{L2}	L2 carrier phase measurement
$\Phi'_{L1/L2}(t_i)$	L1 carrier phase measurement with relatively ionospheric correction applied
k	epoch number
K	Kalman gain matrix
λ	carrier wavelength
l	observation vector
L1/L2	ionosphererically corrected measurement
n	order of the interpolator or number of the satellites tracked
N	carrier phase integer ambiguity
ρ	range from receiver to satellite
Q	spectral density matrix

$\sigma^2_{\Phi'_{L1/L2}}$	noise variance of the L1 carrier phase measurement with the relative ionospheric correction applied
$\sigma^2_{\Phi_{L1}}$	noise variance of the L1 carrier phase measurement
$\sigma^2_{\Phi_{L2}}$	noise variance of the L2 carrier phase measurement
t	interpolated epoch
t_k	given time
Δt	time interval
$\mathbf{w}$	system process noise vector
$\mathbf{x}$	state vector
Δx	increment vector over two successive epochs
$x^s(t)$	interpolated satellite coordinate at epoch t
$x^s(t_k)$	known satellite coordinate value at t_k
$\mathbf{x}_r$	estimated position vector of the remote
x_r, y_r, z_r	estimated cartesian coordinates of the receiver
X_r, Y_r, Z_r	cartesian coordinates of the remote, r
X^i, Y^i, Z^i	cartesian coordinates of the satellite, i

ii) **Defined Operators**

(-)	predicted quantity
(+)	updated quantity
^	estimated quantity
$\mathbf{A}^{T}$	matrix transpose
$\mathbf{C}^{-1}$	matrix inverse
Δ	double difference
$\prod$	product of
$\sum$	summation of

iii) **Acronyms**

C / A-code	coarse acquisition code
Cc	cross correlation
DD	double difference
GDOP	geometric dilution of precision
GPS	Global Positioning System
P-code	precise code
PDOP	position dilution of precision
PRN	pseudorandom noise
RMS	root mean square
SA	selective availability
SNR	signal to noise ratio

CHAPTER 1

INTRODUCTION

1.1 BACKGROUND AND OBJECTIVES

The advent of the Global Positioning System (GPS) has led to technical revolutions in navigation as well as in fields related to surveying. The GPS system, an all-weather satellite-based radio navigation system, can provide users on a world-wide basis with navigation, positioning, and time information, which is not possible with conventional navigation and surveying methods. By using GPS carrier phase measurements, this system can also provide an ability to determine the trajectory of a moving platform with respect to a fixed monitor station to a precision of several centimetres for a monitor-remote separation less than 30 km. This precise relative kinematic GPS positioning technique was demonstrated by Remondi (1985, 1986) and Mader (1986) in the early developmental stage. Since then, this technique has been investigated and tested in various environments (Krabill and Martin, 1987; Hein et al., 1988; Cannon and Schwarz, 1990; Mader and Lucas, 1989; Cannon, 1990; Lachapelle et al., 1993). The reported results have demonstrated that the theoretical accuracy, which is at the centimetre level, can be achieved over short baselines (less than 30 km

monitor to remote separation). With the completion of the GPS constellation, the kinematic GPS technique will be widely used in a variety land, marine, and aircraft positioning applications.

Precise airborne GPS positioning is a very important component of kinematic GPS applications, and it will provide precise navigation information for many engineering applications and scientific investigations, such as photogrammetric aerotriangulation without ground control, airborne remote sensing, airborne laser systems for precise topographic mapping, and geophysical and oceanographic exploration (Mader and Lucas, 1989; Krabill and Martin, 1989; Colombo, 1991). According to Merrell et al. (1989), a viable GPS photogrammetric control system should position the camera in space to a precision of 3 to 10 cm and the accuracy level should be repeatable.

To study the potential of kinematic GPS in an aircraft environment, a variety of airborne GPS positioning experiments have been conducted since the mid 1980's, see for instance Mader (1986), Mader et al. (1989), Krabill et al. (1987, 1989), Hein et al. (1988), Keel et al. (1989), Cannon et al. (1990 and 1992). Some of the reported results have demonstrated that the positional accuracy of the aircraft with respect to the ground monitor receiver is at the centimetre level (Mader, 1986; Mader at al., 1989) or decimeter level (Keel et al., 1989; Cannon et al., 1990, 1992) when using double difference carrier phase measurements. Most of these experiments were carried out over small test areas from several km to about 30 km. Under such circumstances, many errors tend to cancel, which leads to a high achievable accuracy. However, with monitor-remote separations

increasing to several tens of km, many errors such as ionospheric and orbital effects become the limiting factors in the error budget.

Based on experiments of a land vehicle moving at high speeds with a monitor-remote separation of 165 km, Henderson and Leach (1990) reported that a positioning accuracy better than 25 cm can be achieved. Colombo (1991) demonstrated, according to simulation results, that airborne differential GPS positioning is possible at the decimetre level over very long distances (monitor-remote separations of 1300 km) when properly accounting for errors. The achievable accuracy of airborne positioning with monitor-remote separations of 50 to 200 km using real data has not been demonstrated when taking all critical error sources into account.

The objective of this thesis is: 1) to investigate high accuracy airborne differential GPS positioning with carrier phase measurements using a multi-receiver configuration, 2) to demonstrate the achievable accuracy of differential GPS aircraft positioning over a large operational area (50 to 200 km), and 3) to identify and assess the critical errors for separations ranging from 50 to 200 km using airborne test data. The issues related to kinematic GPS algorithms, data processing, and accuracy evaluation methods are studied. Data from recent flight tests where four Trimble 4000 SSE receivers were used (two as ground monitors and two in the aircraft) is processed using a variety of strategies which are presented in the thesis. The investigations in this thesis are based on the use of double difference carrier phase measurements and resolved ambiguities fixed to the correct integer values.

1.2 THESIS OUTLINE

In Chapter 2, the fundamental GPS observables and carrier phase measurement models are summarized. Various critical errors, such as tropospheric, ionospheric, nominal orbital, Selective Availability (SA) and multipath errors are described with emphasis on their effects on the carrier phase measurement. Methods to eliminate or mitigate the effects are reviewed and discussed.

In Chapter 3, two frequently used kinematic GPS algorithms are analyzed with emphasis on their features and relationships. The mathematical relationship and the computational equivalence of these two algorithms are demonstrated. A sophisticated formula is derived for analytical estimation of orbital error effects and the dependency of positioning solutions from different receiver pairs in a triple receiver system is mathematically proven.

In Chapter 4, the error budget from the relevant GPS error sources that limit the achievable accuracy is given. Based on these errors, some solutions to the configuration of GPS receivers on the ground and aircraft, optimum monitor-remote separations, as well as operational procedures for high accuracy GPS positioning are given.

In Chapter 5, general data processing strategies are summarized and several methods for accuracy checking and analysis are presented. These

methods are suitable for airborne GPS positioning with a multi-receiver configuration.

In Chapter 6, results from an airborne GPS positioning test using a multi-receiver configuration are presented using the data processing strategies and accuracy checking methods presented in Chapter 5. In the test, four Trimble SSE receivers were used, two as ground monitors and two in the aircraft with monitor-remote separations of up to 200 km. Results are examined and discussed with respect to high accuracy airborne positioning as well as to the relevant theoretical analyses presented in Chapter 3. Effects of critical errors from the troposphere, ionosphere, orbit and multipath are investigated using the test data.

A summary of the research as well as the main conclusions and recommendations are presented in Chapter 7.

CHAPTER 2

ERROR SOURCES AND CORRECTIONS

For high accuracy airborne differential GPS positioning over a large area (monitor-remote separation of 50 to 200 km), residual errors from the atmosphere and orbit, and multipath effects are the main error sources which limit the potential positioning accuracy. In this chapter, fundamental GPS observables and carrier phase measurement models are summarized. Various critical errors, such as tropospheric, ionospheric, nominal orbital, Selective Availability (SA) and multipath errors, are described with emphasis on their effects on carrier phase measurements. Methods to eliminate or mitigate these effects are reviewed and discussed.

2.1 GPS OBSERVABLES AND ERRORS

GPS provides users with three fundamental observables, namely, the code pseudorange, carrier phase and Doppler frequency. They are available on two frequencies in P-code mode, i.e. L1 (1575.42 MHz, a wavelength of 19 cm) and L2 (1227.60 MHz, a wavelength of 24 cm), and only on L1 in C/A-code mode.

A code pseudorange measurement contains absolute positioning information, and is the spatial distance from the receiver to the satellite biased by the difference between the receiver and satellite clock errors and the atmospheric effect. The pseudorange measurements thus can be used for a stand-alone positioning. In differential mode with pseudorange measurements, several metres to submetre level positioning accuracy can be achieved depending on the code measurement noise (2 to 3 dm for P-code, 2 to 3 m for C/A-code) and monitor-remote separation.

The second fundamental measurement is the carrier phase, which is the phase difference between the receiver-generated reference carrier signal and the received Doppler-shifted carrier signal. Because of its low noise (several millimetres) and relative measurement information, the carrier phase measurement is used in high accuracy relative positioning applications.

The third measurement is the Doppler frequency, which is the Doppler shift of the received carrier signal. Hence, it provides information regarding the relative motion of a receiver with respect to a satellite and mainly contributes to the estimation of the receiver velocity.

For high accuracy kinematic positioning, the carrier phase measurement has to be used as the fundamental observable while the other two measurements can be treated as auxiliary observables. The nonlinearized carrier phase observation equation can be expressed as (Wells et al., 1986; Lachapelle, 1990):

$$\Phi = \rho + c(dt - dT) + \lambda N - d_{ion} + d_{trop} + d\rho + \varepsilon(\Phi) \qquad (2.1.1)$$

where Φ is the carrier phase observation (m)

ρ is the range from receiver to satellite (m)

c is the speed of light (m/s)

dt is the satellite clock error (s)

dT is the receiver clock error (s)

λ is the carrier wavelength (m/cycle)

N is the carrier phase integer ambiguity (cycle)

d_{ion} is the ionospheric delay (m)

d_{trop} is the tropospheric delay (m)

$d\rho = d\rho_n + d\rho_{SA}$

$d\rho_n$ is the nominal orbital error (m)

$d\rho_{SA}$ is the orbital error due to SA (m)

$\varepsilon(\Phi) = \varepsilon(\Phi_{rx}) + \varepsilon(\Phi_{mult})$

$\varepsilon(\Phi_{rx})$ is the receiver noise (m)

and $\varepsilon(\Phi_{mult})$ is the multipath error (m)

The corresponding observation equation for the code pseudorange has a similar form, and can be given by eliminating the ambiguity term and changing the sign

of the ionospheric delay term of equation (2.1.1) (see Wells et al., 1986 and Lachapelle, 1990). The observation equation for the Doppler frequency can be obtained by taking the derivative with respect to time on both sides of equation (2.1.1) and considering the ambiguity as constant, see Cannon (1991).

It is evident in equation (2.1.1) that the carrier phase measurement is affected by numerous errors. To take full advantage of the millimetre measurement noise, systematic errors such as clock errors, atmospheric and orbital errors have to be removed. One effective technique called double differencing is extensively used in precise positioning. The double difference measurement is formed by differencing two single difference measurements. One single difference measurement is generated by subtracting two measurements from two receivers (a monitor and a remote) to one satellite; the other by differencing two measurements from the same two receivers to another satellite. A double difference observation equation is given as:

$$\Delta\Phi = \Delta\rho + \lambda \Delta N - \Delta d_{ion} + \Delta d_{trop} + \Delta d\rho + \Delta\varepsilon(\Phi) \qquad (2.1.2)$$

where Δ is the double difference operator (between two receivers and two satellites).

As can be seen from equation (2.1.2), in double difference mode the receiver and satellite clock errors have been canceled, and the atmospheric and orbital errors, which are spatially correlated, have been reduced. It should be noted that the residual orbital error term, $\Delta d\rho$, can be further derived as an

explicit function of the satellite orbital errors. This will be further discussed in Section 3.2. The estimated position of the remote is implicit in $\Delta\rho$, and the ambiguity term, ΔN, is theoretically an integer value.

Generally, it is agreed that with a small monitor-remote separation (say less 20 km), the residual atmospheric and orbital errors are small so that the ambiguity term still can maintain its integer nature (i.e. it can be estimated to be an integer value). In this case, centimetre level accuracy can be achieved. When the separation increases to several tens of kilometres, baseline dependent errors, i.e. residual tropospheric, ionospheric and orbital errors, become the limiting factors in the error budget which lead to a degradation of the positioning accuracy.

2.2 TROPOSPHERIC ERROR AND CORRECTION

The tropospheric error or delay results from refraction of the GPS signal transmitted through the troposphere which extends from the earth's surface to about 40 km above the earth. The magnitude of the tropospheric error is dependent on the satellite elevation as well as the meteorological conditions. The effect of this error on the height component is highly correlated with the monitor-remote height difference (see Figure 6.4.1). The tropospheric refraction of the GPS signal (in fact any signal at a frequency below 30 GHz) is frequency independent (Leick, 1990), which makes it impossible to eliminate the

tropospheric error with dual frequency measurements. This has lead to the development of numerous models to estimate the tropospheric delay (Hopfield, 1969; Black, 1978; and Goad and Goodman, 1974)

Tropospheric delay can be expressed as the difference between signal paths through the troposphere and a vacuum. The difference can be further separated into two parts, a dry and a wet component (Seeber, 1993). The basic idea is to estimate the tropospheric delay by empirically expressing the dry and wet refractivities as functions of the height above the surface. The tropospheric delay in the zenith direction can be calculated through integrating the functions along the vertical (to 11 km above the earth's surface for the wet component and to 40 km above for the dry). The delay in an arbitrary direction can be obtained by applying a mapping function, which is an approximate cosecant function of the satellite elevation. This projects the tropospheric delay at the zenith to the line of sight (e.g. Hopfield Model, see Hopfield, 1969) The mapping function may alternatively be applied before integrating the functions (e.g. Modified Hopfield Model, see Goad and Goodman, 1974).

The total tropospheric delay in the zenith direction reaches up to 2.5 m, and increases to about 20 m at a 10 degree elevation. The contribution from the dry component accounts for about 90 % of the total tropospheric delay, and can be accurately modeled to within 2 - 5 % with using surface meteorological data, such as temperature, relative humidity and pressure. The wet component, however, contributes to only about 10 % of the total tropospheric delay, and can be modeled to 2 - 5 cm (Leick, 1990).

Another way to cancel or reduce the tropospheric error is through differencing, as mentioned in the previous section, since a high regional correlation of meteorological conditions should be expected over a monitor-remote separation of 50 km (Seeber, 1993).

For precise GPS positioning applications, especially for an application with a large monitor-remote separation, the cut off satellite elevation angle should be set to at least 15 degrees, and the tropospheric model should be applied. The meteorological data used in the model should be representative of the local atmospheric conditions. In addition, in airborne GPS positioning when the monitor-remote height difference may be large, the actual vertical temperature and pressure gradients should be taken into account (Tiemeyer et al., 1994).

2.3 IONOSPHERIC ERROR AND CORRECTION

The ionosphere is the region of the earth's atmosphere between approximately 70 and 1000 km above the earth. Unlike the troposphere, the ionosphere is a dispersive medium, which causes two different effects on signals transmitted through it, namely, the modulated signals on carrier are affected by the dispersion and the carrier signals by the refraction.

For GPS signals, ionospheric errors behave as a time delay on the code measurements and an advance on carrier phase measurements. As far as the first

order approximation is concerned, the magnitude of the ionospheric errors are the same for the code and the carrier but with an opposite sign (Seeber, 1993; Hofmann-Wellenhof et al., 1992).

The ionospheric error is determined by the total electron content (TEC) along the signal path and the frequency of the signal. It is directly proportional to the TEC and inversely proportional to the square of frequency. TEC is a complicated quantity dependent on numerous factors, such as sunspot activity, season, time of day, user position and the line of sight to the satellite. The ionospheric error reaches 15 m in the zenith direction and more than 150 m at elevations near the horizon under extreme conditions (Leick, 1990; Wells et al., 1986).

The fact that the ionospheric error depends on the frequency of the signal makes it possible to eliminate the error by using dual frequency measurements. The ionospheric correction to the L1 carrier phase can be expressed as

$$d_{ion}(t_i) = \frac{f_2^2}{f_1^2 - f_2^2} \left(\Phi_{L1}(t_i) - \Phi_{L2}(t_i) - N_1\lambda_1 + N_2\lambda_2 \right) \qquad (2.3.1)$$

where $d_{ion}(t_i)$ is the ionospheric correction to the L1 carrier phase at epoch t_i (m)

Φ_{L1}, f_1, N_1, λ_1 are the L1 carrier phase measurement (m), frequency (Hz), ambiguity (cycle),

and wavelength (m/cycle), respectively

and $\Phi_{L2}, f_2, N_2, \lambda_2$ are the L2 carrier phase measurement (m), frequency (Hz), ambiguity (cycle) and wavelength (m/cycle), respectively

Since the ambiguity terms are unknown in equation (2.3.1), the absolute correction, $d_{ion}(t_i)$, can not be practically determined. If no cycle slips occur or if they can be recovered, the ambiguity terms remain constant, so the relative ionospheric correction, d'_{ion}, can be formed as

$$d'_{ion}(t_i) = d_{ion}(t_i) - d_{ion}(t_0) \tag{2.3.2}$$

and applied to the L1 carrier phase measurement, i.e.:

$$\Phi'_{L1/L2}(t_i) = \Phi_{L1}(t_i) + d'_{ion}(t_i) \quad . \tag{2.3.3}$$

Using equations (2.3.1) and (2.3.2) in equation (2.3.3), the relatively ionospheric correction applied to L1 carrier phase measurement, $\Phi'_{L1/L2}(t_i)$, is of the form

$$\Phi'_{L1/L2}(t_i) = \frac{f_1^2}{f_1^2 - f_2^2}\Phi_{L1}(t_i) - \frac{f_2^2}{f_1^2 - f_2^2}(\Phi_{L2}(t_i) + \Phi_{L1}(t_0) - \Phi_{L2}(t_0)) \tag{2.3.4}$$

Applying the covariance law, the corresponding noise variance is given by

$$\sigma^2_{\Phi'_{L1/L2}} = \frac{f_1^4 + f_2^4}{(f_1^2 - f_2^2)^2}\sigma^2_{\Phi_{L1}} + \frac{2 f_2^4}{(f_1^2 - f_2^2)^2}\sigma^2_{\Phi_{L2}} \tag{2.3.5}$$

where $\sigma^2_{\Phi'_{L1/L2}}$ is the noise variance of the L1 carrier phase measurement with the relative ionospheric correction applied

$\sigma^2_{\Phi_{L1}}$ is the noise variance of the L1 carrier phase measurement

$\sigma^2_{\Phi_{L2}}$ is the noise variance of the L2 carrier phase measurement

With consideration of the following relation

$$\sigma_{\Phi_{L2}} = \frac{f_1}{f_2} \sigma_{\Phi_{L1}} , \tag{2.3.6}$$

the variance of the relatively ionospheric error free measurement is of the form

$$\sigma_{\Phi'_{L1/L2}} = \frac{f_1^2 + f_2^2}{f_1^2 - f_2^2} \sigma_{\Phi_{L1}} \tag{2.3.7}$$

or

$$\sigma_{\Phi'_{L1/L2}} = 4.09 \, \sigma_{\Phi_{L1}} \quad . \tag{2.3.8}$$

As can be seen, after applying the relative correction, the noise level increases by four times that of the L1 carrier phase. Consequently, the noise level of the relative ionospherically corrected measurement in double difference mode is eight times that of the L1, namely 1 to 2 cm (if an L1 noise of 1 to 3 mm assumed).

2.4 ORBITAL ERROR AND PRECISE ORBIT

GPS satellite orbit information, contained in GPS ephemerides, is essential to GPS applications. The ephemerides can be classified into two categories, predicted ephemerides (i.e., broadcast ephemerides), and post-processed or precise ephemerides. In this section, nominal orbital errors from the broadcast ephemerides as well as Selective Availability (SA) are reviewed. Issues relating to the precise orbit are discussed with emphasis on the implementation of precise ephemerides.

2.4.1 Broadcast Ephemeris Error and Selective Availability

The orbital error is the resultant of the nominal orbital error and the error due to SA. The nominal orbital error results from inaccuracies in the broadcast ephemerides, which are transmitted to users via the navigation message and provide information about satellite position, velocity and satellite system time.

The broadcast ephemerides are predicted orbits which are based on tracking data from five world wide stations which make up the control segment (Wells et al., 1986). Updated ephemeris data sets are broadcast every hour and are valid for only four hours, two hours before and two hours after the ephemeris reference time (Hofmann-Wellenhof et al., 1992). Obviously, these predicted ephemerides are not errorless. According to Remondi and Hofmann-

Wellenhof (1989), nominal orbital errors range from 5 to 10 m. Similar results obtained in the thesis research support these values, see Section 6.4.3.

In GPS two kinds of positioning services are available, the Standard Positioning Service (SPS) to civil users and the Precise Positioning Service (PPS) to authorized users. SPS users will have an absolute horizontal positioning accuracy of 100 m and vertical accuracy of 156 m with a probability of 95 % (PDOP ≤ 3).

SA is the intentional degradation of the GPS signal to limit SPS users from taking full advantage of the GPS system, and may be introduced in the Block II satellites (launched after the early of 1989). SA is a combination of two effects, namely the manipulation of the broadcast ephemeris data and also dithering the satellite clock. These two effects are also called orbital SA and clock SA, respectively.

Clock SA error behaves as a random oscillation with a period of several minutes. Pseudorange errors due to clock SA vary from 40 to 70 m with periods on the order of 5 to 10 minutes (e.g. Braasch et al., 1993). In double difference mode, satellite clock errors including clock SA can be largely reduced or canceled. From this research, it has been found that in double difference kinematic mode with monitor-remote separations of up to 200 km, the maximum coordinate error due to residual satellite clock errors is no more than 1 mm. Therefore, satellite clock errors can be neglected in this research and no further discussion will be given in the sequel.

In contrast, the error due to orbital SA behaves as a long term, non-periodic error trend, and leads to a degradation of the broadcast ephemerides in the 10 to 40 m range (Seeber, 1993). Figure 2.4.1 gives a comparison between satellite orbital errors from Block I (launched before the end of 1985) and Block II. The figure shows the results from this research and is generated by the test data collected on April 27, 1993 when SA was turned on. Orbital errors in the figure are estimated by differencing the broadcast and precise orbits. As seen in the figure, the Block I satellite orbital error in position is within 5 m which is due to nominal orbital error, while the error from the Block II varies from 20 to 40 m which is obviously due to the orbit SA.

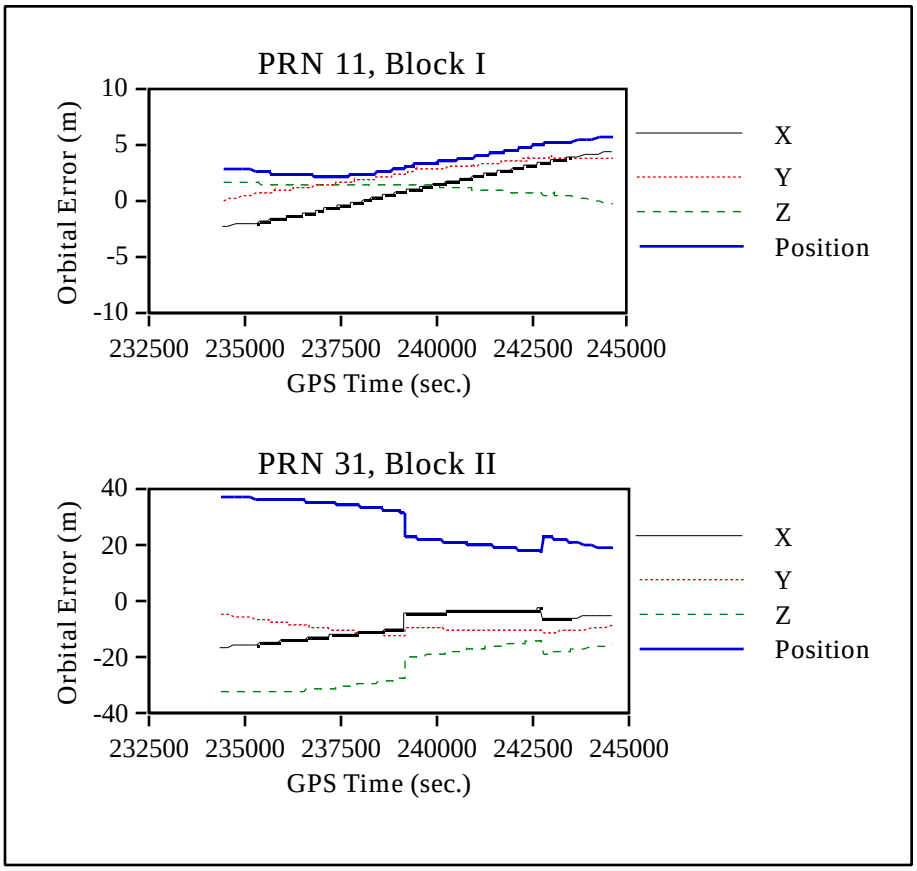

Figure 2.4.1

Comparison Between Orbital Errors from Block I and Block II

When differencing, errors due to orbital SA can be reduced to some extent depending on the monitor-remote separation. Tolman et al. (1990) observed an orbital SA effect of 1 to 2 ppm in medium baselines (250 km), and this translates into an absolute orbital error of 20 to 40 m when not accounting for the effect of satellite geometry. During the test period, an orbital error over one hundred metres due to SA was also detected by Tolman et al. (1990). After the SA implementation in April 1990, the orbital SA was found to be much smaller than

it was during the test period, even approaching the same level as the nominal broadcast error (Tolman et al., 1990 and Braasch et al., 1993). In this thesis investigation, it is also noted that only one of the five Block II satellites tracked in the observation span was significantly affected by orbital SA. The rest are either within or close to the marginal limit of the nominal orbital error. Further discussions of the orbital error effects on positioning will be given in Sections 3.2 and 6.4.3.

2.4.2 Precise Ephemerides and Applications

For some GPS applications with high accuracy requirements, such as geodynamics application and precise relative positioning over hundreds of kilometres, the accuracy of the broadcast ephemerides is not sufficient even when SA is not implemented. Hence, an ephemerides with a metre level accuracy is required. One effective solution is to use post-processed ephemerides, which are usually generated with one week observations from a globally distributed tracking network.

Besides the U.S. Defense Mapping Agency (DMA), several other tracking networks or organizations compute precise ephemerides, e.g. the Cooperative International GPS Network (CIGNET) operated by the U. S. National Geodetic Survey (NGS), International GPS Geodynamics Service (IGS) organized by the International Association of Geodesy (IAG), and Canadian Active Control

System (Seeber, 1993).

Usually, precise ephemerides are available within a few days to a few weeks depending on the organization. Precise orbits of all GPS satellites are expressed as satellite positions and velocities (or positions only) at an even time interval (900, 1350, 1800 or 2400 seconds). Position and velocity values between two given times (in GPS time) can be interpolated with 9th, 11th or 17th order Lagrangian interpolators depending on the time interval used (Remondi, 1989). With an even time interval, the n-th order Lagrangian interpolator can be expressed as

$$x^s(t) = \frac{\Pi_n(t)}{(\Delta t)^n} \sum_{k=1}^{n} \frac{(-1)^{(n-k)}}{(n-k)!\ k!} \frac{x^s(t_k)}{(t - t_k)} \qquad (2.4.1)$$

where $\Pi_n(t) = (t - t_1)(t - t_2) \quad (t - t_{n-1})(t - t_n)$

$t_k = t_1 + k\Delta t$

	t	is the interpolated epoch
	t_k	is the given time
	$x^s(t)$	is the interpolated value at epoch t
	$x^s(t_k)$	is the known value at t_k
	Δt	is the time interval
and	n	is the order of the interpolator

In practical computations, the ASCII file is first converted into binary, creating a direct access data file, then applying equation (2.4.1) and keeping the following relationship:

$$t_{\frac{n}{2}} < t < t_{\frac{n}{2}+1} \qquad (2.4.2)$$

A 9th order interpolator with an interval of 1800 seconds can provide satellite coordinates with an interpolation accuracy of less than 30 cm, or relatively consistent within 0.01 to 0.02 ppm geodetic survey accuracies (Remondi, 1989). The interpolation accuracy depends on the time interval and the order of the interpolator. A smaller interval and a higher order interpolator will give more accurate position or velocity values. It was suggested by Remondi (1989) that one may increase the order of the interpolator rather than decrease the time interval when more accurate results are required.

It is difficult to determine the absolute error in precise orbits. In fact, this is not so important for double differencing, since the precise orbits of all satellites are homogeneous and overlapping differences can be controlled to the centimetre level if the order of the interpolator and the time interval are chosen properly. Even if some uncertainty exists, it is reasonable to expect that the uncertainty effects on all satellite precise orbits are the same. This expectation is correct at least during a limited observation span. The common effects, however, can be canceled out in double differencing (see equation 3.2.15).

2.5 MULTIPATH

The multipath effect causes a signal to arrive via multiple paths and thus to have a phase offset with respect to the direct signal. The resultant signal is a superimposition of the direct and indirect signals due to reflection and diffraction. The signal reflection is caused by surfaces of various objects surrounding the antenna. The signal diffraction, introduced by the edges of the antenna holder such as a circular ground plane, distorts the radiation pattern of the antenna and could lead the reflected signal to be stronger than the direct signal (Braasch & van Graas, 1991).

Multipath errors are frequency dependent and more severe for signals from low elevation satellites than in those from high elevation satellites. As well, multipath effects depend on a receiver's location, such that nearby objects may cause signal reflection, and receiver's motion such that stationary receivers are in general more susceptible to multipath than moving receivers. An amplitude of 20 m errors due to multipath effects on C/A-code measurements were observed in a high multipath environment by Lachapelle et al. (1990). For the carrier phase, the maximum multipath effect is one quarter of the corresponding carrier wavelength (Seeber, 1993). This is only true under the assumption that the reflected signal is weaker than the direct, otherwise, the carrier phase multipath effect could be much larger (Braasch & van Graas, 1991). In this thesis, a height error of 10 cm due to multipath was detected in static mode, see Figure 6.4.15.

In static mode, carrier phase multipath effects can be observed by

examining the residuals which have a sinusoidal behavior with an amplitude of several centimetres and a period of several minutes. The effects on the estimated positions can be minimized by averaging the results over a longer observation span as well as by selecting sites in open areas and using specially designed antennas (e.g. with groundplanes or choke rings).

In an airborne GPS environment, multipath error signatures are generally randomized due to the aircraft motion and flexing. In this randomization process, signal diffraction was found to play a significant role by Braasch & van Graas (1991). It was confirmed with this investigation that the carrier phase multipath error on the aircraft behaves as random noise while in flight (see, Figure 6.4.16), and it was found that a part of the multipath effect could be absorbed by estimated position solutions (1 to 2 cm, see Figure 6.5.5). To mitigate the carrier phase multipath effect in an aircraft environment, one way suggested by Braasch and van Graas (1991) is to use a low grade inertial measurement unit with GPS receivers on the aircraft simultaneously.

CHAPTER 3

ALGORITHMS AND ANALYSIS

Theoretical analysis of kinematic GPS algorithms and additional issues related to the data processing are presented in this chapter. These analyses provide a better understanding of the algorithms' behavior and capabilities, which is beneficial for selecting an algorithm for implementation. Moreover, they are critical for an effective assessment of the accuracy of the results.

The first section reviews two frequently used algorithms, the state space Kalman filter and least squares estimation, and analyzes their features as well as their relationship. In the second section, a complete formula is derived to estimate and analyze the orbital error effect on positions. The third section mathematically reveals the relationship between positioning solutions from different receiver pairs in a triple receiver system. The correctness of the relevant theoretical analysis presented in this chapter will be subsequently confirmed with data collected from flight tests (Chapter 6).

3.1 KINEMATIC GPS ALGORITHMS

Kalman filtering and least squares are two frequently used kinematic GPS algorithms (e.g. Schwarz et al., 1989; Cannon, 1987, 1991; Brown and Hwang, 1992; Georgiadou and Kleusberg, 1991). Each algorithm has its individual features, and under certain circumstances one algorithm is equivalent to the other one in terms of computational results. In kinematic GPS data processing, it is important to understand the features of the algorithms and their relationships.

For the sake of discussion, the Kalman filter equations are summarized as follows (Gelb, 1974):

If the system model and measurement model are of the form

$$\boxed{\mathbf{x}_k = \Phi_{k-1}\,\mathbf{x}_{k-1} + \mathbf{w}_{k-1}}\,, \tag{3.1.1}$$

$$\mathbf{l}_k = \mathbf{A}_{k-1}\,\mathbf{x}_{k-1} + \varepsilon_{k-1} \tag{3.1.2}$$

the prediction equations are of the form

$$\hat{\mathbf{x}}_k(-) = \Phi_{k-1}\,\hat{\mathbf{x}}_{k-1}(+) \tag{3.1.3}$$

$$\mathbf{C}^x_k(-) = \Phi_{k-1}\,\mathbf{C}^x_{k-1}(+)\,\Phi^T_{k-1} + \mathbf{C}^w_{k-1} \tag{3.1.4}$$

and the update equations are given by

$$\hat{\mathbf{x}}_k(+) = \hat{\mathbf{x}}_k(-) + \mathbf{K}_k\,\{\,\mathbf{l}_k - \mathbf{A}_k\hat{\mathbf{x}}_k(-)\,\} \tag{3.1.5}$$

$$\mathbf{C}^x_k(+) = \{\,\mathbf{I} - \mathbf{K}_k\,\mathbf{A}_k\,\}\,\mathbf{C}^x_k(-) \tag{3.1.6}$$

$$\mathbf{K}_k = \mathbf{C}^x_k(-)\,\mathbf{A}^T_k\,\{\,\mathbf{A}_k\mathbf{C}^x_k(-)\,\mathbf{A}^T_k + \mathbf{C}^{-1}_l\,\}^{-1} \tag{3.1.7}$$

where

$\mathbf{x}$	is the state vector
Φ	is the transition matrix
$\mathbf{w}$	is the system process noise vector
$\mathbf{l}$	is the observation vector
$\mathbf{A}$	is the design matrix
$\mathbf{e}$	is the measurement noise vector
k	is the epoch number
$\mathbf{C}^x$	is the covariance matrix of $\mathbf{x}$
$\mathbf{C}^w$	is the covariance matrix of $\mathbf{w}$
$\mathbf{K}$	is the Kalman gain matrix
$\mathbf{C}_l$	is the covariance of $\mathbf{l}$, which is the same for each epoch

and notations, (-), (+) and ^ represent predicted, updated and estimated quantities, respectively.

The choice of the state space model for kinematic GPS leads to different definitions of the transition matrix, Φ (e.g. Schwarz et al., 1989; Brown and Hwang, 1992), and the covariance of the system process noise, $\mathbf{C}^w$, which can be derived from Φ and the spectral density matrix, $\mathbf{Q}$, as

$$\mathbf{C}^w = \int_0^{\Delta t} \Phi(\tau)\, \mathbf{Q}(\tau)\, \Phi^T(\tau)\, d\tau . \qquad (3.1.8)$$

The state space model depends on the system dynamics, state vector

(measurements used), and the assumption on the process behavior of the system (Gelb, 1974; Schwarz et al., 1989; Brown and Hwang, 1992). When the data rate is low, the state space model plays an important role in improving the interpolation accuracy. Schwarz et al. (1989) have demonstrated that with a data rate of three seconds, positioning results improve when using a constant velocity model and velocity results improved when using a constant acceleration model. Since this section is restricted to a discussion of the algorithms, no further discussion of the state space model is given.

As can be seen from the equations summarized above, the Kalman filter can be implemented with different kinematic GPS models as well as different measurements. In addition, the process noise is fully utilized in the filter by means of the spectral density matrix, **Q**, which allows the system to adjust the contribution to the estimates from the observables at the measurement epoch versus a contribution before the epoch. It will be demonstrated later in this section that the spectral density matrix is a key factor in the relationship between Kalman filtering and least squares.

Generally, the Kalman filter is employed in kinematic GPS applications where the remote receiver is installed on a moving platform, while the reference receiver is set up on the ground in stationary mode. However, in the case where both the remote and reference receivers are installed on the platform, a Kalman filter cannot be employed as it is used in the general case. This is because there is no dynamic information (with respect to the monitor) that can be exploited. In practice, this problem can be solved by changing the value of the elements in the

spectral density matrix, which will be discussed later.

It is well known that the least squares algorithm for kinematic GPS does not use dynamic information at all (Georgiadou and Kleusberg, 1991). This means that no assumption is made on the remote motion and no system process noise is involved in the implementation of this algorithm. In the sequel, the approach where *a priori* information about unknown parameters is used, is called the sequential (least squares) approach. When only observables at the measurement epoch are used, it is called the least squares approach. In the literature, sometimes both are referred to as least squares.

If the measurement model is as equation (3.1.2), the expressions of the estimate vector and its covariance matrix in the sequential least squares approach are of the form (Krakiwsky, 1990)

$$\hat{\mathbf{x}}_k(-) = \hat{\mathbf{x}}_{k-1}(+) + \Delta x \tag{3.1.9}$$

$$\mathbf{C}_k^x(-) = \mathbf{C}_{k-1}^x(+) + \mathbf{C}^{\Delta x} \tag{3.1.10}$$

$$\hat{\mathbf{x}}_k = \hat{\mathbf{x}}_k(-) + \{\mathbf{A}_k^T\mathbf{C}_l^{-1}\mathbf{A}_k + [\mathbf{C}_k^x(-)]^{-1}\}^{-1}\mathbf{A}_k^T\mathbf{C}_l^{-1}\{\mathbf{l}_k - \mathbf{A}_k\hat{\mathbf{x}}_k(-)\} \tag{3.1.11}$$

$$\mathbf{C}_k^x = \{\mathbf{A}_k^T\mathbf{C}_l^{-1}\mathbf{A}_k + [\mathbf{C}_k^x(-)]^{-1}\}^{-1}, \tag{3.1.12}$$

where Δx is the increment vector over two successive epochs

$\mathbf{C}^{\Delta x}$ is the covariance of Δx

and the notation (-) denotes an estimate based on data collected before epoch k. The corresponding expressions in the least squares approach are of the form

$$\hat{\mathbf{x}}_k = \{ \mathbf{A}_k^T \mathbf{C}_l^{-1} \mathbf{A}_k \}^{-1} \mathbf{A}_k^T \mathbf{C}_l^{-1} \mathbf{l}_k \quad (3.1.13)$$

$$\mathbf{C}_k^x = \{ \mathbf{A}_k^T \mathbf{C}_l^{-1} \mathbf{A}_k \}^{-1} \quad (3.1.14)$$

In the least squares approach, the discrete position of the remote is determined by only using observables at one epoch, without any requirement of the dynamic assumption or the process noise information. Thus, the positioning solutions in successive epochs are independent. For the purpose of positioning, with a high data rate this approach can be effectively applied to the case when the reference receiver is used either in static or in kinematic mode. From the research in this thesis, it has been found that with a 2 Hz or even 1 Hz data rate, the positions of an aircraft (the aircraft flew at a speed of 80 m per second on a nearly straight flight line) from the Kalman filter algorithm (with a constant velocity model) are identical to those from the least squares approach. This fact indicates two points. The first is that with a high data rate the positioning results tend to be independent with respect to the selection of the kinematic GPS model, and the second is that the correlation between the positioning solutions in successive epochs is so weak that it can be neglected. The second also has been confirmed by a comparison between the positioning results from forward and reverse time processing (Section 6.5.2).

In fact, the Kalman filter algorithm can be mathematically transformed to either the sequential approach or the least squares approach, so this algorithm can provide estimation results which are equivalent to those obtained by the least squares no matter what data rate is used. The mathematical proofs are given in the following.

Using the matrix identity lemmas (Krakiwsky, 1990), equations (3.1.6) and (3.1.7) can be rewritten as

$$\mathbf{C}_k^x(+) = \{[\mathbf{C}_k^x(-)]^{-1} + \mathbf{A}_k^T\mathbf{C}_1^{-1}\mathbf{A}_k\}^{-1} \tag{3.1.15}$$

$$\mathbf{K}_k = \mathbf{C}_k^x(+)\mathbf{A}_k^T\mathbf{C}_1^{-1} \tag{3.1.16}$$

In equation (3.1.4), by letting the transition matrix Φ equal to an identity matrix and redefining $\mathbf{C}^w$ as $\mathbf{C}^{\Delta x}$ in equation (3.1.10), the covariance matrix, i.e., equation (3.1.15), is transformed to that in the sequential approach. Substituting equation (3.1.15) into (3.1.16), and equation (3.1.16) into (3.1.5), the resulting equation is the estimation equation for the sequential approach.

To transform the Kalman filter to the least squares approach, letting the spectral density matrix, **Q**, approach infinity, which leads $[\mathbf{C}_k^x(-)]^{-1}$ in equation (3.1.15) to approach zero considering equations (3.1.8) and (3.1.4), equation (3.1.15) thus becomes

$$\mathbf{C}_k^x(+) = \{\mathbf{A}_k^T\mathbf{C}_1^{-1}\mathbf{A}_k\}^{-1} \tag{3.1.17}$$

Equation (3.1.17) is the transformed expression, i.e., the covariance matrix in the least squares approach. By using equations (3.1.17) and (3.1.16) in equation (3.1.5), the transformed estimation equation is obtained. In the above process, the transition matrix is not changed at all. This feature offers a great advantage in using the Kalman filter algorithm to realize the functions of the least squares approach, since what is needed is to set a large value in the diagonal elements of **Q.**

In summary, least squares has a more concise form of the equations compared with that in the Kalman filter, so it can be exploited in formula derivation to provide a mathematical proof or analysis regarding the positioning results. When the data rate is high, the same results can be achieved by using least squares as those from the state space Kalman filter algorithm. While the Kalman filter has a general form of the equations which are suitable for implementation of different kinematic GPS models and measurements, it also provides flexibility to meet the needs of a practical application in different dynamic environments. In addition, by changing the spectral density matrix, this algorithm can function as the least squares and provide the estimated results which are identical to those from the least squares. But this does not hold the other way round in some cases, e.g. with a low data rate, in a high dynamic environment or less than four satellites.

3.2 ANALYTICAL ESTIMATION OF ORBITAL ERROR EFFECT ON ESTIMATED POSITIONS

The orbital error effect on positions can be estimated by using actual data, i.e. differencing the results using the precise orbit from those using the broadcast ephemerides. The result is a comprehensive effect which comes from a variety of factors, and is often limited by the data sample which is used and the observation conditions. This estimation process using actual data is important for

quantifying the orbital error effect on positioning but has less universality from an error analysis point of view. For error analysis, analytical estimation is more effective. The following equation is a rule of thumb for the estimation of the orbital error effect on the baseline determination (Wells et al., 1986).

$$\frac{db}{b} = \frac{d\rho}{\rho} \tag{3.2.1}$$

where $d\rho$ is the orbital error, db baseline error caused by $d\rho$, b the baseline length and ρ the range. This estimation is based on the effect of one satellite, so it is a simplified estimation. Furthermore, from the research in this thesis, it has been found that in kinematic double difference GPS positioning, the effect of orbital errors on the estimated positions is more dependent on the satellite geometry than the monitor-remote separation or even the magnitude of the orbital errors. This can not be explained with equation (3.2.1). So it is expected that a theoretical basis can be found to provide an explanation. All the above leads to a need for sophisticated analytical estimation of the orbital error effect on estimated positions.

In the following, a complete formula is derived which provides a better understanding of how the orbital errors affect the estimated positions in the kinematic double difference positioning. The derivation is based on the least squares approach. In the formulas in this thesis, the superscript denotes satellite, the subscript denotes receiver, and the variable in bold denotes a vector or matrix.

Disregarding all error terms which can be canceled or reduced in double differencing and letting the noise term be contained in observables, the carrier phase observation equation from a remote receiver can be expressed as

$$\Phi_r^i = \mathbf{a}_r^i \mathbf{x}_r + N_r^i + \rho_r^i + \mathbf{a}_r^i \delta\mathbf{x}^i \qquad (3.2.2)$$

where Φ_r^i is carrier phase measurement from the remote receiver, r, to the satellite, i

$\mathbf{x}_r$ is the estimated position vector of the remote, r, and $\mathbf{x}_r = [\, x_r, y_r, z_r \,]^T$

$\delta\mathbf{x}^i$ is the position error vector of the satellite, i, and $\delta\mathbf{x}^i = [\, \delta x^i, \delta y^i, \delta z^i \,]^T$

N_r^i is the ambiguity of Φ_r^i

ρ_r^i is the range from the remote, r, to the satellite, i, and $\rho_r^i = [\, (X_r - X^i)^2 + (Y_r - Y^i)^2 + (Z_r - Z^i)^2 \,]^{\frac{1}{2}}$ where X_r, Y_r, Z_r are the coordinate of the remote, r , and X^i, Y^i, Z^i are the coordinate of the satellite, i.

$\mathbf{a}_r^i$ is the coefficient vector, and $\mathbf{a}_r^i = \left[\frac{X_r - X^i}{\rho_r^i}, \frac{Y_r - Y^i}{\rho_r^i}, \frac{Z_r - Z^i}{\rho_r^i} \right]$.

The corresponding equation for a monitor receiver is

$$\Phi_m^i = N_m^i + \rho_m^i + \mathbf{a}_m^i \, \delta\mathbf{x}^i \qquad (3.2.3)$$

where m represents the monitor receiver, and the double difference equation is thus of the form

$$\Phi_{rm}^{ik} = (\mathbf{a}_r^i - \mathbf{a}_r^k)\, \mathbf{x}_r + N_{rm}^{ik} + \rho_{rm}^{ik} + \mathbf{dx}^{ik} \qquad (3.2.4)$$

$$i = 1, \ldots, k\text{-}1, k\text{+}1, \ldots, n$$

where k and n represent the base satellite and the number of the satellites tracked, respectively, and

$$\Phi_{rm}^{ik} = \Phi_r^i - \Phi_r^k + \Phi_m^i - \Phi_m^k \qquad (3.2.5)$$

$$N_{rm}^{ik} = N_r^i - N_r^k + N_m^i - N_m^k \qquad (3.2.6)$$

$$\rho_{rm}^{ik} = \rho_r^i - \rho_r^k + \rho_m^i - \rho_m^k \qquad (3.2.7)$$

and
$$\mathbf{dx}^{ik} = (\mathbf{a}_r^i - \mathbf{a}_m^i)\, \delta\mathbf{x}^i - (\mathbf{a}_r^k - \mathbf{a}_m^k)\, \delta\mathbf{x}^k \quad . \qquad (3.2.8)$$

If the correct ambiguities are resolved and fixed, the effect of orbital errors on the estimated position at each epoch is derived as

$$\delta\mathbf{x}_r = \{ \mathbf{A}_r^T \mathbf{C}_l^{-1} \mathbf{A}_r \}^{-1} \mathbf{A}_r^T \mathbf{C}_l^{-1} \begin{bmatrix} \mathbf{dx}^{1k} \\ \vdots \\ \mathbf{dx}^{k\text{-}1k} \\ \mathbf{dx}^{k\text{+}1k} \\ \vdots \\ \mathbf{dx}^{nk} \end{bmatrix} \qquad (3.2.9)$$

where $\delta\mathbf{x}_r$ is the position error vector of the remote, and $\delta\mathbf{x}_r = [\,\delta x_r, \delta y_r, \delta z_r\,]^T$, where $\delta x_r, \delta y_r, \delta z_r$ are the coordinate errors caused by satellite orbital errors

and $$\mathbf{A}_r = [(\mathbf{a}_r^1 - \mathbf{a}_r^k)^T, \ldots, (\mathbf{a}_r^{k-1} - \mathbf{a}_r^k)^T, (\mathbf{a}_r^{k+1} - \mathbf{a}_r^k)^T, \ldots, (\mathbf{a}_r^n - \mathbf{a}_r^k)^T]^T \quad (3.2.10)$$

Equation (3.2.9) is the complete formula which gives the analytical relationship between the orbital error effect on the estimated position and the satellite orbital errors. If the following approximation is assumed:

$$\rho = \rho_r^i = \rho_m^i, \qquad i = 1, \ldots, n, \quad (3.2.11)$$

equation (3.2.8) can be rewritten as

$$\mathbf{dx}^{ik} = \frac{\mathbf{a}_{rm}}{\rho}\,\delta\mathbf{x}^{ik} \quad (3.2.12)$$

where $$\mathbf{a}_{rm} = [\,x_r - x_m, y_r - y_m, z_r - z_m\,] \quad (3.2.13)$$

$$\delta\mathbf{x}^{ik} = \delta\mathbf{x}^i - \delta\mathbf{x}^k \quad . \quad (3.2.14)$$

Using equation (3.2.12) in equation (3.2.9), the approximated formula is thus of the form

$$\delta \mathbf{x}_r = \{ \mathbf{A}_r^T \mathbf{C}_l^{-1} \mathbf{A}_r \}^{-1} \mathbf{A}_r^T \mathbf{C}_l^{-1} \begin{bmatrix} \underline{\mathbf{a}_{rm}}\rho\, \delta \mathbf{x}^{1k} \\ \vdots \\ \underline{\mathbf{a}_{rm}}\rho\, \delta \mathbf{x}^{k-1k} \\ \underline{\mathbf{a}_{rm}}\rho\, \delta \mathbf{x}^{k+1k} \\ \vdots \\ \underline{\mathbf{a}_{rm}}\rho\, \delta \mathbf{x}^{nk} \end{bmatrix} \qquad (3.2.15)$$

As can be seen from the equation above, through an approximation of equation (3.2.11), equation (3.2.9) is presented in a more significant form with regard to error analysis. On the right hand side of equation (3.2.15), the first factor, $\{ \mathbf{A}_r^T \mathbf{C}_l^{-1} \mathbf{A}_r \}^{-1}$, is the covariance matrix of the estimated position; $\mathbf{a}_{rm}$ is the baseline vector formed by the monitor and the remote receiver (equation (3.2.13)); and $\delta \mathbf{x}^{ik}$ is a difference vector between the position error vector of one satellite and that of the base satellite (equation (3.2.14)). By comparison with equation (3.2.15), equation (3.2.1) obviously can be a special case reduced from equation (3.2.15).

The following four points which are implied in equation (3.2.15) should be pointed out:

1) As an indicator of the satellite geometry, the covariance (or standard deviation) of the estimated position plays a critical role in dictating the orbital error effect on positions. Through the covariance, poor satellite geometry can be an amplifier of orbital errors ,

2) With other conditions being equal, the orbital error effect is directly proportional to the monitor-remote separation,

3) Elements of the column vector on the right hand side of the equation are inner products. This indicates that the orbital error effect on the position also depends on the direction of the vector formed by the monitor and the remote receiver as well as on that of the satellite position error vectors,

4) In double difference mode, it is the relative orbital error (the position error vector of one satellite with respect to that of the base satellite) that effects the estimated position, rather than the absolute one.

3.3 THEORETICAL ANALYSIS ON SOLUTIONS FROM A TRIPLE RECEIVER SYSTEM

A triple receiver system, as the term suggests, is composed of three separate receivers. It is frequently employed in an application of double difference GPS positioning either in static or kinematic mode. In the case of one remote receiver and two monitor receivers, it often happens that the positioning accuracy of the remote is assessed through the difference in solutions determined from two monitors. The magnitude of the difference is usually taken as an indicator of the remote positioning accuracy. This practice, as a means of accuracy assessment, is not only accepted but taken for granted as well. In fact, this assessment is ineffective in double difference GPS positioning, since the

measurement information from the remote is eliminated when differencing one monitor solution from the other. This concept is analogous to systematic error terms in GPS observables being canceled or reduced in double difference mode. Also, this concept can be mathematically verified. The following proof is still based on the least squares approach, and assumed in kinematic mode.

One remote and two monitors form three different receiver pairs, i.e., two remote-monitor pairs and one monitor-monitor pair. At each epoch, the observable equation sets from the two remote-monitor pairs can be expressed as

$$\mathbf{l}_{rj} = \mathbf{A}_r \mathbf{x}_{rj} + \mathbf{n}_{rj}, \qquad j = 1, 2 \tag{3.3.1}$$

where the first subscript represents the estimated receiver, the second represents the reference receiver; r, 1, and 2 represent the remote and two monitors, respectively, $\mathbf{n}_{rj}$ is the ambiguity vector, $\mathbf{l}_{rj}$ is the misclosure vector and

$$\mathbf{n}_{rj} = [\, N_{rj}^{1k}, \ldots, N_{rj}^{k-1k}, N_{rj}^{k+1k}, \ldots, N_{rj}^{nk} \,]^T \tag{3.3.2}$$

$$\mathbf{l}_{rj} = [\, \Phi_{rj}^{1k} - \rho_{rj}^{1k}, \ldots, \Phi_{rj}^{k-1k} - \rho_{rj}^{k-1k}, \Phi_{rj}^{k+1k} - \rho_{rj}^{k+1k}, \ldots, \Phi_{rj}^{nk} - \rho_{rj}^{nk} \,]^T \tag{3.3.3}$$

and the definitions for $\mathbf{x}$, Φ, N, r, and $\mathbf{A}$, see equations (3.2.2), (3.2.5), (3.2.6), (3.2.7) and (3.2.10).

Assuming that the ambiguities are resolved and fixed, the estimated remote position at each epoch with respect to the two monitors is thus of the form

$$\mathbf{x}_{rj} = \{ \mathbf{A}_r^T \mathbf{C}_l^{-1} \mathbf{A}_r \}^{-1} \mathbf{A}_r^T \mathbf{C}_l^{-1} (\mathbf{l}_{rj} - \mathbf{n}_{rj}), \qquad j = 1, 2 \tag{3.3.4}$$

Data from the monitor-monitor pair, however, also can be processed in kinematic mode. If the first monitor is still used as the reference station, the corresponding observable equation and the estimated position of the second monitor are of the form

$$\mathbf{l}_{21} = \mathbf{A}_2 \mathbf{x}_{21} + \mathbf{n}_{21} \tag{3.3.5}$$

$$\mathbf{x}_{21} = \{ \mathbf{A}_2^T \mathbf{C}_l^{-1} \mathbf{A}_2 \}^{-1} \mathbf{A}_2^T \mathbf{C}_l^{-1} (\mathbf{l}_{21} - \mathbf{n}_{21}) \tag{3.3.6}$$

With the realization of equations (3.2.5) to (3.2.7), the following two relations hold:

$$\mathbf{l}_{21} = \mathbf{l}_{r1} - \mathbf{l}_{r2} , \tag{3.3.7}$$

$$\mathbf{n}_{21} = \mathbf{n}_{r1} - \mathbf{n}_{r2} \tag{3.3.8}$$

Using equations (3.3.4), (3.3.7) and (3.3.8), the difference in solutions determined from two monitor stations, $\mathbf{dx}_r$, can be derived as following

$$\mathbf{dx}_r = \{ \mathbf{A}_r^T \mathbf{C}_l^{-1} \mathbf{A}_r \}^{-1} \mathbf{A}_r^T \mathbf{C}_l^{-1} (\mathbf{l}_{21} - \mathbf{n}_{21}) \tag{3.3.9}$$

As seen from the above equation, the measurement information of the remote has been already eliminated, and what remains is information regarding two monitors and the design matrix of the remote. By comparison with equation

(3.3.6), it is clear that $\mathbf{dx}_r$ and $\mathbf{x}_{21}$ are approximately linearly dependent. Thus, as a result of differencing solutions from two monitors, $\mathbf{dx}_r$ obviously cannot act as a measure of the positioning accuracy of the remote. As a matter of fact, when considering equations (3.3.7) and (3.3.8), the estimated positions from the three receiver pairs are dependent, see equations (3.3.4) and (3.3.6). This means one solution can be approximately expressed by a linear combination of the other two.

As a side product from the derivation, an interesting feature regarding the misclosure in a triple receiver system is discovered. When differencing equation (3.3.9) from equation (3.3.6), the misclosure formed by the three receiver pairs, $\Delta\mathbf{x}_{r\,12}$, is generated, i.e.,

$$\Delta\mathbf{x}_{r\,12} = \left(\{ \mathbf{A}_2^T \mathbf{C}_l^{-1} \mathbf{A}_2 \}^{-1} \mathbf{A}_2^T - \{ \mathbf{A}_r^T \mathbf{C}_l^{-1} \mathbf{A}_r \}^{-1} \mathbf{A}_r^T \right) \mathbf{C}_l^{-1} \left(\mathbf{l}_{21} - \mathbf{n}_{21} \right) \qquad (3.3.10)$$

It is generally agreed that if successful data processing is achieved using a triple receiver system, the misclosure should always be close to zero, while equation (3.3.10) demonstrates that this is not necessarily to be true in some cases. When the separation between two estimated receivers (herein i.e., the remote and the second monitor) is large (e.g. over 50 km), which leads to a large difference in the corresponding design matrices, the misclosure may not be close to zero, even though successful data processing is achieved in all three receiver pairs (e.g. Figure 6.5.8). In practice, with small separations (less than 30 km), the difference in the design matrices may be neglected as far as the misclosure

computation is concerned. In other words, a zero misclosure may be expected in this case.

Although the proof and demonstration above are based on the assumption of one remote and two monitors, the concept and relevant features can be, without loss of generality, applied to any kind of a triple receiver system, no matter which of the three receivers is used in kinematic or static mode.

CHAPTER 4

CONFIGURATIONS AND OPERATIONAL STRATEGIES

For airborne photogrammetry and remote sensing without the use of ground control, aircraft positions at the 10 cm level are required, for instance for a viable GPS photogrammetric control system used in precise mapping (Merrell et al., 1989) or for a large scale airborne photogrammetry, e.g. 1:3000 to 1:6000 (see Schwarz et al., 1994). To ensure that this accuracy level can be achieved, issues relating to the use of a multi-receiver GPS configuration have to be investigated. These include the configuration of GPS receivers on the ground and aircraft, optimum separations between the monitor receivers and the aircraft, and operational procedures. Solutions of the problem are affected by many factors, such as available equipment, size of the test area and distance between the airport and the operational area.

In this chapter, an error budget comprising the relevant GPS error sources which limit the achievable accuracy is given. Some possible solutions to minimize these errors for high accuracy GPS positioning are developed.

4.1 ERROR BUDGET AND LIMITATIONS

When using the differential GPS technique as discussed in Chapter 2, the main error sources that limit the accuracy of aircraft positioning are residual tropospheric, ionospheric, orbital effects and multipath. Orbital errors as well as tropospheric and ionospheric errors are spatially correlated, so their magnitudes are a function of the separation between the monitor and remote stations, and can be expressed in terms of relative accuracy, e.g. in parts per million (ppm). Generally, residual tropospheric error ranges from 0.2 to 0.4 ppm after the tropospheric correction is applied (Beutler, 1988). The ionospheric effect greatly depends on the user's position, observation time and satellite elevation. Under normal conditions, the residual ionospheric error can be estimated within 0.25 to 3 ppm (see Georgiadou and Kleusberg, 1988; Cannon, 1991; and Section 6.4.2). Based on the discussions in Sections 2.4.1 and 3.2 as well as on the results in Section 6.4.3, and considering the effects of satellite geometry under favorable conditions (six satellites in view and with a factor varying from 1 to 1.5 due to the standard deviation of the estimated position), the residual nominal orbital and orbital SA errors can be approximately estimated to within 0.5 to 1 ppm and 1 to 2 ppm, respectively.

Table 4.1 summarizes the magnitudes of these residual errors for the case when using L1 measurements under SA. The total error budget, which is estimated as the square root of the sum of the squares of the individual component errors (Cannon, 1991), is also given as is the percentage contribution

of the individual errors.

Table 4.1

Residual GPS Errors for the Case of L1 Measurements with SA on

Error Source (Residual)	Magnitude (ppm)	Contribution to Error Budget
Troposphere	0.2 - 0.4	1 % - 3 %
Ionosphere (L1 only)	0.3 - 3	7 % - 64 %
Orbit (Broadcast)	0.5 - 1	7 % - 13 %
Orbit (SA)	1 - 2	28 % - 72 %
Total Error Budget	1.2 - 3.8	100 %

One error that is not listed in Table 4.1 is the effect of multipath. Multipath is not spatially correlated and will, therefore, not be decreased by differential processing. The multipath effect on the carrier phase measurement is a main error source in the airborne GPS positioning environment either while stationary or in flight. The multipath error has a random behavior and the effects on the estimated position can be a few centimetres (see Section 6.4.5).

In Table 4.1, the total residual error ranges from approximately 1.2 - 3.8 ppm, of which the contributions of the ionosphere and the orbital SA account for 64% and 72 %, respectively. Since SA is turned on indefinitely, it will be one of the critical error sources. Under this assumption, if the monitor-remote separation is 30 km, the total error will range from 3.6 to 11.4 cm. To achieve aircraft positions at the 10 cm level, the monitor-remote separation should be

limited to a range less than 30 km. Beyond this range, the integer nature of the double differenced ambiguities will not be maintained, and this will degrade the accuracy of the remote positions (Cannon, 1991). The general case for differential GPS applications involves the use of a L1 receiver with SA on. This is treated as the case on which the following discussion on GPS receiver configurations will be based.

Table 4.2 gives the magnitude of each of the residual GPS errors when using L1/L2 measurements with SA turned on. The residual ionospheric error term is neglected in Table 4.2, since the residual effect can be assumed negligible after ionospheric correction using dual frequency measurements (Wells et al., 1986). As shown, the total residual error ranges between 1.1 and 2.3 ppm. Compared with Table 4.1, the error decreases by 1.5 ppm for the worst case after removing the ionospheric bias.

Table 4.2

Residual GPS Errors for the Case of L1/ L2 Measurements with SA On

Error Source (Residual)	Magnitude (ppm)	Contribution to Error Budget
Troposphere	0.2 - 0.4	3 %
Orbit (Broadcast)	0.5 - 1	19 %
Orbit (SA)	1 - 3	78 %
Total Error Budget	1.1 - 2.3	100 %

The effect of the orbital SA error can be avoided by using post-mission precise ephemerides. The contribution of residual error due to the precise ephemerides is less than 0.1 ppm (Remondi, 1989), so it can be neglected. Summarized in Table 4.3 are the magnitude of residual GPS errors in the case when using L1 measurements with precise ephemerides. The total residual error is within a range of 0.4 to 3 ppm, which is about a 25% error improvement over the broadcast ephemerides case.

Table 4.3
Residual GPS Errors for the Case of L1 Measurements with Precise Ephemerides

Error Source (Residual)	Magnitude (ppm)	Contribution to Error Budget
Troposphere	0.2 - 0.4	2 % - 31 %
Ionosphere (L1 only)	0.3 - 3	69 % - 98 %
Total Error Budget	0.4 - 3	100 %

In the case when using L1/L2 measurements with precise ephemerides, the total residual error will be significantly reduced to a level of less than 0.5 ppm. Since civilian users cannot exploit the advantages of using a P-code receiver anymore, the use of L1/L2 measurements with post-mission precise ephemerides is a realistic and effective solution to avoid the effects due to the ionosphere and orbital SA errors to improve positioning accuracy.

4.2 CONFIGURATION OF GPS RECEIVERS

4.2.1 Configuration on the Ground

The configuration of GPS receivers should be designed to ensure that the accuracy requirements of the aircraft positions can be maintained throughout a mission and that they can be checked. To reach this goal, it is important to limit the area controlled by a single monitor receiver. Based on the previous discussion about the use of L1 measurements under SA, the area should be limited to within 40 X 40 km with the monitor station in the centre. If the flying height of the aircraft is about 5000 m, the maximum distance between the monitor station to the aircraft will then be less than 30 km. Within this distance, the ambiguities can generally be resolved on-the-fly during the post-processing, so that ambiguity initialization is not required. If the entire operational area is accessible, the positioning accuracy of the aircraft over the area can be controlled by the monitor stations set up based on the above guideline.

An alternative scenario is to initialize the ambiguities before the mission. This needs at least one additional monitor receiver to be set up within a range of several kilometres (preferably several tens of metres) from the aircraft. This ensures that the initial ambiguities can be correctly resolved from a static survey at the beginning and end of a mission and, thus, fixed to their integer values during the mission. If the airport is more than 30 km away from the operational area, more monitor receivers may be required along the flight line in order to

transfer initialized ambiguities to the operational area (see Shi & Cannon, 1993). In this scenario, the configuration of monitor receivers depends not only on the size of the operational area, but also on the distance between the airport and the operational area. Compared with the scenario where ambiguity resolution on-the-fly is exploited, this scenario is less cost effective but more reliable, since it is usually not difficult to resolve integer ambiguities between the monitors.

In case the operational area is inaccessible, such as mountainous or forested areas, and also far away from the airport (over 100 kilometres), receivers with a function providing the L2 measurements (e.g. cross correlation L2 and the L2 in the Z-Tracking mode, see Ashjaee and Lorenz, 1992) and ambiguity initialization are needed if the required positioning accuracy is of the order of 10 cm. In this case, at least one monitor should be set up at the airport for ambiguity initialization, and another installed on the aircraft. If one additional receiver is available, it should be installed on the aircraft to increase the redundancy of kinematic data. However, the ideal configuration in this case is to use two monitors (if more than three receivers are available) with a separation of several kilometres. This configuration can provide an independent comparison for accuracy evaluation, see Sections 5.2 and 6.5.4.

4.2.2 Configuration on the Aircraft

For the purpose of airborne GPS positioning, the basic configuration on the aircraft involves the use of a single receiver. The main drawback of using a

single receiver is that no checking can be performed. If more than one monitor is used in this case, as explained in Section 3.3, any aircraft position errors will be eliminated when differencing aircraft positions estimated with respect to two monitor stations. An alternative configuration is that two or more receivers are installed on the aircraft, which has the following advantages:

1) Provides an alternative for detection of cycle slips on the aircraft. Since the distance between the two antennas is known, the computed baseline can be compared with the known length to determine if cycle slips occur on either of the aircraft receivers.

2) Provides a spatial vector defined by a pair of antennas on the aircraft at each measurement epoch so that a comparison can be made between this vector and the solutions determined with respect to the monitor station(s). This will also be helpful in assessing multipath effects since any differences in these two solutions can only be attributed to multipath errors assuming all cycle slips are correctly resolved.

3) Provides more measurement information than from a single antenna, so that the reliability of the aircraft positions will be increased.

4) Allows aircraft heading determination in the case of two receivers and attitude in the case of three or more receivers.

4.3 OPERATIONAL STRATEGIES

In planning the operational scheme, the most important criterion is that the required accuracy is met. Furthermore, the operational scheme should also be designed in such a way that more additional accuracy checking and analysis methods can be provided.

Considering the high dynamics of an aircraft, it is required that all GPS receivers collect data at a high data rate (not lower than 2 Hz). It is beneficial for the interpolation of GPS positions (for instance, to the time of exposure in airborne photogrammetry) as well as for carrier phase cycle slip detection. The tracking loop bandwidth of each remote receiver on the aircraft should be set to 16 Hz which is the ideal setting for an aircraft dynamic environment. A 16 Hz bandwidth allows phase lock under accelerations of up to several tens of m/s^2 with only a small probability of cycle slips (Braasch & van Grass, 1993).

In selecting the optimal observation span, it is strongly recommended that the GDOP be less than three within the operational area, and that more than five satellites are visible during a mission since the satellite geometry plays a critical role. An ideal observation span has four or more satellites covering the entire kinematic positioning period (preferably covering the entire observation span) to avoid multiple satellite switching and to keep the positioning accuracy consistent.

An open environment is required at each monitor station and each monitor antenna should be equipped with a choke ring or a radio frequency

absorbing groundplane so that the effect of multipath can be minimized. The satellite elevation cut-off angle should be between 10 and 15 degrees, leaving some optional space for the post mission data processing.

Before and after the flight, the aircraft should remain stationary for 30 minutes to acquire sufficient data for ambiguity resolution as well as for examining the multipath effects on the aircraft in static mode. The observation span for monitor receivers should not be less than two hours in order that the baselines between the monitors can be correctly determined.

CHAPTER 5

DATA PROCESSING STRATEGIES AND ACCURACY EVALUATION

Effective data processing strategies are essential in order to achieve successful positioning results, while accuracy checking and analysis methods are very important in verifying the positioning accuracy. General data processing strategies are summarized and several methods for accuracy checking and analysis are presented in this chapter. The strategies and methods are suited for airborne GPS positioning with a multi-receiver configuration.

5.1 DATA PROCESSING STRATEGIES

The post mission data processing can be divided into three stages according to the receiver configurations and operational strategies discussed in the previous chapter.

In the first stage, all static data from the various monitor stations are processed to determine their relative coordinates. Based on these monitor coordinates, the trajectory of the aircraft will be determined in the following stages.

The second stage is the processing of the static initialization data collected before aircraft take off and also after landing. All integer ambiguities should be correctly resolved so that they can be fixed during kinematic data processing. With resolved ambiguities, the aircraft coordinates can be determined at the centimetre level with respect to the monitor at the airport before take off and after landing. These known coordinates can be used for flight misclosure tests at the start or end of the mission (see the next section).

Kinematic processing of the aircraft data is performed in the last stage. Positions of the aircraft at each measurement epoch are determined using the double difference method with fixed integer ambiguities. For ionospherically corrected measurements, however, the ambiguities should be fixed to their floating solutions rather than their nearest integer values, since the integer nature of the ambiguities will not be maintained after the ionospheric correction is applied.

During kinematic data processing, the following considerations can be made:

1) When two or more receivers are installed on the aircraft, one can be used as a pseudo-reference station. Based on the trajectory of the pseudo-

reference station generated with respect to a monitor station on the ground, the positions of the other aircraft receiver(s) with respect to the pseudo-reference station can be determined. In this case, one should use a least squares algorithm or a Kalman filter as given in Section 3.1.

2) To keep the positioning accuracy consistent, frequent satellite switching should be avoided. In addition, one should use the most recently updated ephemerides which correspond to the period during the largest monitor-remote separation, rather than switching to updated ephemerides every hour (see Section 6.4.3).

3) To increase reliability and provide an accuracy checking method, both kinematic and static initialization data should be processed in forward and reverse time.

4) For applications with a large monitor-remote separation (over 50 km), a minimum of four satellites are required without losing phase lock during the kinematic period if no inertial measurement unit (INS) is used on the aircraft.

5.2 METHODS FOR ACCURACY CHECKING AND ANALYSIS

In order to assess the quality of the results, methods for accuracy checking and analysis have to be studied. For airborne GPS positioning, the following

accuracy checking and analysis methods are available. Some of them are dependent on the receiver configuration.

1) Flight Misclosure Test

The flight misclosure test can be used at the end or the start of the flight. A misclosure at the end of the flight is generated by differencing the aircraft position at the end of the mission with the known coordinates determined using static data collected after landing. A misclosure at the start of the flight is generated by differencing the aircraft position at the start of the mission with the coordinates determined from the static data collected before take off (e.g. data processing in reverse time). If the flight misclosures are at the centimetre level, it indicates that the integer ambiguities are correct at the start and end of the mission. Centimetre level misclosures are a basic requirement for a successful kinematic run. However, they do not guarantee that successful data processing has been achieved during the entire kinematic run.

2) Comparison Between Forward and Reverse Processing

The trajectory of the aircraft determined from forward time processing can be compared with that from the reverse, so that the consistency of the results can be checked. This is critical when some satellites rise or set during flight. This method can be used to examine the correctness of the new satellite ambiguities, and to detect if a problem occurred during the fight. Consistent results from forward and reverse processing are expected when successful data processing

has been achieved in both directions.

3) Comparison with Known Baseline on the Aircraft

When two receivers are installed on the aircraft with a known separation, the GPS derived distance between them can be compared. Three different GPS derived distances can be generated from three methods. The first one is to directly estimate the relative position of one aircraft receiver with respect to the other (using a pseudo-reference station). The second is to difference two aircraft trajectories determined from one monitor receiver on the ground. A third method is to difference two aircraft trajectories which are determined from two monitors. These two trajectories are independent. Differences in the known and GPS-derived aircraft antenna separations reflect the internal positioning accuracy, the consistency of different positioning solutions, multipath effects and measurement noise.

4) Triangle Misclosure Test

Two receivers on the aircraft and one monitor receiver on the ground form three different kinematic vectors. A triangle misclosure in each coordinate component can be generated with the three kinematic vectors at each epoch. Based on the demonstration given in Section 3.3, this misclosure should be very close to zero. But a zero misclosure is only a required indicator for three

successfully processed kinematic runs.

5) Residual Analysis

Residual analysis can be performed by examining the residuals of the double difference carrier phase measurements. The level of residual errors (atmospheric, orbital errors as well as amplified measurement noise due to differencing) remaining after differential processing can be quantified through this analysis.

6) Systematic Error Effect Analysis

Effects of systematic residual errors can be isolated and quantified through comparisons between solutions from different scenarios, such as 1) solutions with tropospheric corrections applied, versus those without the corrections, 2) results using the ionospheric effect free measurement versus those using the L1 only, and 3) precise ephemerides versus the broadcast (see Section 6.4).

CHAPTER 6

TEST DESCRIPTION, RESULTS AND ANALYSIS

To demonstrate the achievable accuracy of GPS in an aircraft environment, results from an airborne GPS positioning test using a multi-receiver configuration are presented in this chapter. The relevant theoretical analysis presented in Chapter 3 is confirmed by the results from the test data**.** Data processing strategies and accuracy check methods presented in Chapter 5 are applied to the data processing, and the results are examined and discussed. In addition, the effects of critical errors from the troposphere, ionosphere, orbit and multipath on the estimated positions are investigated using the test data.

6.1 TEST DESCRIPTION

A series of airborne GPS positioning tests were undertaken during April, 1993, in order to assess the achievable accuracy of GPS for precise positioning in an aircraft environment. The tests were conducted in the Lake Ontario region

and consisted of several flight runs over Lake Ontario on several days. Four Trimble 4000 SSE receivers were used, two as remote stations on the aircraft and two as monitor stations on the ground. The SSE receivers have the capability of using P-code L1 and L2 when available and the C/A-code L1 and cross-correlation mode on L2 when the P-code is denied. In cross-correlation mode, a full wavelength L2 carrier measurement is available so processing options such as ionospheric corrections and widelaning are possible. Both modes were tested during the campaign.

A Cessna 310R twin engine aircraft was used during the test. Two antennas, herein called FORE and AFT were mounted on the fuselage with a separation of 93.7 cm manually measured by tape. One monitor station, OSHA was set up at Oshawa Municipal Airport, and the second one, WLAK, at Westlake on Quinte Island, Prince Edward County, about 131 kilometres away. Both monitor stations were in open areas and equipped with Trimble Geodetic antennas with a 19 cm radius groundplane in order to minimize multipath effects. The OSHA site was about 43 metres away from the aircraft before take off (and after landing) to allow for an adequate static initialization. Figure 6.1.1 shows a sketch of the GPS receiver configuration used in the tests. During the flight tests, Selective Availability (SA) was on and there were 5 to 7 satellites in view above 15 degrees during the entire mission, see Figure 6.1.2 which gives the satellite skyplots (azimuth versus elevation) during the two 30 minute periods, before the aircraft take off and after landing. The PDOP was generally about 3.

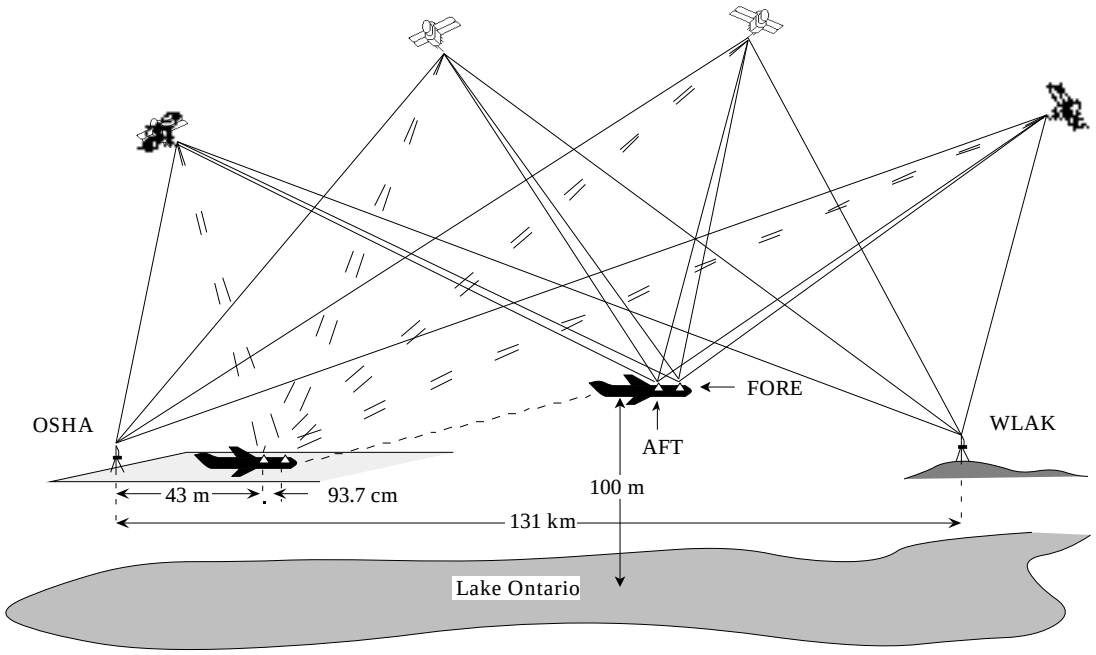

Figure 6.1.1
GPS Receiver Configurations on the Ground and on the Aircraft

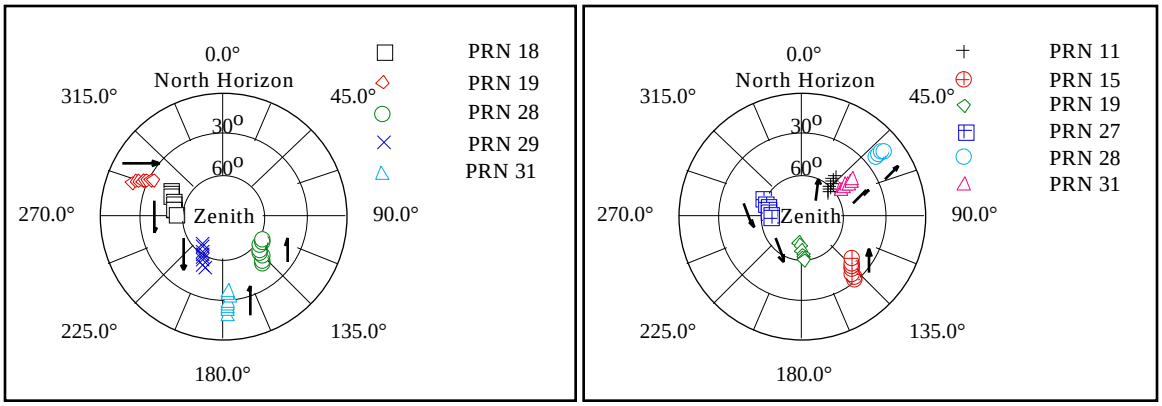

Before take off **After landing**

Figure 6.1.2
Satellite Skyplot

The flight test on an individual day was carried out according to the following procedure: before take off, the aircraft remained static on the tarmac and at least 30 minutes of GPS data was logged to ensure correct and reliable ambiguity initialization. Then the aircraft-mounted receivers were switched to kinematic mode and the aircraft took off and flew an east-west line over the lake. The altitude was about 100 metres over the lake, and the aircraft speed reached 80 m/s. After completing two or three flight lines on the same track, the aircraft returned to the airport and landed close to the same place as before take off. Another half hour of data was then collected in stationary mode. All four receivers logged raw data at a 2 Hz rate during the 3 and half hour mission.

Data from April 27 and 28 were selected for post-processing in which the receiver was set to P code mode and P codeless mode (i.e. cross-correlation), respectively. Figure 6.1.3 shows the flight path on April 27 in terms of northing versus easting, and Figure 6.1.4 shows the flight path changing in latitude, longitude and height versus GPS time. The flight path on April 28 is similar to those shown in Figures 6.1.3 and 6.1.4.

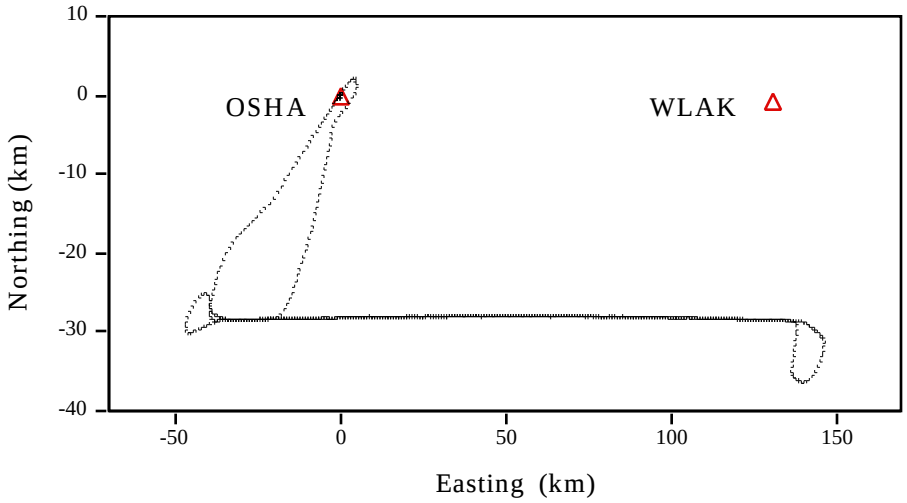

Figure 6.1.3
Flight Path on April 27, 1993

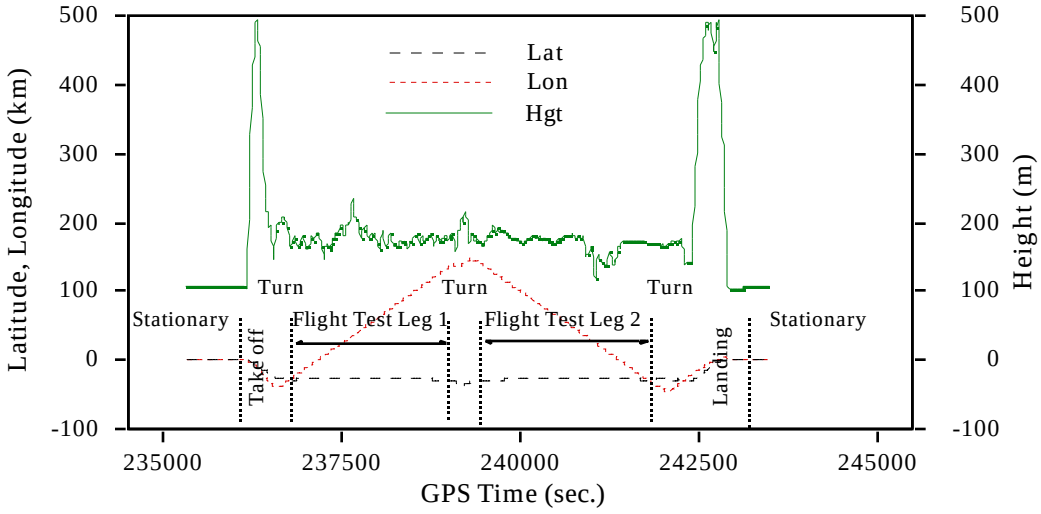

Figure 6.1.4
Flight Path Changing in Latitude, Longitude and Height over GPS Time (April 27, 1993)

6.2 DATA PROCESSING

Data processing was implemented in two stages. Firstly, the static initialization data before aircraft take off and also after landing were processed to determine the position of the aircraft with respect to OSHA to the centimetre level. These relative positions can then be used to check the misclosure between the start and end of the mission which can be used to verify the quality of the results. Data from these static baselines were successfully processed to generate integer ambiguity carrier phase solutions.

The second stage was the kinematic processing of the aircraft data. Several strategies were implemented in order to check a variety of processing options. These scenarios are listed in Table 6.2.1. Each of the monitor receivers (i.e. OSHA and WLAK) were processed with respect to each of the aircraft antennas (i.e. FORE and AFT). As well, the two aircraft antennas were processed with respect to each other, as were the two monitor stations. For the April 27 test, in which the receiver was in P-code mode, both L1, L2 and ionospherically corrected L1 (i.e. L1/L2) data was processed for the longer baselines. On April 28, the receiver was in C/A-code mode and only the L1 and cross-correlation L2 data (i.e. Cc L2) data were analyzed. Problems were experienced with using the cross-correlation data for ionospheric corrections (see Section 6.4.2), so this option was not further investigated. The data was processed in forward and reverse time to check the consistency of these two solutions.

Table 6.2.1
Kinematic Data Processing Scenario

Antenna Pair	Day	Carrier Phase Measurement Used*	Ephemerides Used
OSHA-FORE	April 27 April 28	P-code L1, L2, L1/L2 C/A-code L1, Cc L2	Broadcast & Precise Broadcast
OSHA-AFT	April 27 April 28	P-code L1, L2, L1/L2 C/A-code L1, Cc L2	Broadcast & Precise Broadcast
FORE-AFT	April 27 April 28	P-code L1, L2 C/A-code L1, Cc L2	Broadcast
AFT-FORE	April 27 April 28	P-code L1, L2 C/A-code L1, Cc L2	Broadcast
WLAK-FORE	April 27	P-code L1/L2	Precise
WLAK-AFT	April 27	P-code L1/L2	Precise
OSHA-WLAK	April 27	P-code L1/L2	Precise

* Cc L2 -- Cross-correlation L2; L1/L2 -- Ionospherically corrected

In most cases, the carrier phase ambiguities were fixed to integers. The software used in the data processing is the SEMIKIN™ program, developed at The University of Calgary (Cannon, 1990), which utilizes a double differencing approach. The program was modified in this research to allow for the use of precise orbit and a pseudo-reference station on the aircraft. Data from several satellites were rejected due to frequent cycle slips on April 27. With the remaining data, at least five satellites were in view during the entire mission.

One satellite was rejected from April 28 due to cycle slips, however at least six satellites were visible throughout the mission.

Since four receivers were used in the test, solutions from different antenna pairs can be compared in different ways. The four methods that were selected for the evaluation of the results are: 1) flight misclosure test, 2) comparison of the estimated distance between two antennas on the aircraft using GPS with the measured distance, 3) comparison of aircraft trajectories from forward and reverse time processing solutions, and 4) triangle misclosure test. These methods have been explained in Section 5.2.

6.3 POSITIONING RESULTS

Kinematic positioning results with four types of measurements are presented herein to demonstrate the potential internal accuracy of airborne differential GPS positioning with a monitor-remote separation of 200 km. Data quality and validation, ambiguity correctness, and noise level of each type of measurement are examined through flight misclosure tests and residual analysis.

6.3.1 Results with P-code L1 and C/A-code L1

C/A-code L1 carrier phase is one of the fundamental observables and is generally used in various high accuracy positioning applications. The noise level

of this observable is 0.2 to 3 mm. P-code L1 carrier phase has a similar characteristic to C/A-code L1, but with slightly higher noise level dependent on the type of the receiver.

Tables 6.3.1 and 6.3.2 summarize flight misclosures of different antenna pairs using P-code L1 on April 27 and C/A-code L1 on April 28. The flight misclosures are the differences between the position of the aircraft at the end of the flight (or start if data is processed in reverse time) with the known coordinates determined from the static initialization stages.

As can be seen in Table 6.3.1, the misclosures for P-code L1 are less than 2 cm in all cases while Table 6.3.2 shows that the C/A-code L1 is generally less than 2 cm except for one case of 4.8 cm in height. In both cases this illustrates that the carrier phase ambiguities are at the correct integer value at the start and end of the mission. Generally, a centimetre level flight misclosure does not guarantee that the entire mission is successful, but it is one of the necessary indicators for successful kinematic positioning. If the ambiguities were incorrect at the start (in reverse processing) and the end (in forward processing) of the run, the misclosure would be significantly poorer than those in Table 6.3.1 and 6.3.2. Since no cycle slips occur in both cases, it can be reasonably estimated that with the correct integer ambiguities the internal positioning accuracy during the flight should be at the centimetre level, which will be verified in Section 6.5.

Table 6.3.1
Flight Misclosures, P-code L1, April 27

Antenna Pair	End of the Flight (cm)			Start of the Flight (cm)		
	Δϕ	Δλ	Δh	Δϕ	Δλ	Δh
OSHA-FORE	-0.6	0.0	0.9	-0.6	0.0	1.0
OSHA-AFT	0.0	0.0	-0.3	0.3	-0.2	0.9
FORE-AFT	-0.6	0.2	1.0	-0.3	0.0	1.7
AFT-FORE	0.3	0.0	-0.3	0.3	-0.2	-0.9

Table 6.3.2
Flight Misclosures, C/A-code L1, April 28

Antenna Pair	End of the Flight (cm)			Start of the Flight (cm)		
	Δϕ	Δλ	Δh	Δϕ	Δλ	Δh
OSHA-FORE	0.0	-0.4	1.6	-0.3	0.0	0.0
OSHA-AFT	0.0	-1.5	-0.6	0.0	-1.3	-0.7
FORE-AFT	0.0	-1.5	4.8	0.0	-1.3	-0.7
AFT-FORE	0.0	-1.5	-0.6	-0.3	0.0	0.0

In evaluating the data quality and internal accuracy of kinematic positioning during the flight, residual examination is a necessary and efficient means. Figures 6.3.1 and 6.3.2 show the double difference residuals behaviors for PRNs 31-11 and PRNs 19-11, respectively, during the entire flight using the OSHA-AFT kinematic run with P-code L1 on April 27. The separation (in units of 10 km) between the monitor OSHA and the aircraft is also plotted in the figures

to illustrate the correlation between the residuals and the separation.

Since the ambiguities have been fixed to the correct integer values at the start of the flight as well as for the ambiguities of the satellites rising during the flight, the residual error effect which remains in the residuals in Figures 6.3.1 and 6.3.2 is the sum of the ionospheric error, orbital error, multipath and measurement noise. In comparing with other errors, the ionospheric error effect is a dominant residual error which shows a long term systematic effect and is not necessarily proportional to the separation (see Figures 6.3.1 and 6.3.2). Similar results are shown in Figures 6.3.3 and 6.3.4 for PRNs 31-11 and PRNs 28-11, respectively, with C/A-code L1 on April 28. As can be seen in Figures 6.3.1 and 6.3.3, the maximum residual is up to 10 cm likely due to residual ionospheric effects over a 100 kilometer monitor-remote separation.

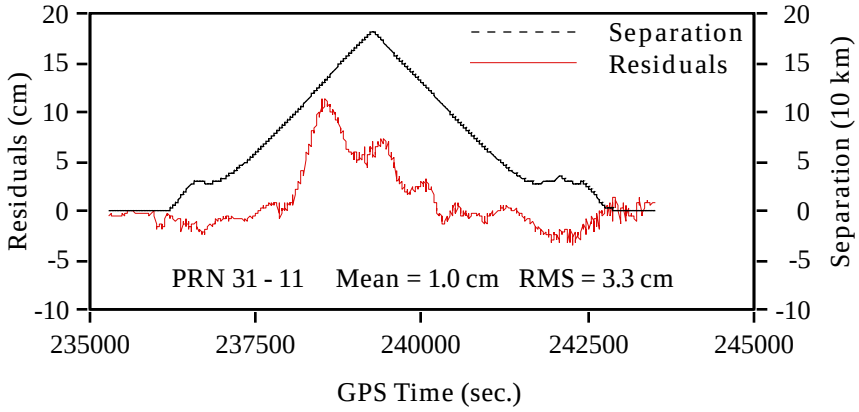

Figure 6.3.1
DD Residuals for PRNs 31-11 Using the OSHA-AFT Kinematic Run
(P-code L1, on April 27)

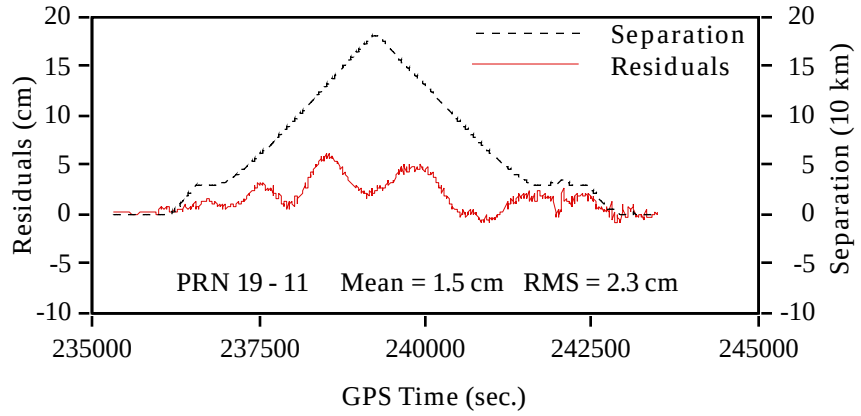

Figure 6.3.2

DD Residuals for PRNs 19-11 Using the OSHA-AFT Kinematic Run (P-code L1, on April 27)

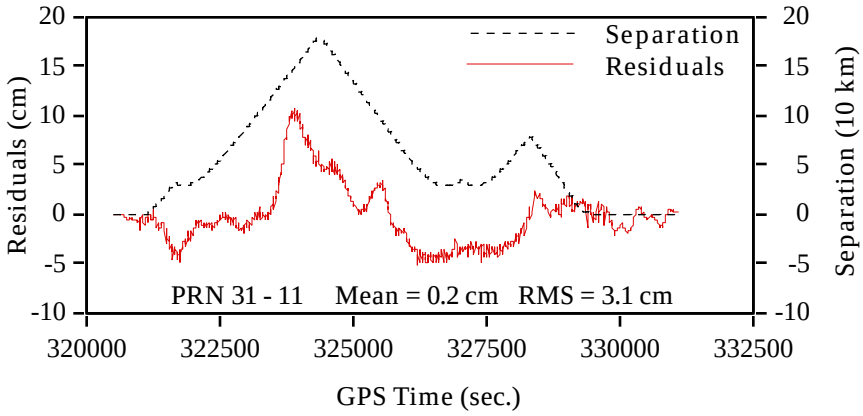

Figure 6.3.3

DD Residuals for PRNs 31-11 Using the OSHA-AFT Kinematic Run (C/A-code L1, on April 28)

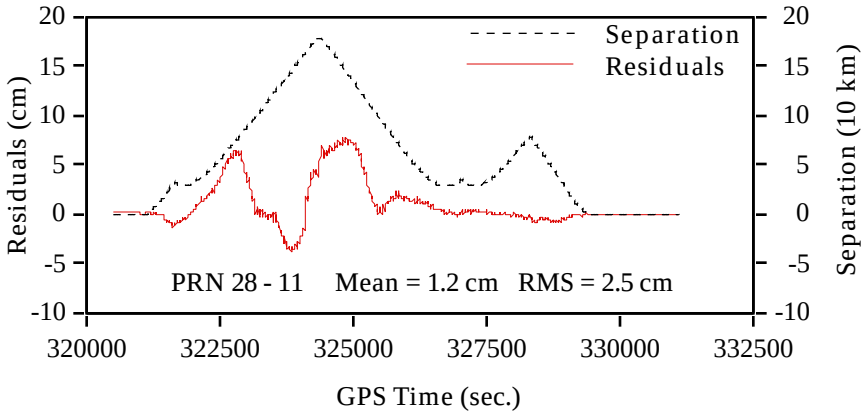

Figure 6.3.4
DD Residuals for PRNs 28-11 Using the OSHA-AFT Kinematic Run (C/A-code L1, on April 28)

In order to evaluate the quality of data on the aircraft and relative positioning accuracy between the two aircraft receivers, FORE or AFT is used as the pseudo-reference station, respectively, to determine the position of the other antenna. In this case, only multipath effects and receiver noise remain in the residuals if the ambiguities are set to the correct integer value. Figures 6.3.5 and 6.3.6 show the residuals for PRNs 19-11 using the FORE-AFT kinematic run on April 27 with P-code L1 and April 28 with C/A-code L1, respectively. As shown in the figures, the residuals are within 1 cm throughout the entire straight flight line, and some larger ones occur during aircraft turns. Compared with the results using the OSHA-AFT kinematic run, the residual mean and RMS of using the FORE-AFT are significantly reduced because all spatially related errors are canceled, see Table 6.3.3 where the statistics of the residuals for all PRNs in both cases are summarized.

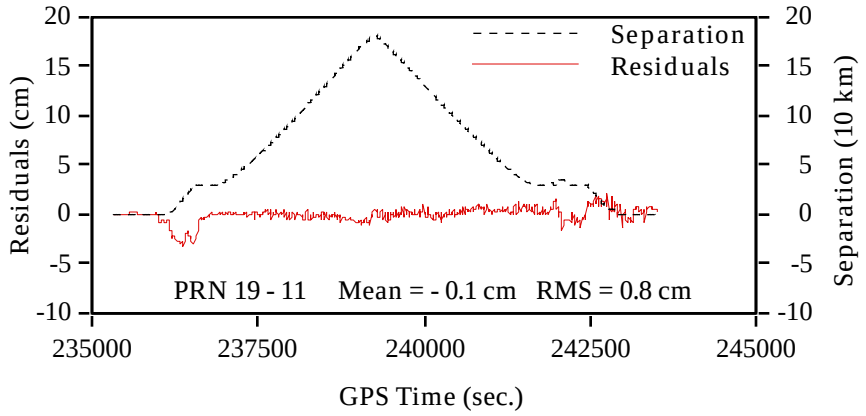

Figure 6.3.5
DD Residuals for PRNs 19-11 Using the FORE-AFT Kinematic Run
(P-code L1, on April 27)

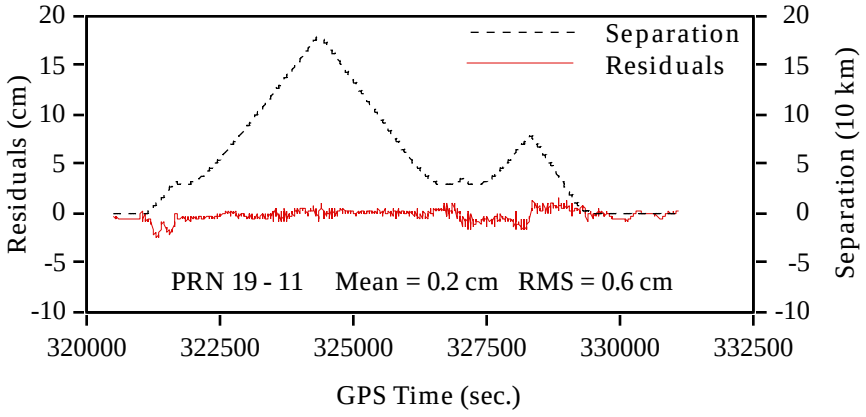

Figure 6.3.6
DD Residuals for PRNs 19-11 Using the FORE-AFT Kinematic Run
(C/A-code L1, on April 28)

Table 6.3.3
Contrast of DD Residuals Statistics Between the OSHA-AFT and FORE-AFT Kinematic Runs (C/A-code L1, April 28)

PRN	Number of Epochs	OSHA -AFT (cm)		FORE - AFT (cm)	
		Mean	RMS	Mean	RMS
31	21192	0.2	3.1	0.0	1.0
29	7159	1.6	4.4	0.0	1.1
28	17748	1.2	2.7	-0.4	1.5
27	14004	-1.1	2.1	-0.2	0.9
19	21192	0.4	1.3	0.2	0.6
18	15563	0.7	3.1	-0.4	1.5

6.3.2 Results with P-code L2

When the P-code is available, P-code L2 carrier phase can be used to generate the widelane measurement (with a wavelength of 86 cm) and the ionospherically corrected measurement with the combination of the P-code L1, as discussed in the Section 2.3. The accuracy of P-code L2 carrier phase is slightly lower than the P-code L1, not only because of the larger wavelength of the P-code L2 (carrier phase noise level is about 1.6% of the wavelength, see Seeber, 1993) but also because of the lower received power level at P-code L2 (Lachapelle, 1993). The noise level of the P-code L2 is related to that of P-code L1 by the factor of 1.28, which is the ratio of the wavelength of L2 to L1.

Flight misclosures for the antenna pairs using P-code L2 are listed in Table 6.3.4, and are generally less than 3 cm, which means that the correct integer

ambiguities are kept at the start and end of the flight and the basic necessary prerequisite for the successful kinematic positioning is met. A single cycle slip is detected on PRN 28 from the AFT and the ambiguity is correctly recovered during the flight.

The double difference residual behavior for PRNs 31-11 during the entire flight using the OSHA-AFT kinematic run with P-code L2 is illustrated in Figure 6.3.7, where the larger scale of the ionospheric effect can be seen clearly compared with Figure 6.3.1 because of the lower frequency of L2. The theoretical ratio of the ionospheric delay at L2 to that at L1 is 1.65 when only considering the first order effect, while the estimated ratio of the P-code L2 to L1 from the test data using RMS varies from 1.60 to 1.90 with different PRNs. Table 6.3.5 shows the contrast between P-code L1 and P-code L2 double difference residuals statistics in term of mean and RMS, using the OSHA-AFT kinematic run.

Table 6.3.4
Flight Misclosures, P-code L2, April 27

Antenna Pair	End of the Flight (cm)			Start of the Flight (cm)		
	Δϕ	Δλ	Δh	Δϕ	Δλ	Δh
OSHA-FORE	0.3	0.4	0.1	1.5	-0.6	1.5
OSHA-AFT	0.0	-3.2	0.9	-0.9	-0.2	-2.2
FORE-AFT	0.3	0.6	0.2	0.0	-3.2	0.9
AFT-FORE	1.8	-0.6	2.2	-0.9	-0.2	-2.3

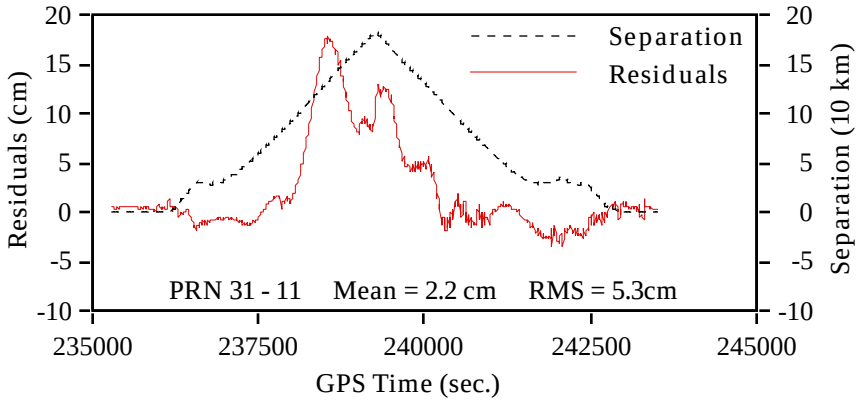

Figure 6.3.7
DD Residuals for PRNs 31-11 Using the OSHA-AFT kinematic run (P-code L2, on April 27)

Table 6.3.5
Contrast Between P-code L1 and P-code L2 DD Residuals Statistics (The OSHA-AFT Kinematic Run, April 27)

PRN	Number of Epochs	P-code L1 Carrier Phase (cm)		P-code L2 Carrier Phase (cm)	
		Mean	RMS	Mean	RMS
31	8185	1.0	3.3	2.2	5.3
28	8185	-0.2	1.1	-0.2	2.0
27	5654	-0.7	1.2	-1.3	2.3
19	8185	1.5	2.3	2.7	4.0
18	5665	-0.7	1.4	-0.8	2.4

6.3.3 Results with Cross Correlation L2

The cross-correlation L2 carrier phase is a codeless measurement which is produced by cross-correlating the L1 and L2 signals. In comparison with the squaring L2, the cross-correlation L2 has the advantage of a full wavelength measurement and a 3 dB higher SNR (Ashjaee and Lorenz, 1992). The cross-correlation L2 can be used when the P-code is denied to civil users after the completion of GPS system. The substantial drawback is that this L2 measurement suffers a 27 dB lower SNR than the P-code L2 carrier phase. This is a critical factor which prevents the cross-correlation L2 from being effectively exploited, which will be discussed in the following section.

Due to the increased measurement noise through the cross-correlation process, the misclosure results for the cross-correlation L2 listed in Table 6.3.6 are significantly poorer, especially on the height component. The results are also amplified due to poorer satellite geometry at the end of the mission (PRN 28 was rejected before landing, see Figure 6.1.2), see Tables 6.3.2 and 6.3.6 with comparisons between the results at the end of the flight versus those at the start.

To compare with the other misclosure results, Figure 6.3.8 illustrates the RMS in all cases and shows that all the results are compatible with the exception of the cross-correlation L2. In contrast to Figure 6.3.6, Figure 6.3.9 shows noisier behavior of the cross-correlation L2 measurement in terms of the residuals. A further investigation into the characteristics of the cross-correlation L2 is

discussed in Sections 6.4 and 6.5.1.

Table 6.3.6
Flight Misclosures, Cross-correlation L2, April 28

Antenna Pair	End of the Flight (cm)			Start of the Flight (cm)		
	Δϕ	Δλ	Δh	Δϕ	Δλ	Δh
OSHA-FORE	-0.9	-2.8	13.5	2.4	-1.9	-1.7
OSHA-AFT	0.6	-0.9	-8.0	-1.5	0.0	-2.1
FORE-AFT	-0.9	-2.8	13.1	-1.5	0.0	-2.1
AFT-FORE	-0.3	-7.1	-3.4	2.4	-1.9	-1.7

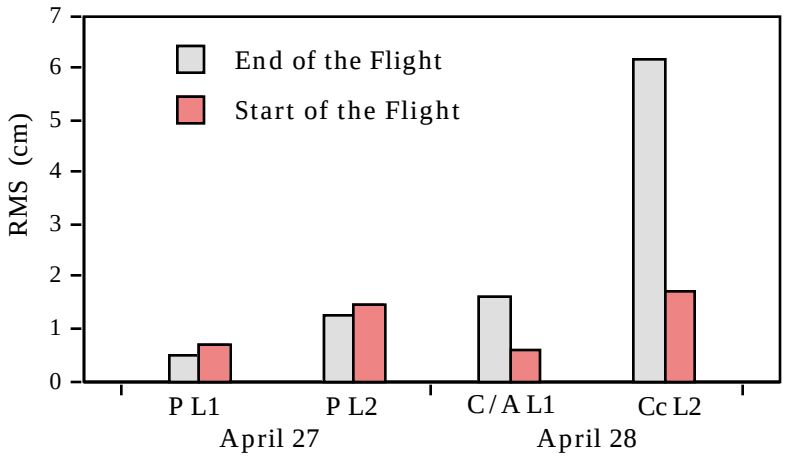

Figure 6.3.8
RMS of Flight Misclosures on April 27 and 28

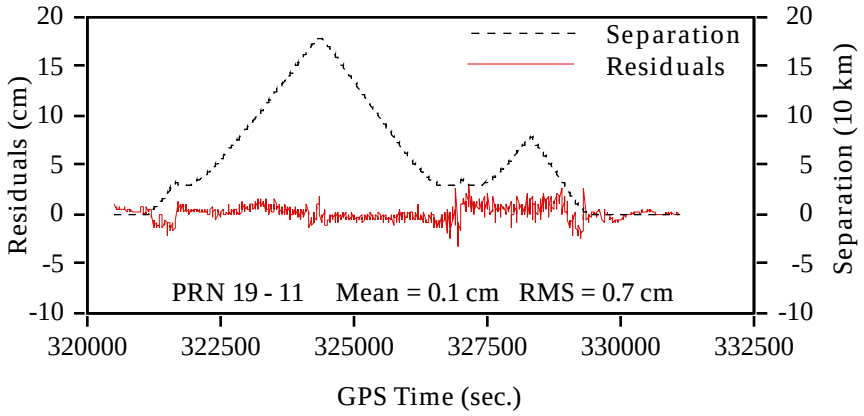

Figure 6.3.9
DD Residuals for PRNs 19-11 Using the FORE-AFT Kinematic Run
(Cross-correlation L2, on April 28)

6.4 CRITICAL ERROR EFFECTS AND ANALYSIS

Residual tropospheric, ionospheric, and nominal orbital errors are critical for airborne kinematic positioning over large areas, since they are spatially correlated. Multipath effects are also a key error source considering the environment for aircraft applications (Braasch & van Graas, 1991). The magnitude and peculiarity of these effects need to be extensively investigated, because the achievable accuracy of airborne positioning is greatly dependent on how to eliminate or mitigate these effects. The real effects due to these errors on the flight test were computed, examined and analyzed.

6.4.1 Tropospheric Effect

For the entire data processing schedule, the Modified Hopfield model (Goad and Goodman, 1974) was used to compute the tropospheric correction with consideration of the vertical temperature and pressure gradients based on the standard atmosphere model. The effect due to residual tropospheric error on the aircraft position is computed by differencing the trajectory without the correction from that with the correction applied.

Figure 6.4.1 shows the residual tropospheric effect on the aircraft positioning using C/A-code L1 and the corresponding profile of the aircraft height on April 28. In the figure, it is apparent that the effect on the height component is greatly correlated with the monitor-remote height difference. This is caused by the mapping function of the model which, as mentioned in Section 2.2, projects the tropospheric refraction correction at the zenith on the line of sight according to the satellite elevation. As can be seen in the figure, during the stable flight stage, the effect is about 6 cm on the height, corresponding to the average height difference of 60 m (100 m above the lake), and 2 mm on the horizontal components. The maximum effects on the latitude , longitude and height are 3.6 cm, - 2.7 cm and 46.1 cm, respectively, corresponding to the largest height difference of 774 m. It is obvious that tropospheric correction has to be applied in a high accuracy airborne GPS positioning.

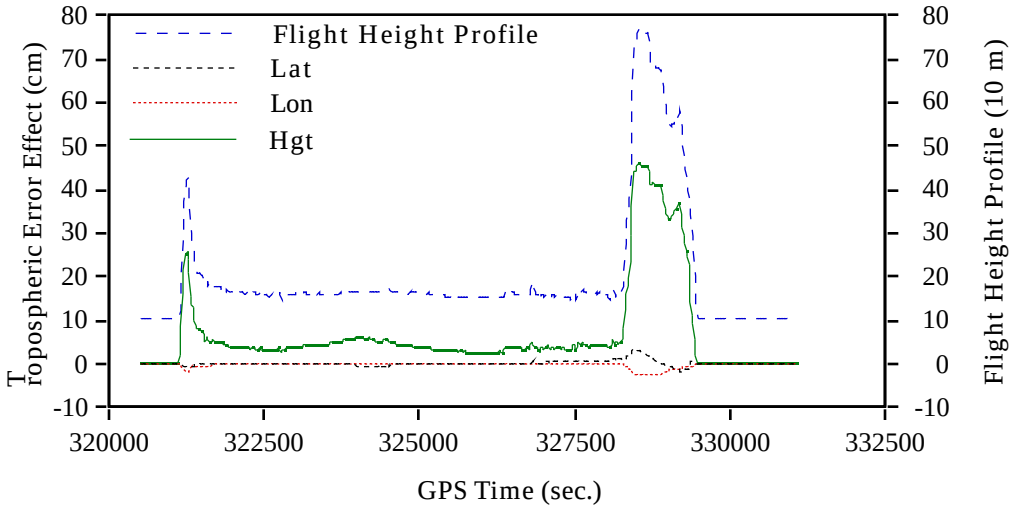

Figure 6.4.1
Tropospheric Error Effect on the Position of the FORE Antenna Using the OSHA-FORE Kinematic Run (C/A-code L1, April 28)

By examining the statistics of the measurement residuals from solutions with and without the tropospheric correction applied, it is found that the difference between the statistics from the two cases is very small, within several millimetres (see Table 6.4.1). This is quite different from the results obtained by Tiemeyer et al. (1994) where a several centimetre difference was observed with monitor-remote height differences of 400 m and 6000 m. This can be explained from two aspects. Firstly, the average height difference is only 60 m in this flight test, so the tropospheric effect is not so critical in the solution. Secondly, the effect can not be apparently reflected through the residual statistics, where the ionospheric error effect is dominant because of a large monitor-remote separation.

Table 6.4.1
DD Residuals Statistics Comparison Between with and without Tropospheric Correction Solutions
(The OSHA-FORE Kinematic Run, C/A-code, April 28)

PRN	Number of Epochs	Residuals with Tropospheric Correction (cm)			Residuals without Tropospheric Correction (cm)		
		Mean	RMS	Max.	Mean	RMS	Max.
31	21195	-0.1	3.1	-9.2	-0.1	3.1	-9.6
29	7189	1.3	3.9	10.6	1.2	3.9	10.5
28	17750	1.0	2.6	7.6	0.9	2.7	7.8
27	14199	-1.1	2.1	-6.3	-1.1	2.2	-6.5
19	21195	0.5	1.5	5.2	0.4	1.7	5.2
18	15565	0.7	2.7	8.3	0.7	2.8	8.5
15	5641	0.1	0.2	-2.8	0.3	0.4	-2.3

6.4.2 Ionospheric Effect

The ionospheric effect on the L1 or L2 trajectories can be estimated by comparing with the trajectory using the ionospherically corrected measurement. To generate an ionospheric error free carrier phase measurement, only the relative ionospheric correction can be applied in double difference mode, as discussed in Section 2.3. A disadvantage of performing this correction, besides the fact that the ambiguities are not integers anymore, is that the noise level of the measurement is greatly amplified due to the linear combination of the L1 and L2, up to four times that of the L1 in terms of standard deviation (see Section 2.3).

For a high accuracy GPS application with a large monitor-remote separation, this is the price to pay to eliminate ionospheric errors.

A comparison of residuals using P-code L1, L2 and ionospherically corrected measurements for PRNs 31-11 and 19-11 are shown in Figure 6.4.2, where no ionospheric effect can be seen in the L1/L2 results, however the residuals are noisier. Table 6.4.2 gives the corresponding statistics. The RMS for all satellites range from 1.2 to 1.8 cm, which are in agreement with the theoretical values from 0.8 to 1.6 cm for the relative ionospherically corrected measurement in double difference mode if the noise level of P-code L1 is assumed from 1 to 2 mm (see Section 2.3).

Table 6.4.2
Statistics of Residuals Using Ionospherically Corrected Measurement
(OSHA-AFT Kinematic Run, April 27)

PRN	Number of Epochs	Residuals (cm) Mean	RMS
31	8189	-0.4	1.7
28	8182	0.6	1.3
27	5655	-0.6	1.2
19	8189	0.6	1.8
18	5662	0.6	1.6

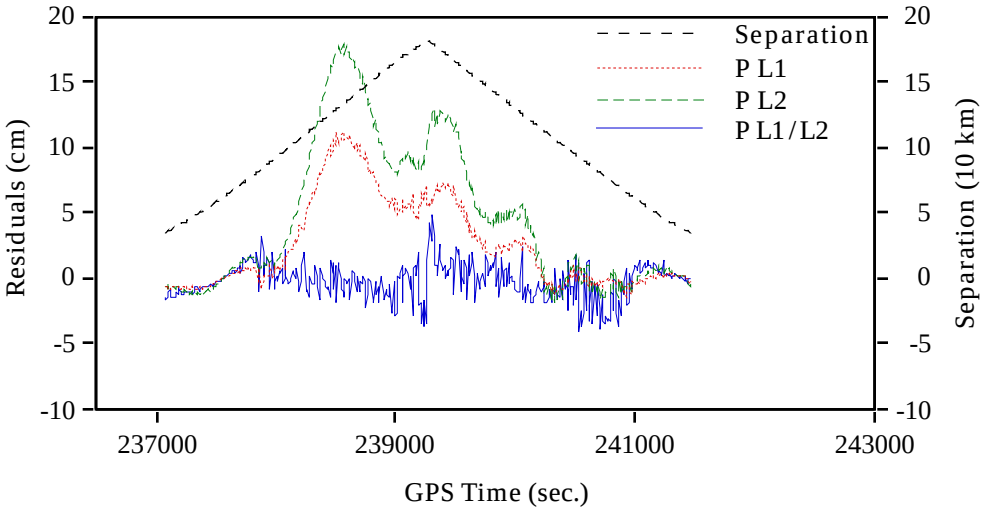

Figure 6.4.2 (a) DD Residuals for PRNs 31-11

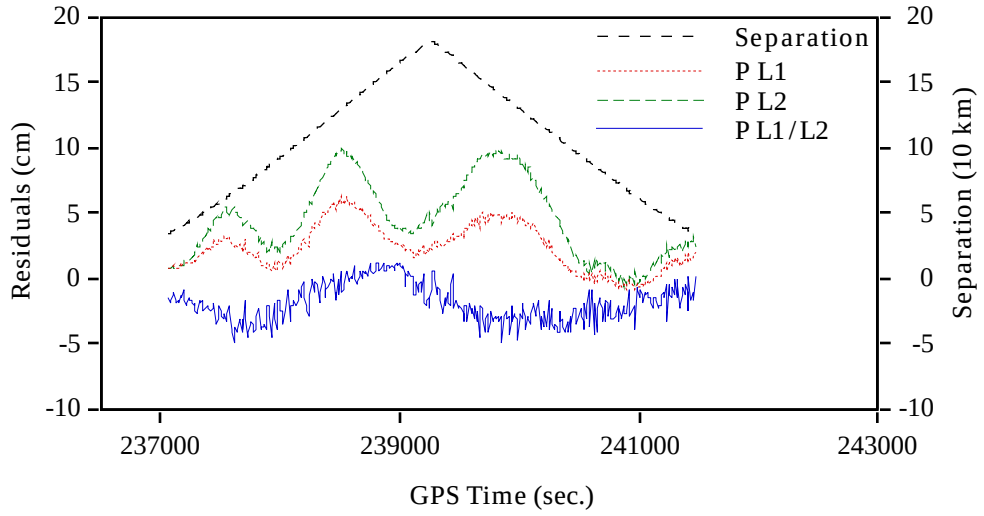

Figure 6.4.2 (b) DD Residuals for PRNs 19-11

Figure 6.4.2
Comparison of Residuals Using P-code L1, L2 and L1/L2 Measurements
(OSHA-AFT Kinematic Run, April 27)

Unfortunately, an attempt to use the cross-correlation L2 for ionospheric error free measurements failed. By observing and analyzing the characteristics of the cross-correlation L2 measurement in kinematic mode, the reason for the failure may be partly explained by comparing the relation between the C/A-code L1 and cross-correlation L2, with that between P-code L1 and L2 in terms of ionospheric refraction delay. Theoretically, the ratio of the delay at P-code L2 to that at P-code L1 should be 1.65. The practical ratio from the flight test data can be estimated by the ratio of the RMS of the L2 residuals to that of the L1, since for a kinematic run the dominant systematic and measurement dependent error is the residual ionospheric error. Figure 6.4.3 illustrates a comparison of PRN 31 residuals using P-code L1 and L2 versus the monitor-remote separation, while Figure 6.4.4 shows the similar result but using the C/A-code L1 and cross-correlation L2. From the figures, the similar behavior of the C/A-code L1 residuals to the P-code L1 can be seen, which is more clearly shown in Figure 6.4.5, while the cross-correlation L2 is quite different from the P-code L2.

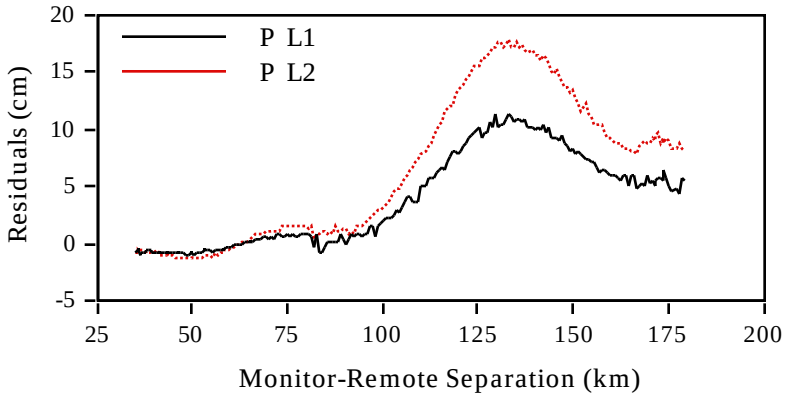

Figure 6.4.3
Comparison Between Residuals Using P-code L1 and L2 versus Monitor-Remote Separation (PRN 31, OSHA-AFT Kinematic Run)

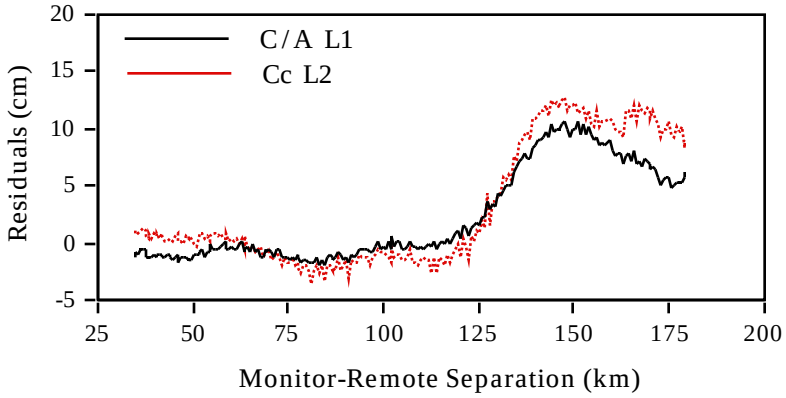

Figure 6.4.4
Comparison Between Residuals Using C/A-code L1 and Cross-correlation L2 versus Monitor-Remote Separation (PRN 31, OSHA-AFT Kinematic Run)

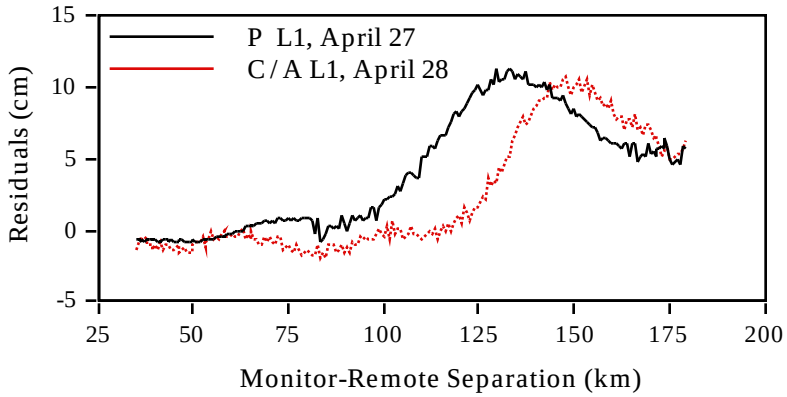

Figure 6.4.5
Comparison Between Residuals Using P-code L1 on April 27 and C/A-code L1 on April 28 versus Monitor-Remote Separation (PRN 31, OSHA-AFT Kinematic Run)

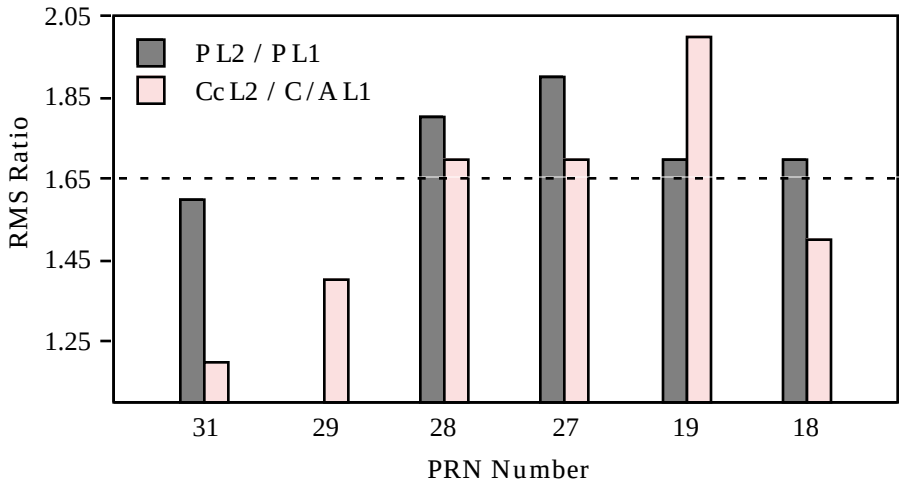

Figure 6.4.6
Ratios of Residual RMS Using P-code L2 to P-code L1 and Using Cross-correlation L2 to C/A-code L1 (OSHA-AFT Kinematic Run)

Since the flight test was repeated on the same flight line on April 27 and 28, Figure 6.4.5 gives us an understanding regarding the change of the atmospheric conditions over the test area. Figure 6.4.6 graphically summarizes the two kind of ratios (P-code L2 to L1 and cross-correlation L2 to C/A-code L1) for all tracked satellites to demonstrate the two different features. It is clear that all the ratios of P-code L2 to L1 are generally close to and consistent with the theoretical value 1.65, while those of cross-correlation L2 to C/A-code L1 generally diverse from the value, and some diverge greatly. This might be the reason that caused the failure in successfully exploiting the ionospherically corrected measurements generated by the cross-correlation L2. Since the positioning results with the cross-correlation L2 seem to be quite good, as presented in Section 6.3.2, further investigations on using the cross-correlation L2 to form ionospheric error free measurements are needed.

As an important aspect of this investigation, the ionospheric error effect on the positioning results was estimated by differencing an L1 only carrier phase trajectory from an ionospheric error free trajectory (i.e. P-code L1/L2). Figure 6.4.7 shows these differences for the three coordinate components for the April 27 data between the aircraft and the OSHA monitor station. From the figure, it is clear that the effect on height is correlated to the monitor-aircraft separation and ranges from 20 to 60 cm with a separation from 60 to 180 km. The effects on horizontal components generally are less than 15 cm and independent of the separation. The total effect on the position is up to 3 ppm and is mostly in the height.

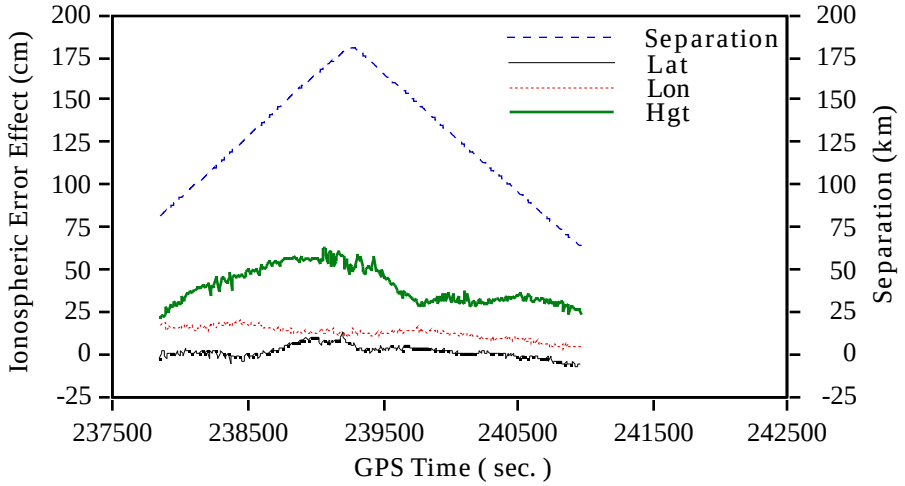

Figure 6.4.7
Difference Between Aircraft Trajectories Using P-code L1 and L1/L2 Measurements, April 27

6.4.3 Orbital Error Effect

Unlike atmospheric error effects, the orbital error can not be simply eliminated by modeling. As mentioned in Section 2.4, the orbital error is made up of the nominal broadcast orbital error and SA, while the magnitude of the error on positioning can be significantly affected by the satellite geometry represented through the position standard deviation (see equation 3.2.15) and sometimes by switching to an updated broadcast ephemerides. In this section, these statements will be examined and confirmed using flight data.

The orbital error can actually be computed by differencing the results

using the precise orbit from those using the broadcast ephemerides, assuming that the error in the precise orbit is negligible. Figure 6.4.8 graphically presents the orbital error (in position) behaviors for all satellites used on April 27. Table 6.4.3 lists the statistics of an individual satellite orbital error, the Block number and the epochs when switching to an updated broadcast ephemerides. In the figure, it can be seen that the sudden changes of PRNs 31 and 19 happen at the switching epochs according to Table 6.4.3, which are due to updated broadcast ephemerides. Some slight changes also can be observed on PRNs 11 and 27. No differences due to ephemerides updating can be found on PRNs 18 and 28.

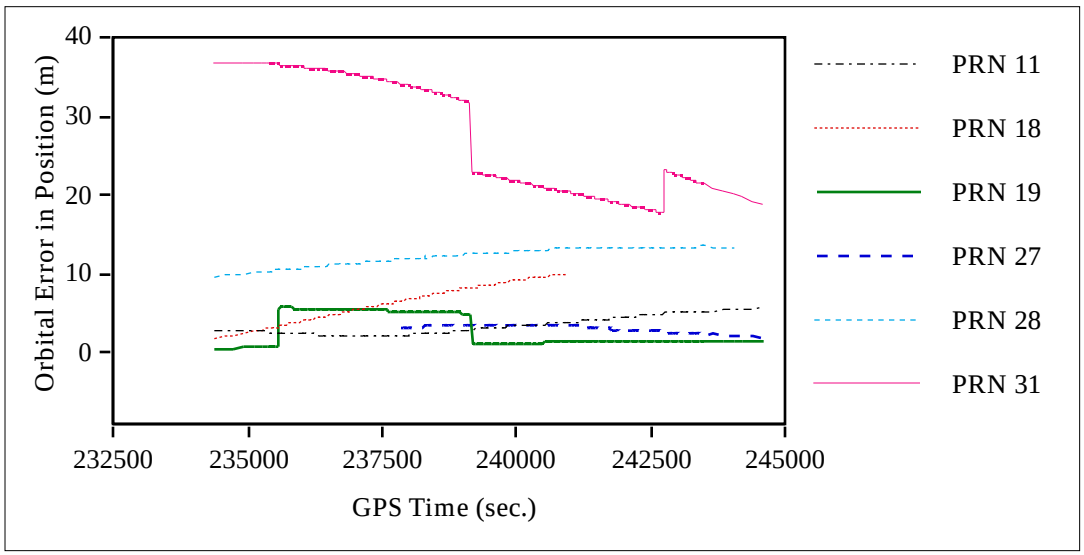

Figure 6.4.8
Differences Between Broadcast and Precise Orbits for All Satellites Used on April 27

Table 6.4.3
Statistics of the Satellite Orbital Error in Position and Related Features

Satellite ID	Block Number	Mean (m)	RMS (m)	Std. Dev. (m)	Max. (m)	Switching epoch
PRN 11	I	3.34	3.50	1.06	5.72	239400, 243000
PRN 18	II	6.68	7.04	2.21	10.11	239152
PRN 19	II	3.02	3.62	2.00	5.71	235552, 239152
PRN 27	II	3.11	3.13	0.40	3.57	241200
PRN 28	II	12.30	12.34	1.02	13.47	241200
PRN 31	II	27.22	28.16	7.23	36.80	239152, 244304

It was reported that the broadcast orbital error for Block I satellites is about 5 m in range (Remondi and Hofmann-Wellenhof, 1989) and the error due to orbital SA ranges from 10 to 40 m in range (Seeber, 1993). Results given in Table 6.4.3 are in agreement with these estimations, see results of PRNs 11, 18, 28, and 31 for example.

When assessing orbital error, the main concern is the effect on positioning. Figure 6.4.9 illustrates the orbital effect in position in terms of the difference between trajectories (AFT with respect to OSHA) determined using broadcast and precise ephemerides. The separation between the aircraft and monitor as well as the standard deviation of estimated aircraft positions are also plotted. This standard deviation divides the mission into four distinct periods: during the first and third periods, only five satellites were tracked, and thus the corresponding standard deviation is larger than for the second and fourth periods when six satellites were tracked. This means that the satellite geometry was weaker in the first and third periods. Considering the monitor-aircraft separation, it can be seen

that the broadcast orbital error effect in position varies from 3 to 5 ppm (standard deviation from 2 to 3.5 cm) in the first period, and decreases to 0.5 to 1 ppm (standard deviation from 1.1 to 1.7 cm) in the second period. In the third period, it again increases to 2 to 10 ppm (standard deviation from 4.8 to 7.0 cm) which indicates that poor satellite geometry can significantly amplify orbital effects in that range. This correlation of the position error due to the residual orbital error, with the position standard deviation and the separation can be mathematically explained by equation 3.2.15. The sudden change in position error at 239152 s (the corresponding monitor-remote separation is about 175 km) is caused by sudden changes in the two satellite (PRNs 19 and 31) orbital errors due to switching to their updated broadcast ephemerides, see Figure 6.4.8. In Figure 6.4.9, no sudden changes in position error can be found at 235552 and 244304 s when the orbital errors of the two satellites also suddenly changed respectively, because the corresponding separation is only several tens of metres so the resulting errors are too small to be detected.

To avoid sudden changes in position error, the proper broadcast ephemerides has to be chosen. The prime principle is to choose the most recently updated ephemerides which correspond to the largest monitor-remote separation. Usually, a set of broadcast ephemerides is valid for four hours, two hours before and two hours after the ephemerides reference time (Hofmann-Wellenhof et al., 1992). Figure 6.4.10 shows that the sudden change disappears and the orbital error effect is decreased when only one set of broadcast ephemerides is used during the mission.

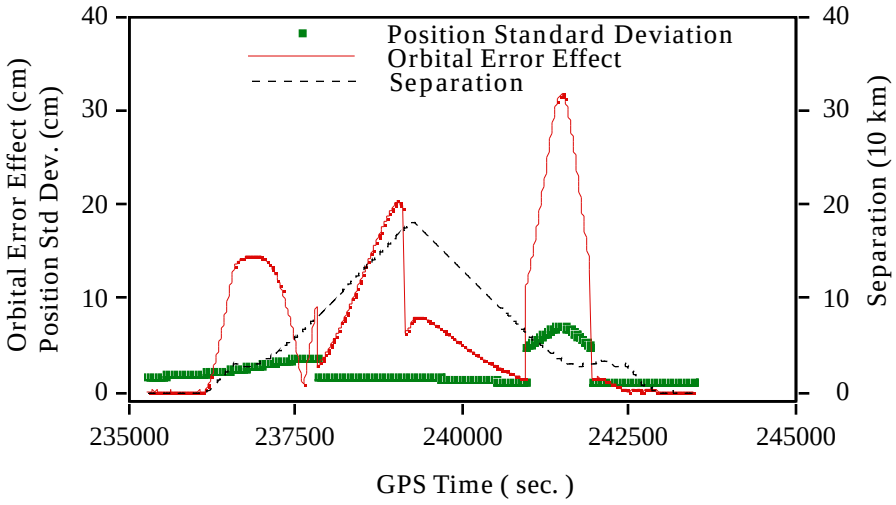

Figure 6.4.9
Difference Between Aircraft Trajectories Using Precise and Broadcast Orbits on April 27 (OSHA-AFT Kinematic Run with P-code L1)

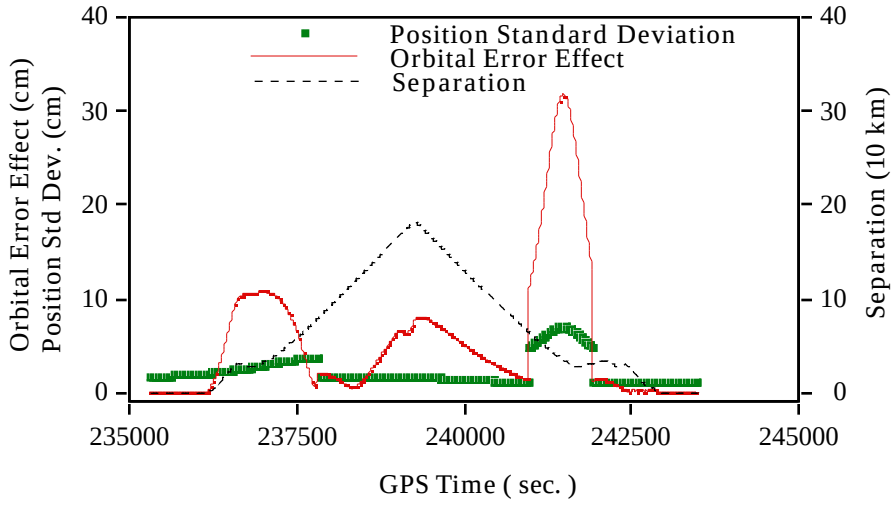

Figure 6.4.10
Difference Between Aircraft Trajectories Using Precise and Broadcast Orbits on April 27 (OSHA-AFT Kinematic Run with P-code L1 and No Broadcast Updating During Mission)

Figure 6.4.11 gives us a general illustration of the orbital error effect on positioning under good satellite geometry on April 28 when at least six satellites had been tracked until the aircraft landing stage. As can be seen in the figure, the corresponding position standard deviation varies from 1.0 to 2.5 cm, and the position error generally ranges from 0.5 to 1.0 ppm. Sudden changes in the error at about 324000 and 328280 s are mainly caused by satellite changes (PRN 27 rises at 323999 s, PRN 29 sets at 324094 s, PRN 15 rises at 328281 s, and PRN 18 sets at 328285 s), since the corresponding position standard deviations only change slightly. The change at 325552 s is still due to the updated ephemerides of PRNs 19 and 31, which happens exactly 24 hours after the same phenomenon on April 27. By the end of the mission, although the standard deviation increases rapidly because the satellite geometry weakens due to rejecting PRN 28 before the landing (see Figure 6.1.2), the position error does not change at all. This is again because of the short baseline. It is also apparent in Figures 6.4.9. through 6.4.11 that the position error is proportional to the monitor-remote separation.

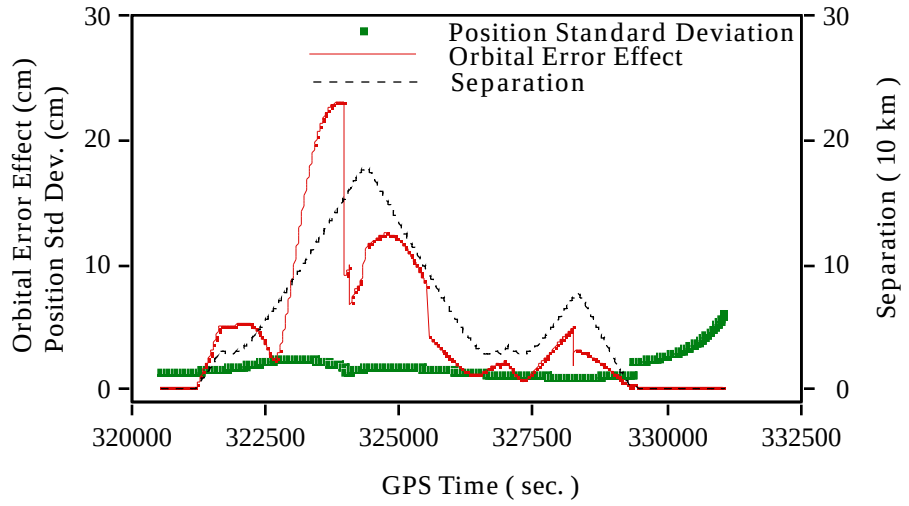

Figure 6.4.11

Difference Between Aircraft Trajectories Using Precise and Broadcast Orbits on April 28 (OSHA-FORE Kinematic Run with C/A-code L1)

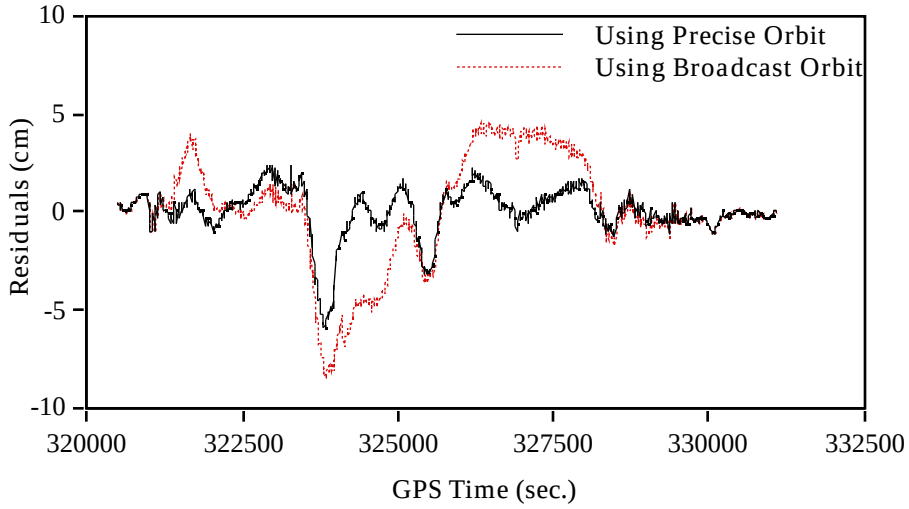

Figure 6.4.12

Comparison Between Residuals Using Precise and Broadcast Orbit (OSHA-FORE Kinematic Run with C/A-code L1 on April 28)

Table 6.4.4
Comparison Between Statistics of Residuals Using Broadcast and Precise Orbits (OSHA-FORE Kinematic Run, C/A-code L1, April 28)

PRN	Number of Epochs	Residuals (cm) Using Broadcast Orbit			Residuals (cm) Using Precise Orbit		
		Mean	RMS	Max.	Mean	RMS	Max.
31	21195	-0.1	3.1	-9.2	0.0	1.3	-6.1
29	7189	1.3	3.9	10.6	1.3	3.2	9.2
28	17750	1.0	2.6	7.6	0.2	1.9	7.3
27	14199	-1.1	2.1	-6.3	-0.2	1.0	-3.6
19	21195	0.5	1.5	5.2	0.1	1.3	5.1
18	5641	0.7	2.7	-8.3	0.2	1.9	-5.5

Orbital error contributes to the residuals as well as positions, and this can be found when comparing the residuals when the precise orbit is applied. A comparison of the residual statistics is summarized in Table 6.4.4. For the sake of contrast, Figure 6.4.12 shows PRN 31 residuals using both the broadcast and precise ephemerides. It is clear that the orbital error effect on the residuals is a long term error and can reach up to several centimetres which may be critical for correctly resolving ambiguities on-the-fly over large separations.

6.4.4 Multipath Effect

Multipath was confirmed to be the dominant error source for GPS aircraft

attitude determination by Braasch and van Graas (1991). They also found and demonstrated the randomized multipath behavior in an airborne environment. Although their investigation was based on the code measurement, it was stated that the same conclusion may be applied to the carrier because of the intimate relation between these two measurements.

In the flight test, multipath effects on airborne positions using carrier phase measurements can be examined since two antennas were mounted on the aircraft with a known separation. The examination consists of the following four scenarios:

1) examining the multipath effect on residuals from the monitor-remote antenna pairs and remote-remote antenna pairs in the static mode on known short baselines, and by processing static data in kinematic mode with fixed integer ambiguities;

2) estimating the coordinate error due to multipath by processing static data in kinematic mode with fixed integer ambiguities;

3) examining residuals from the remote-remote antenna pair while in flight;

4) comparing the estimated distance between the two antennas on the aircraft using GPS with the measured distance.

The scenarios listed above are based on the fact that all errors other than multipath and measurement noise tend to cancel due to the short monitor-remote or remote-remote separation. The first three are discussed in order herein,

leaving the fourth in Section 6.5.1.

As results of the first scenario, Figure 6.4.13 shows the residuals from the FORE-AFT, OSHA-AFT, OSHA-FORE antenna pairs during static data processing after landing. The sinusoidal behavior of multipath are apparent in the residuals with periods of 5 to 10 minutes and magnitudes of 1 to 2 cm. Comparing Figure 6.4.13 (c) to 6.4.13 (b), it is obvious that multipath is much smaller on the FORE antenna than on the AFT, by 1 to 2 times in terms of RMS. In comparing Figure 6.4.13 (a) with 6.4.13 (b) and 6.4.13 (c), it is found that the antenna pair on the aircraft suffers from multipath more than either of the two monitor-remote pairs. These features also can be observed from Figure 6.4.14, where residuals from processing the static data in kinematic mode are presented. In contrast with Figure 6.4.13, it is found that multipath effects in Figure 6.4.14 have similar periods but very different magnitudes, particularly see PRN 27 residuals in both figures. This is due to the fact that a part of the multipath effect contributes to coordinate errors.

In the second scenario, coordinate errors caused by multipath are estimated by differencing the known coordinates from those determined by processing static data in kinematic mode with fixed integer ambiguities. Results are given in Figure 6.4.15 show a larger multipath effect on the height component, up to 10 cm in Figure 6.4.15 (a). The horizontal component errors due to multipath are generally less than 2 cm in all antenna pairs. Features regarding the magnitude of multipath on different antennas mentioned in the discussion of the first scenario are confirmed in Figure 6.4.15. For instance, the

position error due to multipath on AFT is three times that on FORE in terms of RMS. For further confirmation, static data collected before take off is also processed according to the two scenarios and similar results are obtained.

From the above discussion, the conclusion is that multipath is significant either in the residuals or in the coordinates when the aircraft is stationary. While in flight, if only one receiver is onboard, estimation of multipath becomes complicated since the effect on coordinates can not be detected from the positioning solution as in the second scenario. With two receivers onboard, the effect on residuals can be examined because only multipath and noise errors remain in the residuals of the two onboard receivers. Due to aircraft motion, multipath error is expected to be observed as random in the residuals. This expectation is verified in the third scenario.

To demonstrate the noise-like multipath effect on residuals while in flight, PRN 31 residuals using the AFT-FORE kinematic run on the flight test leg 2 (see Figure 6.1.4) with four types of measurements (i.e. P-code L1, L2, C/A-code L1 and Cross-correlation L2) are illustrated in Figure 6.4.16. It is clear that no typical sinusoidal multipath signature can be observed. Since noise should be at the millimetre level, multipath effects are obviously dominant in the residuals.

When comparing with results using P-code L1 or C/A-code L1, those using P-code L2 or Cross-correlation L2 are more corrupted by multipath due to their longer wavelength and lower SNR. It can be inferred that similar results should be expected on the position error caused by multipath when these

measurements are used, for a discussion see Section 6.5.1.

In summarizing the above results, the findings are listed as follows:

1) Very different magnitudes (by two times in position RMS) of multipath effect have been detected in static mode on the two antennas mounted on the aircraft with only about one metre separation;

2) A part of the multipath effect is absorbed by the positions when static data is processed in kinematic mode. This is supposed to be true in the pure kinematic mode;

3) A randomized multipath behavior on residuals has been observed while in flight.

4) The multipath effect on the carrier phase measurement is confirmed to be a main error source in the airborne GPS positioning environment either while stationary or in flight.

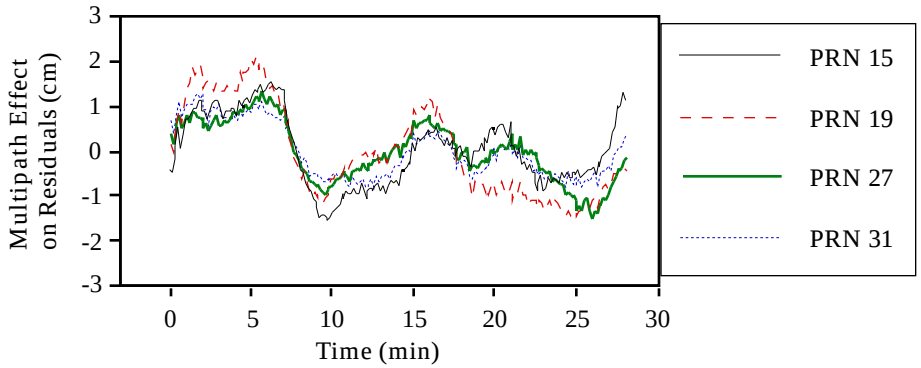

Figure 6.4.13 (a) The FORE-AFT Receiver Pair

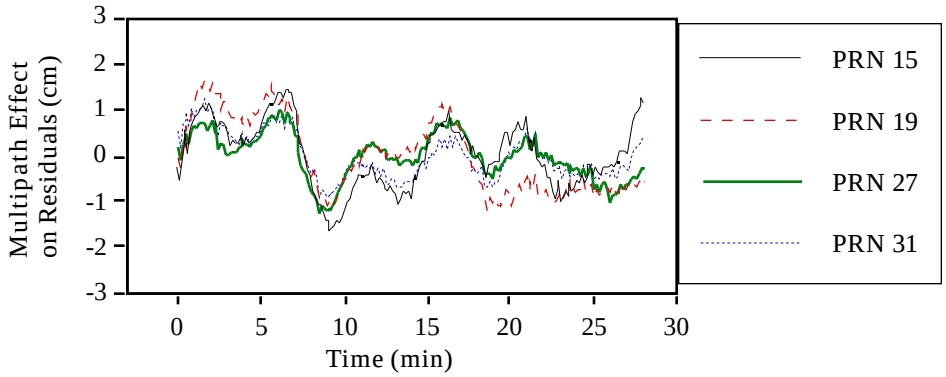

Figure 6.4.13 (b) The OSHA-AFT Receiver Pair

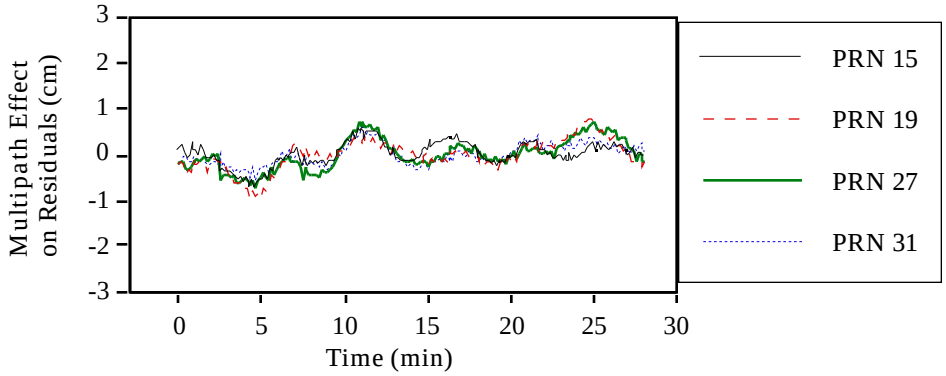

Figure 6.4.13 (c) The OSHA-FORE Receiver Pair

Figure 6.4.13
Multipath Effect on Residuals in Static Mode after Landing
(C/ A-code L1, April 28)

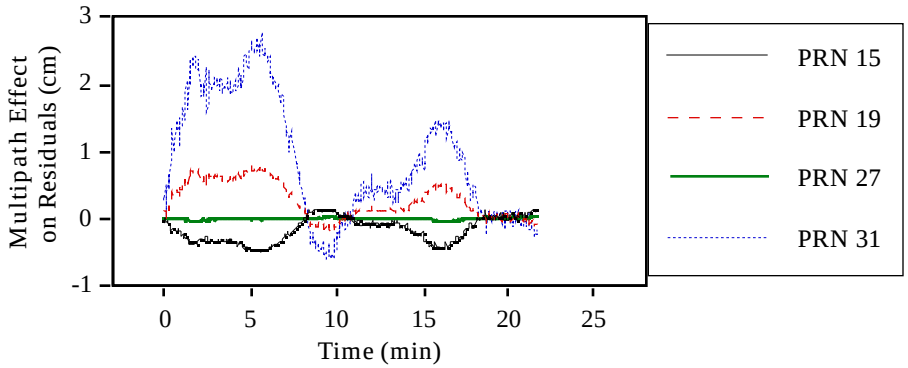

Figure 6.4.14(a) The FORE-AFT Receiver Pair

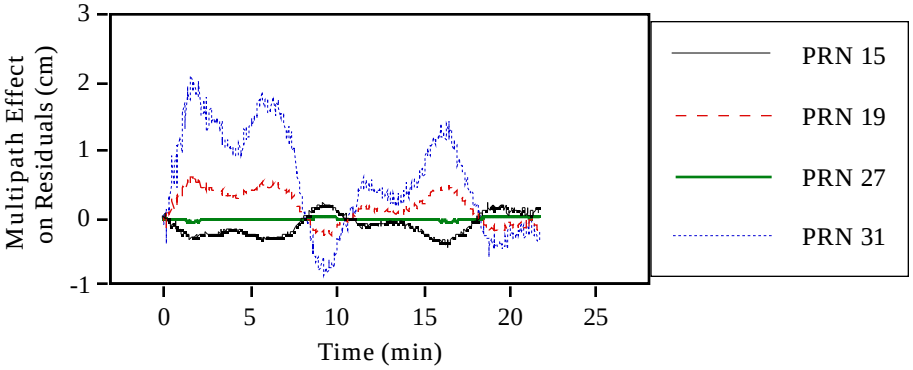

Figure 6.4.14(b) The OSHA-AFT Receiver Pair

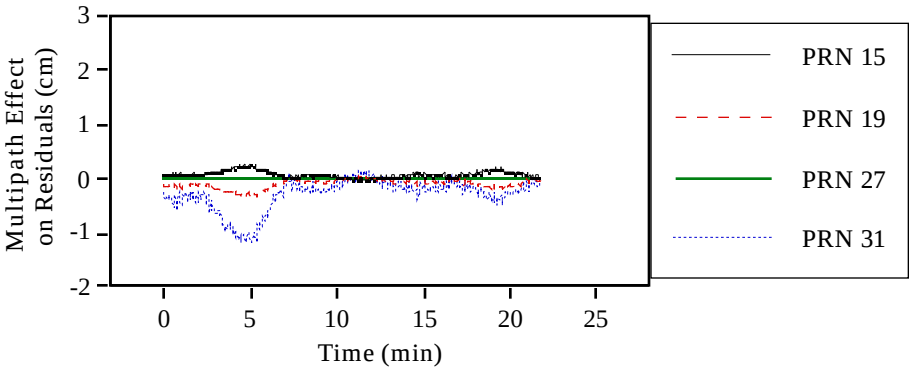

Figure 6.4.14(c) The OSHA-FORE Receiver Pair

Figure 6.4.14
Multipath Effect on Residuals by Using Static Data in Kinematic Mode after Landing (C/ A-code L1, April 28)

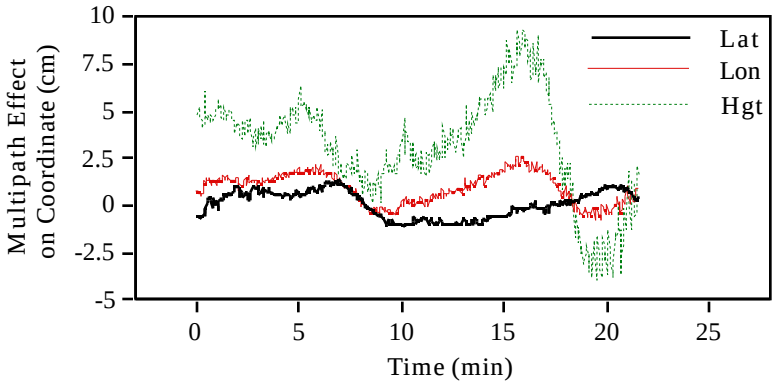

Figure 6.4.15(a) The FORE-AFT Receiver Pair

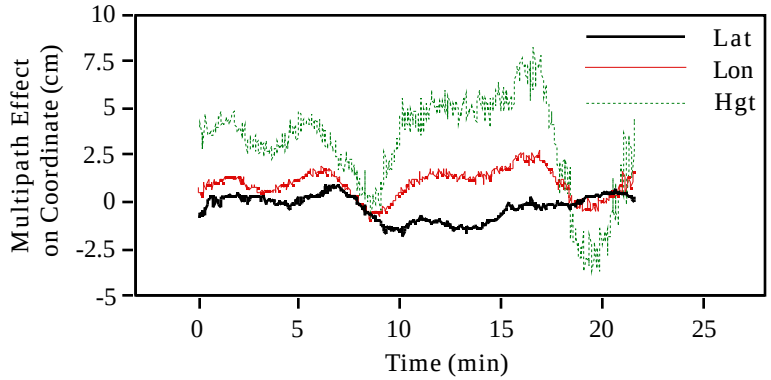

Figure 6.4.15(b) The OSHA-AFT Receiver Pair

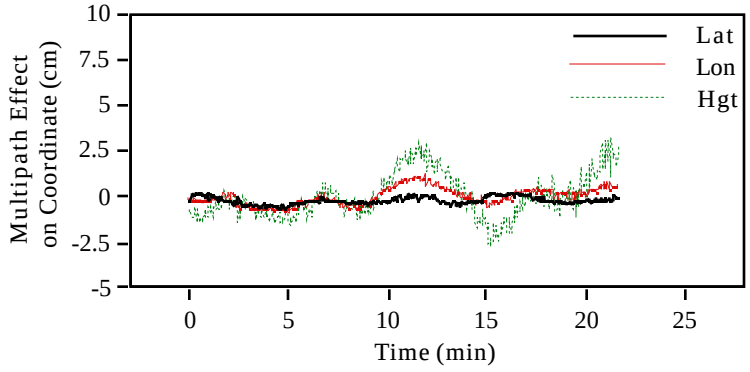

Figure 6.4.15(c) The OSHA-FORE Receiver Pair

Figure 6.4.15
Multipath Effect on Coordinates by Using Static Data in Kinematic Mode after Landing (C/ A-code L1, April 28)

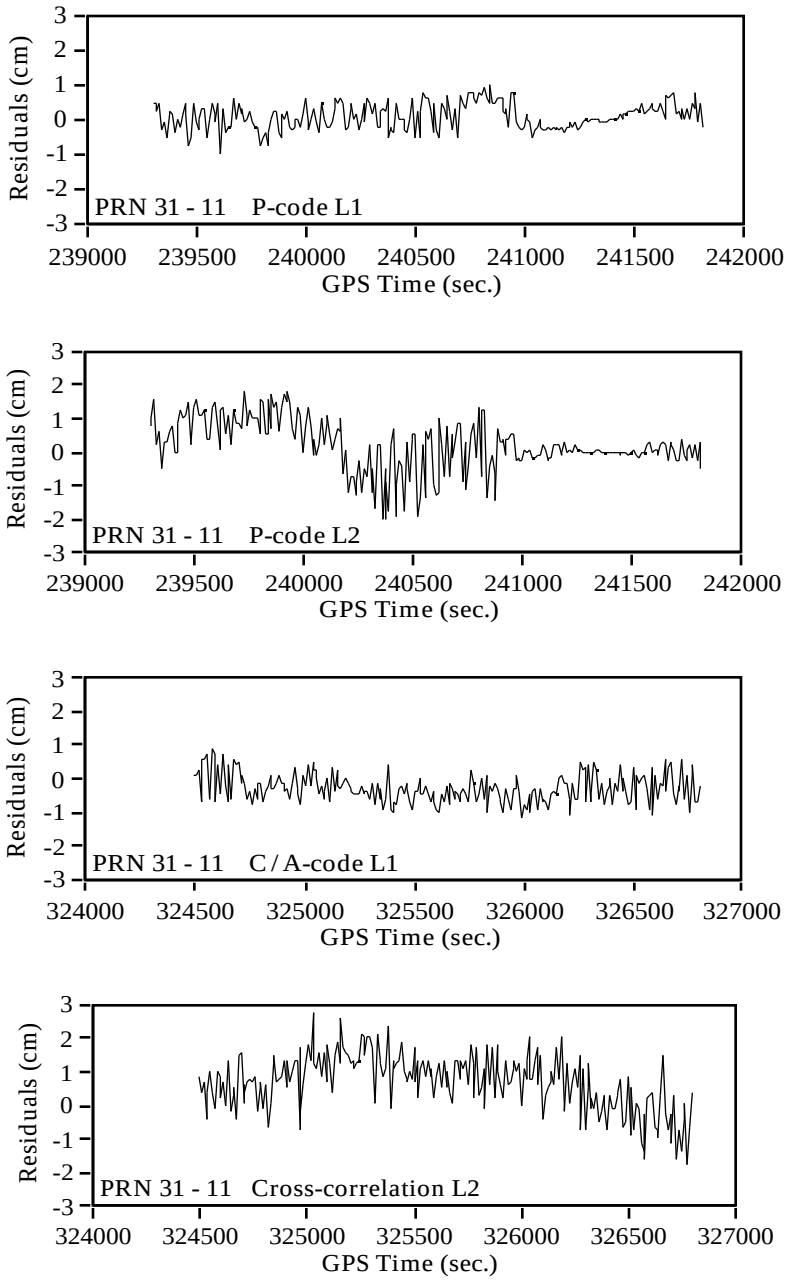

Figure 6.4.16

Residuals Using the AFT-FORE Kinematic Run on the Flight Test Leg 2 (P-code L1, P-code L2, C/A-code L1, and Cross-correlation L2)

6.5 COMPARISON AND ACCURACY EVALUATION

The multi-receiver configuration used in the flight test provides several means to effectively evaluate the internal positioning accuracy of the system. In this section, results using the following methods are discussed: 1) a comparison of the estimated distance between antennas on the aircraft using GPS with the known baseline, 2) a comparison of aircraft trajectories from forward and reverse time processing solutions, 3) the triangle misclosure test, and 4) a comparison of aircraft trajectories from different monitor stations. These methods serve three purposes: 1) to examine the consistency of results from different ways; 2) to further analyze carrier phase multipath effects on aircraft positions while in flight; and 3) to demonstrate the achievable accuracy of airborne GPS positioning with large monitor-remote separations.

6.5.1 Comparison with Known Baseline on the Aircraft

Considering the triangle relation among the OSHA monitor and the two remote receivers, the direct and indirect (through the OSHA) comparisons can be made with the known baseline formed by two aircraft antennas (93.7 cm). From the indirect comparison, Figure 6.5.1 shows the difference between the known aircraft antenna separation and the estimated separation computed from the difference between the OSHA-FORE and OSHA-AFT kinematic vectors. This was computed using P-code L1 data on April 27. The difference is within 2.5 cm

and the RMS is 1.1 cm which shows that the two aircraft positions are consistent and the internal accuracy is high.

Figure 6.5.2 shows results from the direct comparison, where FORE is used as a pseudo-reference station. In this case, both the pseudo-reference and rover antennas are moving and the baseline length is constant. Comparing Figures 6.5.1 and 6.5.2, three error peaks of up to 5 cm can be seen in Figure 6.5.2 which corresponds to aircraft turns. This is due to the fact that the reference receiver is moving which is not consistent with the general Kalman filter model under a 1 Hz data rate used in data processing on April 27. In general, the results during the turns are not of interest for most applications.

From corresponding results on April 28 when data was collected at a 2 Hz rate in C/A-code mode shown in Figures 6.5.3 and 6.5.4, no differences are found. In fact, results from the indirect comparison should be the same as those from the direct comparison, and this has been proven theoretically in Section 3.3.

The above results show that the relative position accuracy between the two antennas on the aircraft reaches a few centimetre level. If it is assumed that each coordinate component has a equal amount of contribution to the error budget, the coordinate accuracy should not be worse than the position accuracy. Remaining errors include multipath and carrier phase noise.

To isolate the carrier phase multipath effect on the aircraft position, analysis has to focus on results from the direct comparison during the straight flight line. Figure 6.5.5 shows results with four types of measurements (P-code

L1, L2, C/A-code L1 and cross correlation L2) using the AFT-FORE kinematic run on the flight leg 2 (see Figure 6.1.4). From the figure, it can be observed that there is a bias-like trend in all cases, which is likely due to the common multipath effect. The random behavior of the differences is composed of the random part of multipath and measurement noise. In Figure 6.5.5, the random part of P-code L1 results is similar to that of C/A-code L1, and noisier behavior of the cross-correlation L2 results is evident compared with the P-code L2 results. Cross-correlation results are twice as poor as the P-code L2 results in terms of the standard deviation.

From the above results, it is found that the multipath effect on the position generally ranges from 1 to 2 cm while in flight, and a bias-like trend from multipath is observed although the effect on residuals seems to be random, see Figure 6.4.16.

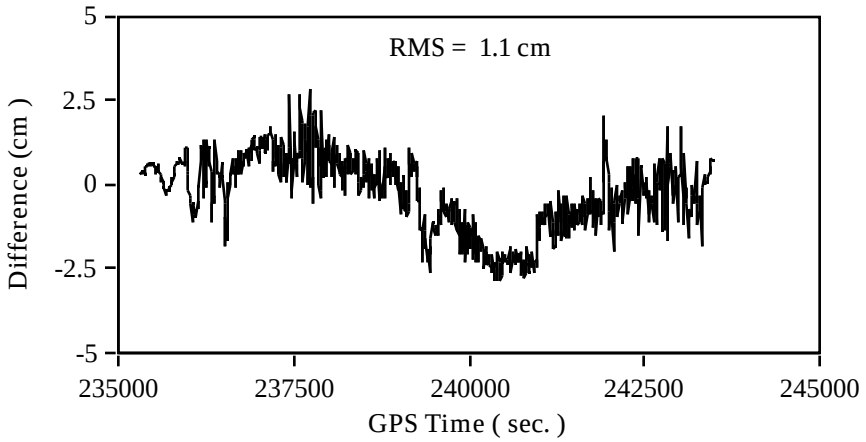

Figure 6.5.1
Difference in Known and Estimated Aircraft Antenna Separation Using the OSHA-FORE and OSHA-AFT Kinematic Runs (P-code L1, April 27)

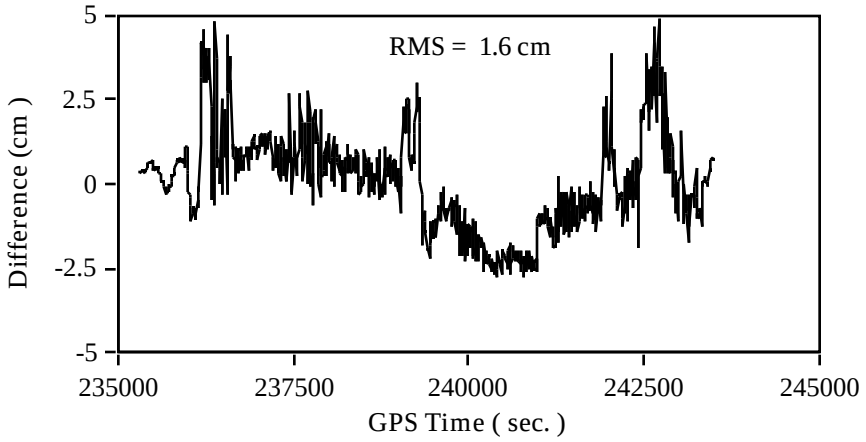

Figure 6.5.2
Difference in Known and Estimated Aircraft Antenna Separation Using the FORE-AFT Kinematic Run (P-code L1, April 27)

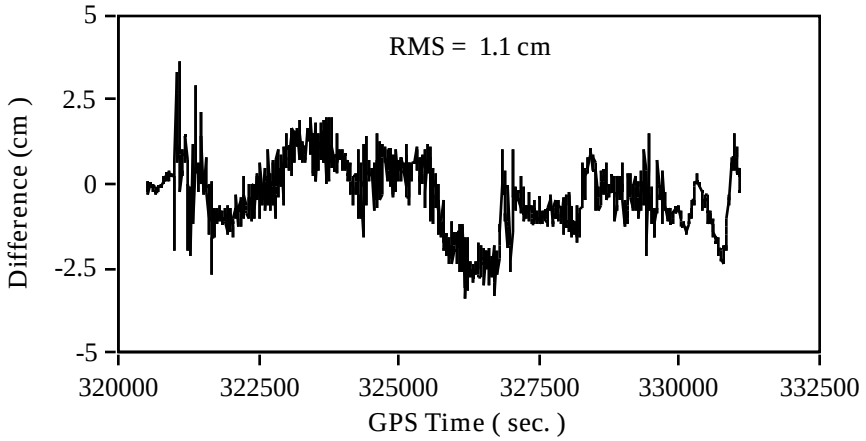

Figure 6.5.3
Difference in Known and Estimated Aircraft Antenna Separation Using the OSHA-FORE and OSHA-AFT Kinematic Runs (C/A-code L1 , April 28)

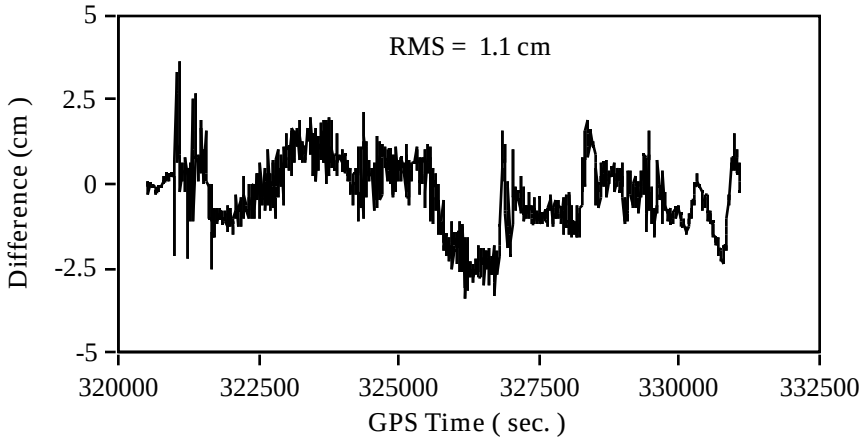

Figure 6.5.4
Difference in Known and Estimated Aircraft Antenna Separation Using the FORE-AFT Kinematic Run (C/A-code L1, April 28)

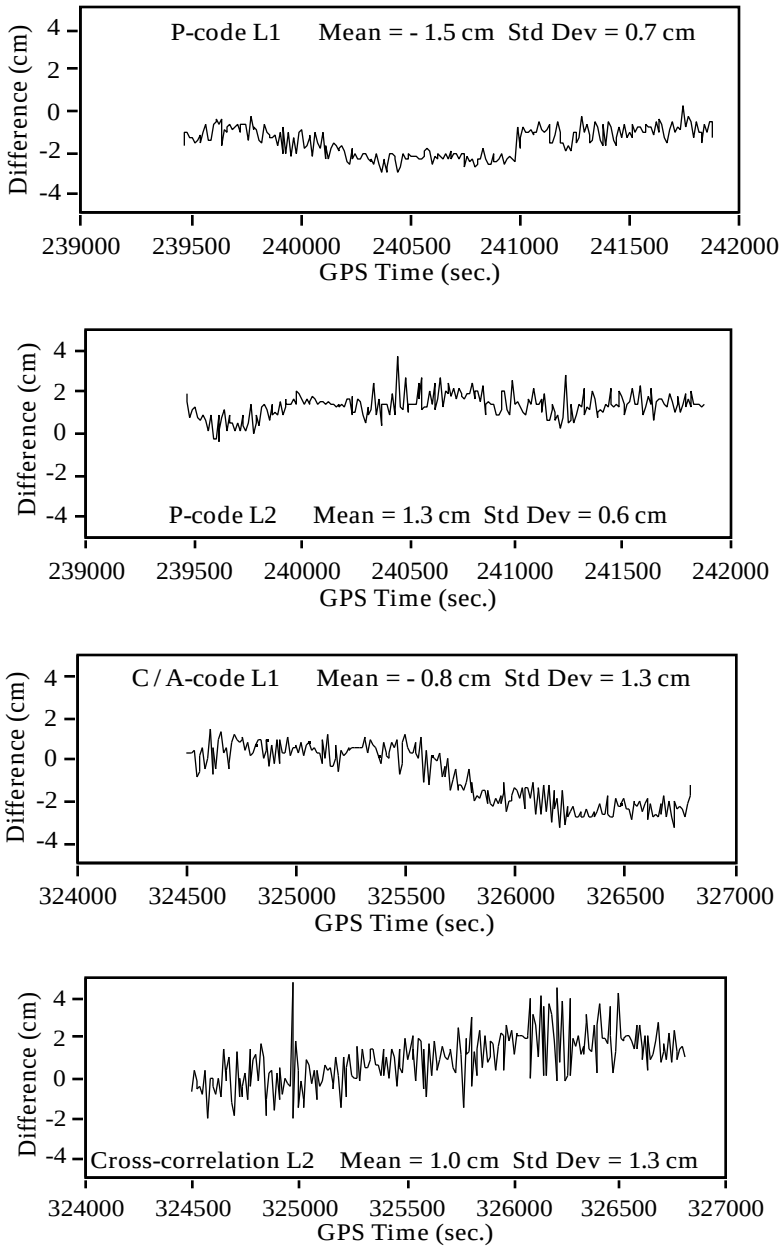

Figure 6.5.5

Difference in Known and Estimated Aircraft Antenna Separation Using the AFT-FORE Kinematic Run on the Flight Test Leg 2 (P-code L1, P-code L2, C/A-code L1, and Cross-correlation L2)

6.5.2 Comparison Between Forward and Reverse Processing

The benefit of comparing the trajectory from forward processing with that from the reverse is that the consistency of the results can be checked. Consistent results are expected when kinematic data is successfully processed in both forward and reverse time.

Figure 6.5.6 shows the differences between trajectories from forward and reverse processing using the OSHA-AFT kinematic run in P-code L1 mode on April 27. The differences in all three coordinate components are generally less than 1 cm, with the maximum RMS being 0.5 cm in the height component. The larger differences in Figure 6.5.6 occur during aircraft turns and also during weaker satellite geometry (when 5 satellites are tracked, see Figure 6.4.9 in contrast to Figure 6.5.6).

Statistics of the differences between trajectories are summarized in Table 6.5.1, and show that the maximum differences in the three components for April 28 are less than 3 cm. Better results for April 28 are due to higher data rates which greatly improve results during aircraft turns. In fact, differences on the flight test leg 1 and 2 for April 28 vary within a few millimetres. This indicates that a high consistency in the aircraft positions from the forward and reverse processing has been achieved.

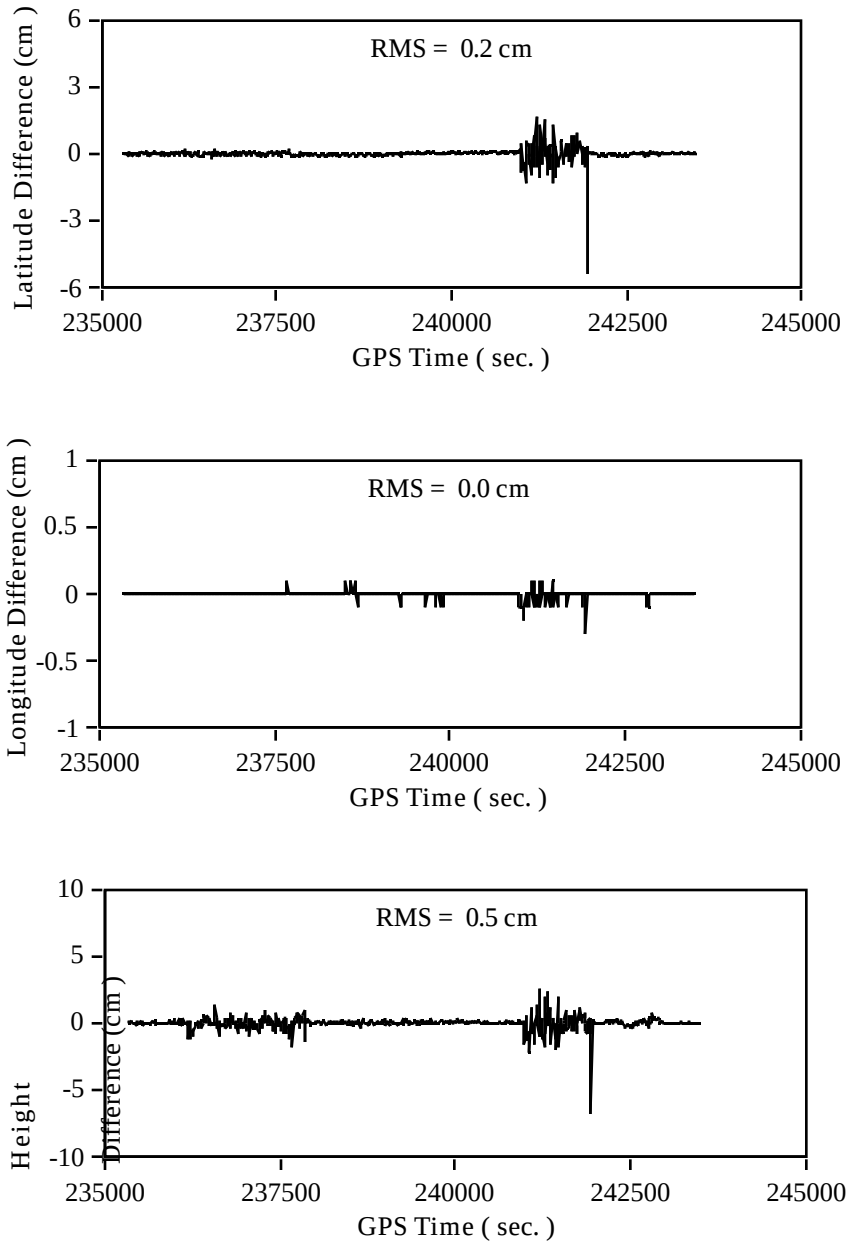

Figure 6.5.6
Trajectory Differences Between Forward and Reverse Time Processing Solutions (P-code L1, April 27)

Table 6.5.1
Statistics of Difference Between Trajectories from Forward and Reverse Time Processing (P-code L1 and C/A-code L1)

Antenna Pair	Coordinate Component	P L1(1 Hz), April 27 Difference (cm)			C / A L1(2 Hz), April 28 Difference (cm)		
		Mean	RMS	Max.	Mean	RMS	Max.
OSHA-FORE	Latitude	0.0	0.2	5.7	0.0	0.0	2.7
	Longitude	0.0	0.0	0.8	0.0	0.0	-2.4
	Height	0.0	0.5	-15.0	0.0	0.1	2.7
OSHA-AFT	Latitude	0.0	0.2	-6.3	0.0	0.0	2.0
	Longitude	0.0	0.0	-0.5	0.0	0.0	-1.8
	Height	0.0	0.5	-10.3	0.0	0.1	-2.7

It should be noted that the above differences also verify the fact that the positioning solutions from successive epochs are weakly correlated with each other. Otherwise, larger differences between trajectories from the forward and reverse processing would be observed.

6.5.3 Triangle Misclosure Test

Triangle misclosure checking is an auxiliary method for examining the internal accuracy of a multi-receiver configuration. This method also has been applied to the test data. A misclosure in each coordinate component can be computed at each epoch from three kinematic vectors formed by OSHA, FORE and AFT. From the discussion in Section 3.3, this misclosure should be close to

zero if all the kinematic runs have been processed correctly.

Figure 6.5.7 shows misclosures in three coordinate components, formed by the OSHA-FORE, OSHA-AFT and FORE-AFT kinematic vectors using P-code L1 data from April 27. As shown in the figure, on the flight test legs the misclosures are almost zero in the horizontal component and generally less than 1 cm in height. These results are sufficiently good to be an indicator that the necessary condition of a successful kinematic run for each antenna pair is met. The three groups of error peaks in the height misclosure correspond to the three aircraft turns where the results are usually not of interest for most applications. Again, due to the higher data rate, results for April 28 are improved greatly which can be seen in Table 6.5.2 where the statistics of the misclosures are listed.

It should be clearly pointed out that near zero misclosures may not guarantee that a successful kinematic run has been achieved for each antenna pair. Large misclosures do mean something is wrong with at least in one antenna pair.

Table 6.5.2
Statistics of the Triangle Misclosure Formed by OSHA-FORE, OSHA-AFT and FORE-AFT Kinematic Vector (P-code L1 and C/A-code L1)

Coordinate Component	P L1(1 Hz), April 27 Misclosure (cm)			C/A L1(2 Hz), April 28 Misclosure (cm)		
	Mean	RMS	Max.	Mean	RMS	Max.
Latitude	0.0	0.2	4.6	0.0	0.0	0.1
Longitude	0.0	0.0	0.3	0.0	0.0	-0.1
Height	0.1	8.6	-27.2	0.0	3.3	-12.7

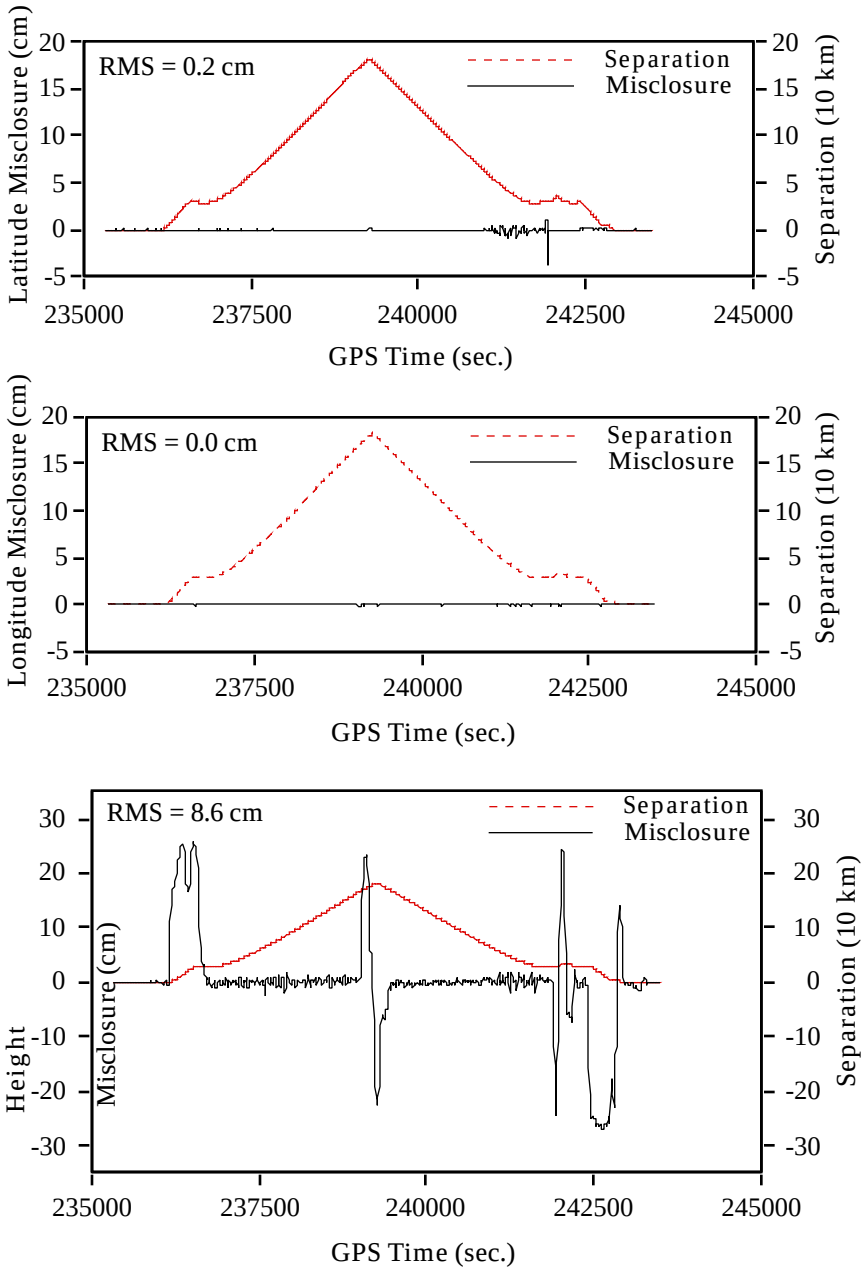

Figure 6.5.7
Misclosure Formed by the OSHA-FORE, OSHA-AFT and FORE-AFT Kinematic Vectors (P-code L1, April 27)

6.5.4 Positioning Solutions from Different Monitor Stations

Comparison strategies discussed in the previous sections only involve one monitor station. With more than one monitor, additional comparison scenarios are available. In this subsection, two scenarios involved with using two monitor receivers to evaluate the aircraft positioning accuracy are presented with emphasis on their effectiveness as well as the corresponding results using the test data. One scenario is to compare trajectories of one remote on the aircraft determined from two monitor stations on the ground, called dependent comparison. The other is to compare the estimated distance between the two remote positions determined from the two monitors (different remote with respect to different monitor) with the measured distance, called independent comparison.

In numerous cases, the positioning accuracy of an aircraft is often assessed using the dependent comparison. The magnitude of the difference from this comparison is sometimes treated as a measure of the positioning accuracy. However, the aircraft information will be eliminated when differencing between solutions from two monitors, and what remains is only information regarding the monitor stations, which has been theoretically proven in Section 3.3. Figure 6.5.8 further illustrates this concept with the test data, where the solid lines are differences between aircraft trajectories determined from the two monitors (OSHA-AFT and WLAK-AFT kinematic runs). The dashed lines represent the error generated by differencing the known monitor position from that

determined by processing the static baseline in kinematic mode (OSHA-WLAK receiver pair). For a clear illustration, only the latitude and height components are given (the results in longitude overlap) in the figure. These two sets of curves are completely correlated over time, and are offset about 10 cm, i.e. the misclosure due to the separation between WLAK and the aircraft as well as the changing satellite geometry. These results confirm what have been already suggested with equations (3.3.4), (3.3.6) and (3.3.10) in Section 3.3, and clearly demonstrate the ineffectiveness of the dependent comparison for the assessment of the positioning accuracy of the aircraft. This ineffectiveness results from the triangle relationship of the three receivers, see Section 3.3.

To evaluate the positioning accuracy of the aircraft, a triangle relationship has to be avoided so an independent kinematic vector is needed. This leads to a need for an independent comparison.

As a final accuracy assessing scenario, the independent comparison is performed by computing two trajectories using ionospheric error free observables with precise ephemerides; AFT with respect to OSHA and FORE with respect to WLAK. These two trajectories are independent, so they can be used to check the internal positioning accuracy by subtracting the known baseline length between the two aircraft antennas from that computed from the two trajectories. The difference results on the flight test leg 2, as well as the corresponding separation between the aircraft and OSHA, are shown in Figure 6.5.9 and clearly demonstrate that the relative accuracy of the two independent trajectories is within 10 cm over separations of 30 to 180 km.

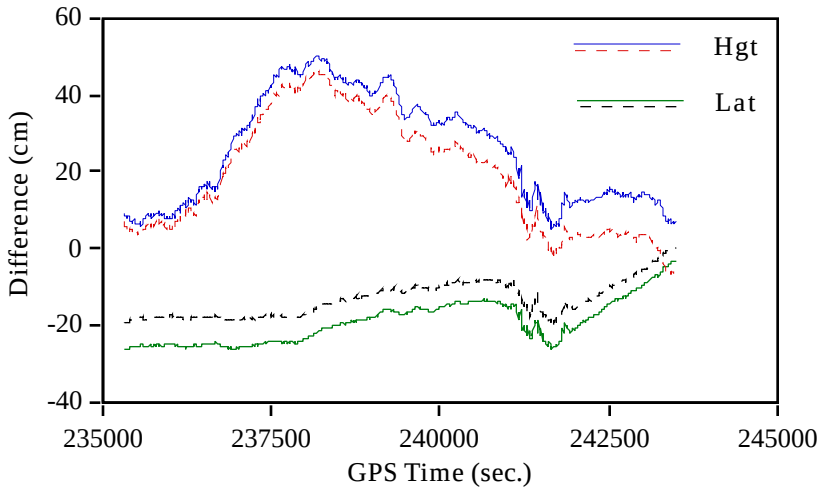

Figure 6.5.8

Correlation Between Aircraft Differences Determined from Two Monitor Receiver and the Error Between Two Monitor Receivers When Processed in Kinematic Mode (L1/L2, April 27)

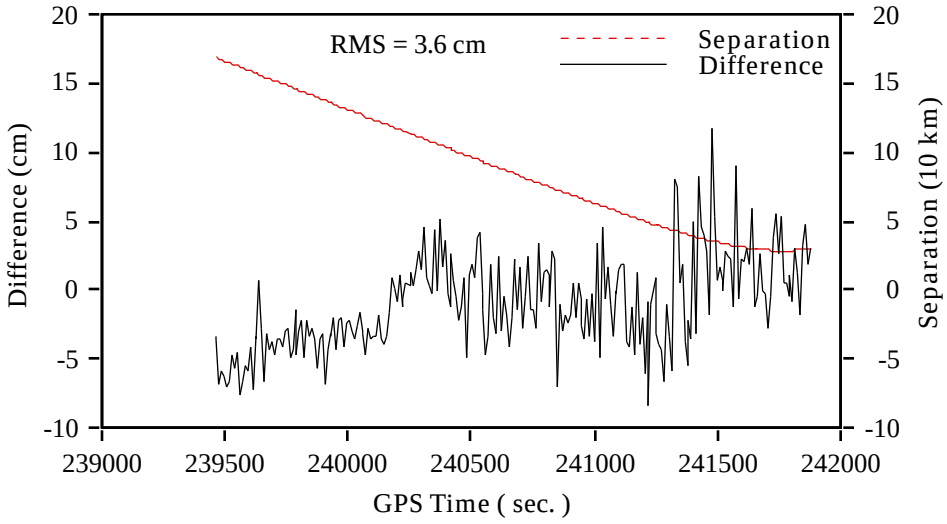

Figure 6.5.9

Difference Between Measured and Estimated Baseline Using Independent Aircraft Trajectories (on the flight test leg 2)

CHAPTER 7

SUMMARY, CONCLUSIONS AND RECOMMENDATIONS

The following summary, conclusions and recommendations are made regarding the research in this thesis.

7.1 SUMMARY OF RESEARCH

Airborne differential GPS positioning techniques open up broad prospects for various positioning applications. The investigations made in this thesis have successfully demonstrated the achievable accuracy over a large operational area (50 to 200 km in extent). Research in this thesis primarily studied the effects of various critical errors on the estimated positions and the issues relevant to kinematic GPS algorithms, data processing, and accuracy evaluation which are applicable for a multi-receiver configuration.

In this thesis, two frequently used kinematic GPS algorithms, namely the state space Kalman filter and least squares estimation, were investigated with

emphasis on their features and relationships. The mathematical relationship and the computational equivalence of these two algorithms were demonstrated. A sophisticated formula for analytical estimation of the orbital effect on positions was derived, and the dependency of positions from different receiver pairs in a triple receiver system was mathematically proven. In addition, optimal GPS receiver configurations, operational and data processing strategies, and accuracy checking methods were investigated and applied to the recent flight tests with a multi-receiver configuration. The theoretical analyses and demonstrations were verified using results from the flight tests. Effects of critical errors from the troposphere, ionosphere, orbit and multipath on estimated positions were analyzed and investigated using the test data. This is another significant component of the thesis.

7.2 CONCLUSIONS

The main conclusions drawn from the investigations in the thesis are summarized below:

1) With a high data rate, the same positioning results can be achieved by using least squares as those from the state space Kalman filter algorithm. In this case, the positioning results tend to be independent with respect to the selection of the kinematic GPS model (state space model) and the correlation between the positioning solutions in successive epochs is so

weak that it can be neglected.

2) The state space Kalman filter algorithm, by changing the spectral density matrix, can function as the least squares and provide the estimated results which are identical to those from the least squares no matter what data rate is used. But this does not hold the other way round in some cases, e.g. with a low data rate and in a high dynamic environment.

3) The satellite geometry plays a critical role in dictating the orbital error (and the other systematic errors) effects on the estimated position. Poor satellite geometry is an amplifier of the orbital errors (and the other systematic errors). Another factor which can significantly change the orbital effect on the estimated position is switching to an updated broadcast ephemerides during the mission.

4) In the double difference mode, it is the relative orbital error that effects the estimated position, rather than the absolute one. The orbital error effect on the position also depends on the direction of the vector formed by the monitor and the remote receiver as well as on that of the relative satellite position error vectors.

5) During the flight test period, the nominal orbital error in position from Block I satellites was confirmed to be at the 5 m level. Only one Block II satellite orbital error varied from 20 to 40 m due to SA, while most of the Block II satellite orbital errors were observed either within or close to the marginal limit of the nominal orbital error. For kinematic positioning, the

orbital error was estimated to contribute 0.5 to 1 ppm to the position error under favorable observation conditions (i.e., six satellites in view). In the analysis, there was no evidence to indicate that SA contributed significantly to the estimated position errors.

6) The residual tropospheric effect on the height component is greatly correlated to the monitor-remote height difference which is caused by the mapping function of the tropospheric model. The ionospheric effect on height is also correlated to the monitor-aircraft separation, ranging from 20 to 60 cm with a separation between 60 to 180 km, while the effect on the horizontal components generally are less than 15 cm and independent of separation. The total ionospheric effect on the position is 2 to 3 ppm, resulting mostly from the error in the height.

7) Multipath effect on the carrier phase measurement is confirmed to be a main error source in the airborne GPS positioning environment either while stationary or in flight. A part of the multipath effect is absorbed by the position solutions when static data is processed in kinematic mode. In this case, a severe multipath effect on the height component of up to 10 cm was detected, while the horizontal component errors due to multipath are generally less than 2 cm. While in flight, a randomized multipath behavior on residuals, and a bias-like trend on position, were observed. The multipath effect on position generally ranges from 1 to 2 cm while in flight.

8) The assessment of the remote positioning accuracy through the difference in solutions determined from two monitors is ineffective, since in a triple receiver system the estimated solutions from the three receiver pairs are dependent. The misclosure formed by the three receiver vectors may not be close to zero in some cases, for instance in the case where the separation of the two estimated receivers is large (e.g. over 50 km).

9) To effectively evaluate the positioning accuracy of the aircraft, an independent kinematic vector is required. The flight misclosure test, comparison between forward and reverse time processing, and comparison with the known baseline on the aircraft are effective to examine and assess the internal positioning accuracy and consistency of positioning solutions.

10) Reliable ambiguity initialization is still required for high accuracy kinematic applications with monitor-remote separations over 30 kilometres, when reliable ambiguity determination on-the-fly may be difficult to implement.

11) Results from the flight tests demonstrate that under the satellite constellation during the tests, and accounting for effects due to atmospheric and orbital errors, the accuracy of airborne GPS positioning with monitor-remote separations of 50 to 200 km is at the level of 10 cm using high quality receivers.

7.3 RECOMMENDATIONS

The following recommendations are given either for proper implementation of airborne GPS positioning or for further investigations in the future.

1) When conducting an airborne kinematic survey over large areas, it is recommended that three receivers be used and that two be installed on the moving platform, in order to increase the redundancy of the kinematic data. When this is the case, some checks are available to ensure that the aircraft positions indeed meet the required specifications.

2) To keep the positioning accuracy consistent during a mission, one should keep using the most recent updated ephemerides, which correspond to the period with the largest monitor-remote separation, rather than switching to updated ephemerides every hour. Also frequent satellite switching should be avoided.

3) Since the P-code is denied to civil users, in order to eliminate ionospheric effects, the L2 measurements (e.g. the cross correlation L2 and the L2 in the Z-Tracking mode) should be used. Further elaborate investigations on efficiently using the L2 measurements to form a relative ionospheric error free measurement are required.

4) Investigations on airborne GPS positioning over large areas made in this thesis have been limited to fixing ambiguities to correct values as well as to at least four satellites without loss of lock. The challenge of reliably

implementing airborne GPS positioning with monitor-remote separations of over 50 km is to correctly recover cycle slips 'on-the fly' when multiple loss of lock occurs. One possible solution is to use a low grade inertial measurement unit with GPS receivers on the aircraft to bridge the gap. Another one is using a filtering algorithm to estimate ambiguities as well as other biases. Investigations on these two possible areas should be a continuation of the research in this thesis.

REFERENCES

Ashjaee, J and R. Lorenz (1992), Precision GPS Surveying After Y-Code, Ashtech.

Beutler, G., I. Bauersima, W. Gurtner, M. Rothacher, T. Schidknecht and A. Geiger (1988), Atmospheric Refraction and Other Important Biases in GPS Carrier Phase Observations, Atmospheric Effects on Geodetic Space Measurements, Monograph 12, School of Surveying, University of New South Wales.

Black, H.D. (1978), An Easily Implemented Algorithm for the Tropospheric Range Correction, Journal of Geophysical Research, 83(B4), pp. 1825-1828.

Braasch, M.S. and F. van Graas (1991), Guidance Accuracy Considerations for Realtime GPS Interferometry, Proceedings of ION GPS 91, Albuquerque, New Mexico, September 11 - 13, pp. 373-386.

Braasch, M.S., A. Fink, and K. Duffus (1993), Improved Modeling of GPS Selective Availability, Proceedings of the 1993 ION National Technical Meeting, San Francisco, California, Jan. 20 - 22, pp. 121-130.

Brown, R.G. and P.Y.C. Hwang (1992), Introduction to Random Signals and Applied Kalman Filtering, John Wiley & Sons, Inc., New York.

Cannon, M. E. (1987), Kinematic Positioning Using GPS Pseudorange and Carrier Phase Observations, UCSE Reports No. 20019, Department of Geomatics Engineering, The University of Calgary.

Cannon, M.E. (1990), High-Accuracy GPS Semikinematic Positioning: Modeling and Results, Navigation, Vol. 37, No. 1, pp. 53-64.

Cannon, M.E. (1991), Airborne GPS/INS with an Application to Aerotriangulation, UCSE Report No. 20040, Department of Geomatics Engineering, The University of Calgary.

Cannon, M.E. and K.P. Schwarz (1990), A Discussion of GPS/INS Integration for Airborne Photogrammetric Applications, Preceeding of Kinematic Systems in Geodesy, Surveying, and Remote Sensing (IAG Symposium 107), Banff, Alberta, Canada, September 10 - 13, pp. 443-452.

Cannon, M.E., K.P. Schwarz and M. Wei (1992), A Consistency Test of Airborne GPS Using Multiple Monitor Stations, Bulletin Géodésique, Vol. 66, No. 1, pp. 2-11.

Colombo, Oscar L. (1991), Errors in Long Distance Kinematic GPS, Proceeding of ION GPS 91, Albuquerque, New Mexico, Sept. 11 - 13, pp. 673-680.

Gelb, A (ed.) (1974), Applied Optimal Estimation, The M.I.T. Press, Cambridge, Mass.

Georgiadou, Y. and A. Kleusberg (1988), On the Effect of Ionospheric Delay on

Geodetic GPS Relative Positioning, Manuscripta Geodetica, Vol. 13, No. 2, pp. 1-8.

Georgiadou, Y. and A. Kleusberg (1991), Algorithms and Results of Kinematic GPS Positioning, CISM Journal ACSGC Vol. 45, No. 4, pp. 569-575.

Goad, C. C. and Lt. L. Goodman (1974), A Modified Hopfield Tropospheric Refraction Correction Model, Presented at the Fall Annual Meeting American Geophysical Union, San Francisco, California, Dec. 12 - 17.

Hein, G.W., H. Landau, and G. Baustert (1988), Terrestrial and Aircraft Differential Kinematic GPS Positioning, Presented at the International GPS Workshop Darmstadt, Germany, April 10 - 13.

Henderson, T and M. Leach (1990), An Assessment of the Absolute Accuracy of Long-baseline Kinematic Vehicle, Proceeding of ION GPS 90, Colorado Springs, Colorado, Sept. 19-21, pp. 91-100.

Hofmann-Wellenhof, B., H. Lichtenegger, and J. Collins (1992), GPS Theory and Practice, Springer-Verlag Wien New York.

Hopfield D.S. (1969), Two-quartic Tropospheric Refractivity Profile for Correcting Satellite Data, Journal of Geophysical Research, Vol 74, No. 18, pp. 4487-4499.

Keel, G., H. Jones, G. Lachapelle, R. Moreau and M. Perron (1989), A Test of Airborne Kinematic GPS Positioning for Aerial Photography,

Photogrammetric Engineering and Remote Sensing, Vol. 55, No. 12, pp. 1727-1730.

Krabill, W.B. and C.F. Martin (1987), Aircraft Positioning Using Global Positioning System Carrier Phase Data, Navigation, Vol. 34, No. 1, pp. 1-21.

Krabill, W.B., C.L. Lennon, and E.B. Frederick, (1989), GPS Differential Carrier Phase Applications to the Space Shuttle Landing System, Proceedings of the Fifth International Geodetic Symposium on Satellite Positioning, Las Cruces, New Mexico, March 13 -17, pp. 660-667.

Krabill, W.B. and C.F. Martin (1989), Applying Kinematic GPS to Airborne Laser Remote Sensing, Proceedings of ION GPS 89, Colorado Springs, Colorado. September 27 - 29, pp. 39-43.

Krakiwsky, E.J. (1990), The Method of Least Squares: A Synthesis of Advances, ENGO 629 Lecture Notes, The University of Calgary, Galgary, Alberta.

Kremer, G., R. Kalafus, P. Loomis, J. Reynolds, 1990, The Effect of Selective Availability of Differential GPS Corrections, Navigation, Vol. 37, No. 1, pp. 39-52.

Lachapelle, G. (1990), GPS Observables and Error Sources for Kinematic Positioning, Preceeding of Kinematic Systems in Geodesy, Surveying, and Remote Sensing (IAG Symposium 107), Banff, Alberta, Sept. 10 - 13, pp. 17-26.

Lachapelle, G. (1993), NAVSTAR GPS Theory and Applications, ENGO 625 Lecture Notes, The University of Calgary, Calgary, Alberta.

Lachapelle, G., Messrs. C. Liu, G. Lu and R. Hare (1993), Water Level Profiling with GPS, Proceedings of ION GPS 93, Salt Lake City, Sept. 22 - 24, pp. 1581-1587.

Leick, A. (1990), GPS Satellite Surveying, John Wiley, New York.

Mader, G.L. (1986), Dynamic Positioning Using GPS Carrier Phase Measurements, Manuscripta Geodaetica, Vol. 11, No. 4, pp. 272-277.

Mader, G.L. and J.R. Lucas (1989) Verification of Airborne Positioning Using Global Positioning System Carrier Phase Measurements, Journal of Geophysical Research, Vol. 94, No. B8, pp. 10175-10181.

Merrell, R.L., M.P. Leach and J.R. Clynch (1989), Development of an Operational GPS Controlled Aerial Photography Capability, Proceeding of the Fifth International Geodetic Symposium on Satellite Positioning, Las Cruces, New Mexico, March 13 -17, pp. 634-642.

Remondi, B. (1985) Performing Centimeters Accuracy Relative Surveys in Seconds Using GPS Carrier Phase, Proceedings of the First International Symposium on Precise Position with GPS, Rockville, Vol. 2, pp. 789-797.

Remondi, B. W. (1986) Performing Centimeter-level Surveys in Seconds with GPS Carrier Phase: Initial Results, Proceedings of the First International

Geodetic Symposium on Satellite Positioning, Austin, Texas, April 28 - May 2, Vol. 2, pp. 1229-1249.

Remondi, B. W. (1989), Extending the National Geodetic Survey Standard GPS Orbit Formats, National Information Center, Rockville, Maryland, NOAA Technical Report NOS 133, NGS 46.

Remondi, B. W. and B. Hofmann-Wellenhof (1989), GPS Broadcast Orbits Versus Precise Orbit: A Comparison Study, GPS Bulletin, Vol 2, No. 6, pp. 8-13.

Schwarz, K.P., M.E. Cannon and R.V.C. Wong (1989), A Comparison of GPS Kinematic Models for the Determination of Position and Velocity Along a Trajectory, Manuscripta Geodaetica, Springer-Verlag, Vol. 14, pp. 345-353.

Schwarz, K.P., M.A. Chapman, M.E. Cannon, P. Gong and D. Cosandier (1994), A Precise Positioning/Attitude System In Support of Airborne Remote Sensing, Proceedings of Sixth International Conference on Geographic Information Systems (in press), Ottawa, Canada, June 6 - 10.

Seeber, G., (1993) Satellite Geodesy, Foundations, Methods, and Applications, Walter de Gruyter Berlin New York.

Shi, J. and M.E. Cannon (1993), Configurations for Airborne GPS Positioning Applied to Remote Sensing, Internal Report, Department of Geomatics Engineering, The University of Calgary.

Tiemeyer, B., M.E. Cannon, G. Lachapelle and G. Schanzer(1994), High Precision

Aircraft Navigation with Emphasis on Atmospheric Effects, Proceedings of PLANS' 94, IEEE, New York, pp. 394-401.

Tolman, B.W, J.R. Clynch, D.S. Coco and M.P. Leach (1990), The Effect of Selective Availability on Differential GPS Positioning, Proceedings of ION GPS 90, Colorado Springs, Colorado, Sept. 19 - 21, pp. 579-586.

Wells, D.E., N. Beck, D. Delikaraoglou, A. Kleusberg, E.J. Krakiwsky, G. Lachapelle, R.B. Langley, M. Nakiboglou, K.P. Schwarz, J.M. Tranquilla and P. Vanicek (1986), Guide to GPS Positioning, University of New Brunswick Graphic Services, Fredericton.